

EXTERNAL SHEAR STRENGTHENING OF UNREINFORCED DAMAGED
MASONRY WALLS

A THESIS SUBMITTED TO
THE FACULTY OF ARCHITECTURE AND ENGINEERING
OF
EPOKA UNIVERSITY

BY

ENEA MUSTAFARAJ

IN PARTIAL FULFILLMENT OF THE REQUIREMENTS
FOR
THE DEGREE OF DOCTOR OF PHILOSOPHY
IN
CIVIL ENGINEERING

JUNE, 2016

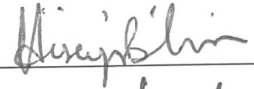
Approval of the thesis:

**EXTERNAL SHEAR STRENGTHENING OF UNREINFORCED DAMAGED
MASONRY WALLS**

submitted by Enea Mustafaraj in partial fulfillment of the requirements for the degree of
Doctor of Philosophy in Department of Civil Engineering, Epoka University by,

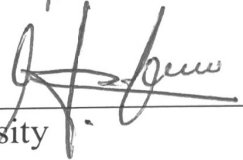
Assoc.Prof. Dr. Hüseyin Bilgin

Dean, Faculty of Architecture and Engineering, Epoka University



Assoc.Prof. Dr. Miriam Ndini

Head of Department, Department of Civil Engineering, Epoka University



Assoc.Prof. Dr. Yavuz Yardım

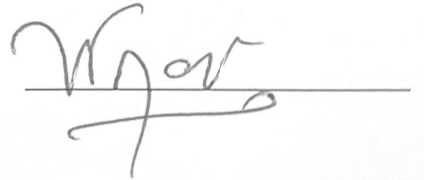
Supervisor, Department of Civil Engineering, Epoka University



Examining Committee Members:

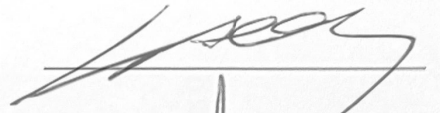
Prof. Dr. Niko Pojani

Faculty of Civil Engineering, Polytechnic University of
Tirana



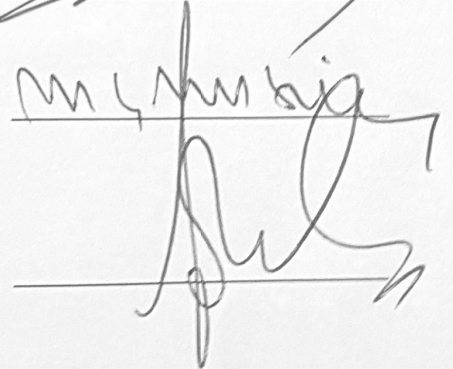
Prof. Dr. Hasan Kaplan

Civil Engineering Department, Pamukkale University



Prof. Dr. Musa Stavileci

Civil Engineering Department, "Hasan Prishtina"
University



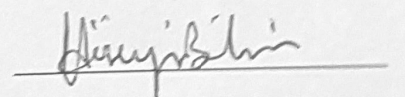
Assoc. Prof. Dr. Fisnik Kadiu

Faculty of Civil Engineering, Polytechnic University of
Tirana



Assoc.Prof. Dr. Hüseyin Bilgin

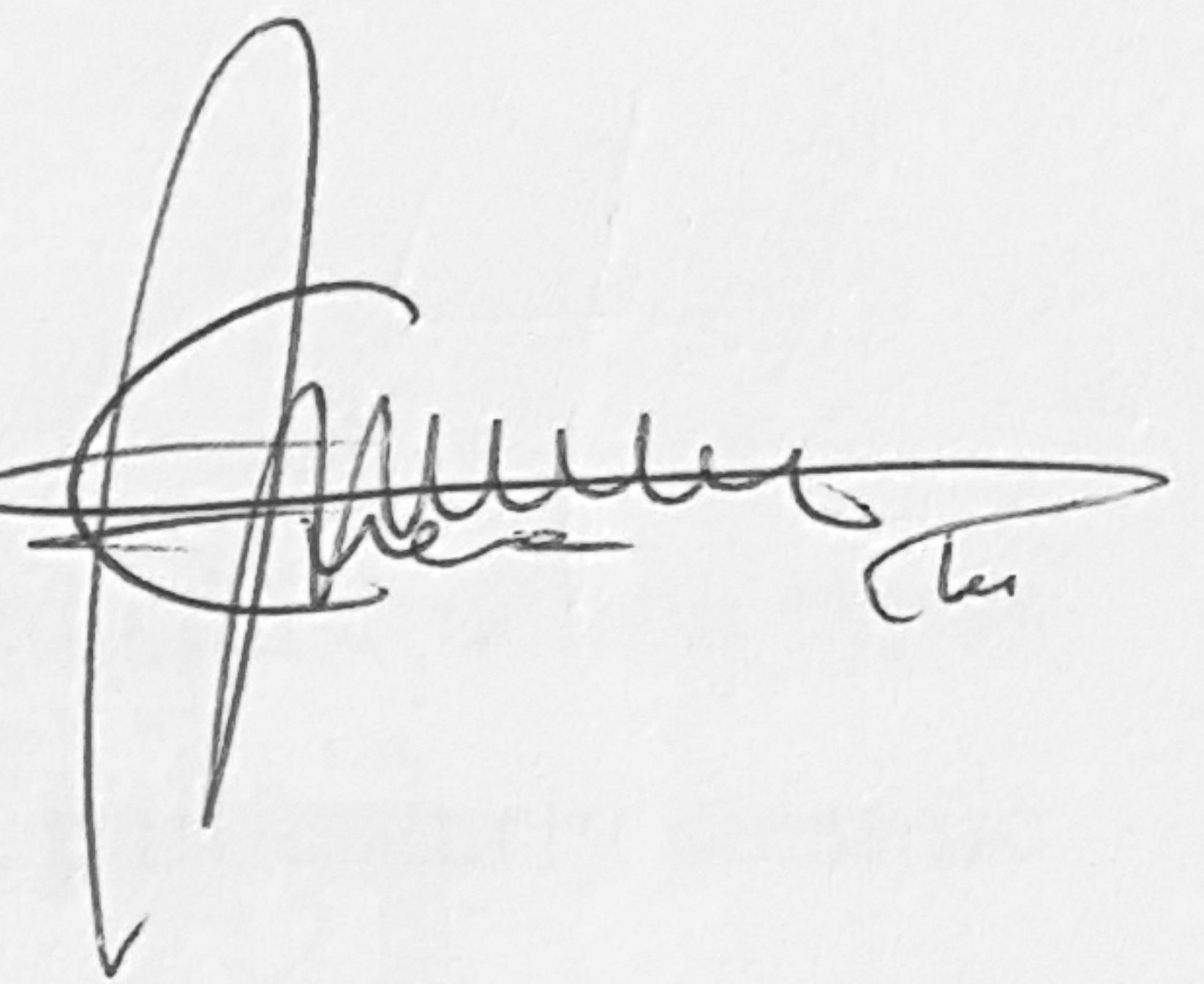
Civil Engineering Department, Epoka University



Date: 16.06.2016

I hereby declare that all information in this document has been obtained and presented in accordance with academic rules and ethical conduct. I also declare that, as required by these rules and conduct, I have fully cited and referenced all material and results that are not original to this work.

Name, Last name: **ENEA MUSTAFARAJ**

Signature: 

ABSTRACT

EXTERNAL SHEAR STRENGTHENING OF UNREINFORCED DAMAGED MASONRY WALLS

Mustafaraj, Enea

M.Sc., Department of Civil Engineering

Supervisor: Assoc.Prof. Dr. Yavuz Yardim

Unreinforced masonry (URM) buildings are one of the most used construction types in the world. Due to the limited capacity to sustain lateral loads, particularly seismic actions, all this building stock is susceptible to damages in the case of an earthquake.

In this study, it is presented the experimental campaign on investigation of structural performance of masonry walls by conducting diagonal compression tests and finite element modelling. A total of 52 diagonal compression tests were conducted in laboratory on 38 specimens of nominal dimensions of 1.2 x 1.2 x 0.25 m. The primary objective was to investigate the structural behavior of three main specimen types: unreinforced, strengthened and repaired masonry panels. Four different strengthening techniques such as ferrocement jacketing (FC), textile reinforced mortar (TRM), glass fiber reinforced polymer (G-FRP) mesh and carbon fiber reinforced polymer (C-FRP) wrap have been used and the structural performance of the panels has been evaluated and compared among each other. The panels were made of two different type of mortars; type “N” representing the modern masonry buildings and type “O” mortars for old buildings of 1950-60s and earlier.

A special attention is paid on the pre-cracked or the so-called damaged panels. After the plain panels were tested until failure, they were repaired using the strengthening methods as ferrocement jacketing, polypropylene plastering and C-FRP repair. The

results among these techniques were compared in terms of increment of improvement in shear strength, drift, as well as energy dissipation.

It was observed that ferrocement jacketing technique, after repairing of the pre-cracked panels, increased the shear strength by 179-476% and ductility 388-1193%.

Additionally, the plain and strengthened panels with ferrocement jacketing and polypropylene reinforced mortar were modelled using discrete micro-modelling of DIANA 9.6 commercial software and a non-linear analysis was conducted for each case. The modelling results showed a good match of experimental and analysis results, highlighting the ferrocement jacketing technique as the most effective one.

As a result, the strengthening techniques had a considerable improvement in shear strength and deformation capacity. The maximum improvement for both, shear strength and ultimate drift was achieved by ferrocement jacketing, 511% and 576% respectively, occurring in panels of Series 2.

At the end of campaign, it was observed that ferrocement jacketing technique apart from increase in shear strength, improved considerably the deformation capacity of the wall specimens in both cases; repaired panels as well as undamaged ones.

Keywords: unreinforced masonry, strengthening, ferrocement jacketing, textile reinforced mortar, fiber reinforced polymers, diagonal compression test, finite element modelling,

ABSTRAKT

PERFORCIMI I JASHEM I MURATURAVE TE DEMUARA NDAJ FORCAVE PRERESE

Mustafaraj, Enea

M.Sc., Department of Civil Engineering

Udhëheqës: As.Prof. Dr. Yavuz Yardım

Konstruksionet e muraturës janë një ndër tipet e ndërtimit më të përdorura në botë. Këto lloj ndrëtimesh kanë aftësi rezistuese të limituar ndaj ngarkesave lateral, në veçanti ndaj tërmeteve.

Në këtë studim paraqitet një fushatë e eksperimenteve mbi investigimin e performancës strukturore të muraturave duke kryer teste diagonalisht në shtypje dhe modelim me elementë të fundëm. Pesëdhjetë e dy (52) teste janë kryer mbi 38 panele me dimensione nominale 1.2 x 1.2 x 0.25 m.

Katër metoda të ndryshme përforcuese janë marrë në konsiderate (suvatim me ferrocement, llaç i përforcuar me fibra (TRM), suvatim me rrijetë polimeri me fibra xhami (G-FRP) dhe përforcim me copa polimeri me fibra karboni (C-FRP)) në mënyrë që të përmirësohet performanca strukturore e mureve gjatë veprimit të forcave sizmike. Muret janë ndërtuar në dy seri me dy lloje të ndryshme llaçi në mënyrë që të simulohej gjëndja e muraturave egzistuese; llaç i tipit “N” për ndërtesat moderne dhe llaç i tipit “O” për ndërtesat e vjetra të ndërtuara gjatë viteve 1950-60 dhe më herët.

Një vëmendje e veçantë i është kushtuar mureve të dëmtuar. Pasi panelet u testuan deri në thyerje të plotë, u riparuan me metodat e përforcimit të mësipërme.

Rezultatet e eksperimenteve u krahasuan në raport me rritjen e rezistencës ndaj forcave prerëse, zhvendosjen laterale dhe absorbimit të energjisë. Gjithashtu, panelet u

modeluan duke përdorur metodën e elementëve të fundëm duke kryer analiza lineare dhe jo-lineare.

Muret e papërforcuar dhe ato të përforcuar me ferrocement dhe polipropilenë, u modeluan me programin DIANA 9.6 duke përdorur metodën “discrete micro-modelling” dhe një analizë jo-lineare u krye për çdo rast. Rezultatet e modelimit treguan një përputhshmëri mjaft të kënaqshme me rezultatet e eksperimenteve duke nxjerrë në pah që teknika e përforcimit me ferrocement ishte më efektive.

Nga rezultatet u pa që teknika e suvatimit me ferrocement, pas riparimit të mureve të dëmtuar, pati një përmirësim të rezistencës në prerje prej 179-476% dhe të duktilitetit në 388-1193%.

Teknikat e përforcimit shkaktuan një rritje të konsiderueshme të rezistencës. Suvatimi me ferrocement ishte metoda që përveç rritjes së rezistencës, solli edhe një rritje të konsiderueshme të duktilitetit si në muret e padëmtuara ashtu edhe në ato të dëmtuar.

Fjalë kyçe: muratura të papërforuara, metoda përforcimi, veshje me ferrocement, llaç i përforcuar me fibra, test diagonal në shypje, modelim me elementë të fundëm

...in loving memory of my father

ACKNOWLEDGEMENTS

I would like to express my special gratitude and thanks to my supervisor Assoc. Prof. Dr. Yavuz Yardım, for his guidance, suggestions, and advices throughout the course of this study.

I am particularly grateful for Epoka University for partly funding this campaign and for the laboratory facilities provided for the experiments and colleagues of the Department of Civil Engineering for their help and support.

I am also deeply thankful to Malvino Turku whose valuable help during testing has been priceless.

Special thanks go to TNO DIANA team and Dr. Maziar Partovi in particular for the technical support during modelling.

I would also like to thank everyone who entered in the laboratory and helped me during the experimental campaign.

No words can express the deepest appreciation to my family, my mother Diana and my brother Ardit, who were always my support in the moments when there was no one to answer my queries.

Enea Mustafaraj

TABLE OF CONTENTS

ABSTRACT.....	ii
ABSTRAKT	iv
ACKNOWLEDGEMENTS	vii
TABLE OF CONTENTS.....	viii
LIST OF TABLES	xiv
LIST OF FIGURES	xvii
LIST OF ABBREVIATIONS.....	xxii
CHAPTER 1	1
INTRODUCTION	1
1.1 Problem Statement	1
1.2 Thesis Objective.....	1
1.3 Scope of work.....	2
1.4 Organization of the thesis.....	3
CHAPTER 2	4
LITERATURE REVIEW	4
2.1. Introduction	4
2.2. Material Properties	7
2.1.1 Bricks	7
2.1.2 Mortar	11

2.1.3	Masonry assemblage	13
2.2.	Non-destructive testing (NDT) techniques	26
2.3.	Scaling of masonry	28
2.4.	Previous research on masonry	29
2.5.	Performance of URM walls.....	32
2.5.1.	Typical failure modes of adobe masonry	41
2.5.2.	Typical failure modes of stone masonry	42
2.6.	Overview of URM buildings in Albania	43
2.6.1.	Seismic Risk in Albania.....	43
2.7.	Strengthening techniques used in existing URM structures.....	45
2.7.1.	Traditional Retrofitting Techniques.....	45
2.7.2.	Summary of Traditional Strengthening Techniques	47
2.7.3.	Modern Strengthening techniques	47
2.7.3.1.	TRM (Textile reinforced mortar)	48
2.7.3.2.	Fiber Reinforced Mortar (FRM)	48
2.7.3.3.	Fiber Reinforce Polymer (FRP) reinforcement	49
2.8.	Review of the Computational Modelling of Masonry Structures	53
2.8.1.	Macro-modelling (Simplified Method via Macro-elements).....	53
2.8.2.	Micro-modelling	54
2.8.3.	Structural Analysis	56
2.9.	Summary of Literature Review	57

CHAPTER 3	58
METHODOLOGY	58
3.1. Introduction	58
3.2. Determination of bricks parameters	58
3.2.1. Physical requirements	58
3.2.2. Sampling and testing procedure.....	59
3.3. Specifications of mortar properties	61
3.3.1. Determination of mortar compressive strength.....	62
3.4. Determination of masonry assemblage compressive strength	62
3.5. Determination of diagonal tensile strength (shear strength)	63
3.6. Stiffness.....	67
3.7. Ductility	67
3.8 Experimental Campaign.....	68
3.9 Construction of Plain Wall Panels (Unstrengthen specimens).....	71
3.10 Reinforcing techniques.....	73
3.10.1 Ferrocement jacketing (W-X-FC).....	73
3.10.2 Textile Reinforced Mortar (TRM) – plastering with polypropylene fibers (W-X-PP)	75
3.10.3 G-FRP jacketing reinforcement (W-X-GFRP)	76
3.10.4 C-FRP reinforcement (W-X-CFRP)	78
3.11 Repairing Strategy.....	79
3.11.1 Repair with Ferrocement jacketing (W-X-R-FC).....	80

3.11.2	Repair with Polypropylene fibers (W-X-R-PP).....	81
3.11.3	Repair with C-FRP (W-X-R-CFRP).....	82
3.12	Summary of methodology	82
CHAPTER 4		84
EXPERIMENTAL RESULTS.....		84
4.1.	Introduction	84
4.2.	Brick Properties.....	84
4.2.1.	Brick Dimensioning	85
4.2.2.	Water Absorption.....	86
4.2.3.	Compressive strength.....	87
4.2.4.	Flexural Strength.....	88
4.2.5	Summary of mechanical properties of bricks	88
4.3	Mortar Properties.....	89
4.4	Masonry Compressive Strength Results	91
4.5	Diagonal Compression Tests Results	93
4.6	Failure modes (crack pattern).....	93
4.6.1	Plain walls (W-X)	94
4.6.2	Ferrocement jacketing reinforced panels (W-X-FC).....	95
4.6.3	Polypropylene reinforced wall panels (W-X-PP)	96
4.6.4	G-FRP reinforced panels (W-X-GFRP).....	97
4.6.5	C-FRP reinforced panels (W-X-CFRP).....	98

4.6.6	Repaired walls with Ferrocement jacketing (W-X-R-FC).....	99
4.6.7	Repaired walls with polypropylene (W-X-R-PP)	99
4.6.8	C-FRP Repaired panels (W-X-R-CFRP).....	100
4.6.9	Summary of failure modes	101
4.7	Shear stress-strain response.....	101
4.7.1	Series 1	102
4.7.2	Series 2	107
4.8	Shear Strength, Stiffness, Ultimate drift and Ductility	114
4.8.1	Plain Wall Panels	114
4.8.2	Ferrocement jacketing reinforced panels (W-FC)	115
4.8.3	Polypropylene Reinforced wall panels	117
4.8.4	G-FRP reinforced wall panels (W-X-GFRP).....	118
4.8.5	C-FRP reinforced wall panels (W-X-CFRP)	118
4.8.6	Ferrocement jacketing repaired panels (W-X-R-FC)	119
4.8.7	Polypropylene repaired wall panels (W-X-R-PP).....	120
4.8.8	C-FRP repaired panels (W-X-R-CFRP)	121
4.8.9	Summary of Shear Strength, Stiffness, Ultimate drift and Ductility .	121
4.9	Summary of diagonal compression test	124
CHAPTER 5		125
FINITE ELEMENT MODELLING.....		125
5.1.	Introduction	125

5.2.	Modelling procedure	125
5.2.1.	Adopted Crack-Shear-Crush (CSC) Interface Material Model.....	127
5.2.2.	FE Model	129
5.2.3.	Assigning of material properties	129
5.2.4.	Boundary constrains and loading.....	130
5.2.5.	Modelling of strengthened walls.....	131
5.3.	Analysis results.....	131
5.4.	Experimental vs Numerical comparisons	136
5.5.	Concluding remarks.....	139
CHAPTER 6		140
CONCLUSIONS.....		140
6.1	Conclusions.....	140
6.2	Recommendations for future research	142
REFERENCES		143
CURRICULUM VITAE.....		158

LIST OF TABLES

Table 1. Examples of historic masonry constructions.	5
Table 2. Physical requirements for bricks, ASTM C 62-04 [11].	10
Table 3. Types of mortar ASTM C 270-03 [20].	12
Table 4. Review of previous diagonal compression tests.	22
Table 5. Various formulas for determining the modulus of elasticity.	25
Table 6. Different shear modulus equations from various researchers.	26
Table 7. Scaling laws for AMS [84].	29
Table 8. Earthquake occurrence during 19 th and 20 th century.	44
Table 9. Height to Thickness Correction Factors for Masonry Prism Compressive Strength [165].	63
Table 10. Wall panels of Series 1.	69
Table 11. Wall panels of Series 2.	70
Table 12. Technical specifications for ferrocement mesh.	75
Table 13. Technical specifications of polypropylene fibers.	75
Table 14. Technical specification for G-FRP mesh (SikaWrap® Hex 106G).	77
Table 15. Technical specification for C-FRP and epoxy.	78
Table 16. Summary of schematic views of strengthening techniques	83
Table 17. Dimensioning of the bricks.	85
Table 18. Determination of weight per unit area of the bricks.	86
Table 19. Determination of water absorption.	87

Table 20. Determination of compressive strength.	87
Table 21. Determination of flexural strength.....	88
Table 22. Summary of brick’s mechanical properties.	88
Table 23. Results of the compressive and flexural strength of mortars from wall panels of Series 1.	90
Table 24. Results of the compressive and flexural strength of mortars from wall panels of Series 2.	91
Table 25. Results of the compressive strength of masonry assemblage.	92
Table 26. Summary of mechanical parameters for plain wall panels of Series 1....	115
Table 27. Summary of mechanical parameters for plain wall panels of Series 2....	115
Table 28. Summary of mechanical parameters for ferrocement jacketing reinforced panels of Series 1.	116
Table 29. Summary of mechanical parameters for ferrocement jacketing reinforced panels of Series 2.	116
Table 30. Summary of mechanical parameters for polypropylene reinforced panels of Series 1.....	117
Table 31. Summary of mechanical parameters for polypropylene reinforced panels of Series 2.....	117
Table 32. Summary of mechanical parameters for G-FRP reinforced panels of Series 1.....	118
Table 33. Summary of mechanical parameters for C-FRP reinforced panels of Series 2.....	118
Table 34. Summary of mechanical parameters for ferrocement jacketing repaired panels of Series 1.	119

Table 35. Summary of mechanical parameters for ferrocement jacketing repaired panels of Series 2.	119
Table 36. Summary of mechanical parameters for polypropylene repaired panels of Series 1.	120
Table 37. Summary of mechanical parameters for polypropylene repaired panels of Series 2.	120
Table 38. Summary of mechanical parameters for C-FRP repaired panels of Series 2.	121
Table 39. Comparison of the average reinforced techniques vs. plain wall panels of Series 1.	122
Table 40. Comparison of the average reinforced techniques vs. plain wall panels of Series 2.	122
Table 41. Material properties used for the model [166]	130
Table 42. Variable parameters for each model type.	130
Table 43. Summary of Linear Analysis Results.	132
Table 44. Summary of nonlinear analysis results.	132

LIST OF FIGURES

Figure 1. Brick-making process in a factory located in Fier, Albania.	8
Figure 2. Air-drying, firing of bricks and the finished product ready for transport (Location: Fier, Albania.	8
Figure 3. The most common types of bonds: (a) American or common bond; (b) English or cross bond; (c) Flemish bond; (d) stack bond; and (e) stretcher bond (reproduced after [26]).	14
Figure 4. a) Compression of masonry prism, b) state of stresses of brick and mortar (reproduced after [32]).	15
Figure 5. Correlation between stress-strain at masonry prism [27].	16
Figure 6. Mechanism of a collapse on the masonry prism [27].	16
Figure 7. a) Saw-like failure and b) straight cracks failure [38].	19
Figure 8. Different tests for masonry specimens subjected to combined shear and axial loading: (a) couplet test, [40], (b) direct shear test [41], (c) shear test [42], (d) triplet test [43] (e) Lourenço and Ramos [44].	20
Figure 9. Typical behavior of quasi-brittle materials and definition of fracture energy: uniaxial tensile loading (a); uniaxial compressive loading (b); pure shear (c) [103].	33
Figure 11. Failure modes of in-plane loaded URM walls: (a) shear failure; (b) sliding failure; (c) rocking failure; and (d) toe crushing failure (Reproduced after [108]). ..	36
Figure 10. a) Experiment set-up, b,c,d,e) Modes of failure of solid clay masonry units under uniaxial compression, f) bi-axial strength by Page [105] [106].	37
Figure 12. Failure modes of masonry.	39

Figure 13. Common failure mechanisms for adobe structures: (i) separation of walls at corners; (ii) diagonal cracking in walls; (iii) separation of roofing from walls; (iv) vertical cracking in walls; (v) out-of-plane wall failure, (extracted from [121]).....	42
Figure 14. Failure modes of masonry prisms (reproduced after [164]).....	63
Figure 15. Loading shoes used for diagonal compression test.	64
Figure 16. Diagonal compression test set-up (example from W-25-R-PP and the schematic view of the system set-up).	65
Figure 17. Construction process of plain walls.....	71
Figure 18. Plastering process with ferrocement jacketing (FC).....	74
Figure 19. Plastering process with polypropylene fibers (PP).....	76
Figure 20. Plastering process with glass fiber reinforced polymer (G-FRP).....	77
Figure 21. Application of carbon fiber reinforced polymer (G-FRP).....	79
Figure 22. Repairing of the damaged walls with ferrocement jacketing (W-X-R-FC).	80
Figure 23. Repairing of the damaged walls with polypropylene fibers (W-X-R-PP).	81
Figure 24. Repairing of the damaged walls with C-FRP (W-X-R-CFRP)	82
Figure 25. Determining brick dimensions.	85
Figure 26. Determination of brick water absorption.....	86
Figure 27. Determination of mortar's flexural and compressive strength.	89
Figure 28. Determination of masonry assemblage compressive strength.....	92
Figure 29. Failure mode of Plain walls of Series 1.....	94
Figure 30. Failure mode of Plain walls of Series 2.....	95

Figure 31. Failure mode of Ferrocement jacketing strengthened wall panels of Series1.	95
Figure 32. Failure mode of Ferrocement jacketing strengthened wall panels of Series2.	96
Figure 33. Failure mode of polypropylene reinforced mortar strengthened wall panels of Series 1.	97
Figure 34. Failure mode of polypropylene reinforced mortar strengthened wall panels of Series 2.	97
Figure 35. Failure mode of GFRP strengthened wall panels of Series 1.....	98
Figure 36. Failure mode of C-FRP strengthened wall panels of Series 2.....	98
Figure 37. Failure mode of ferrocement jacketing repaired wall panels of Series 1.	99
Figure 38. Failure mode of ferrocement jacketing repaired wall panels of Series 2.	99
Figure 39. Failure mode of polypropylene reinforced mortar repaired wall panels of Series 1.....	100
Figure 40. Failure mode of polypropylene reinforced mortar repaired wall panels of Series 2.....	100
Figure 41. Failure mode of C-FRP repaired wall panels of Series 2.	101
Figure 42. Stress-strain response of plain wall panels of Series 1.....	102
Figure 43. Stress-strain response of polypropylene repaired panels vs. plain wall panels of Series 1.	103
Figure 44. Stress-strain response of ferrocement jacketing repaired panels vs. plain wall panels of Series 1.	104
Figure 45. Stress-strain response of ferrocement jacketing reinforced wall panels of Series 1.....	104

Figure 46. Stress-strain response of polypropylene reinforced wall panels of Series 1.	105
Figure 47. Stress-strain response of G-FRP reinforced wall panels of Series 1.	105
Figure 48. Summary of reinforced wall panels of Series 1.....	106
Figure 49. Comparison of strengthening techniques for panels of Series 1.	107
Figure 50. Stress-strain response of plain wall panels of Series 2.....	108
Figure 51. Stress-strain response of polypropylene repaired wall panels of Series 2.	108
Figure 52. Stress-strain response of ferrocement jacketing repaired wall panels of Series 2.....	109
Figure 53. Stress-strain response of C-FRP repaired reinforced wall panels of Series 2.	110
Figure 54. Stress-strain response of ferrocement jacketing reinforced wall panels of Series 2.....	111
Figure 55. Stress-strain response of polypropylene reinforced wall panels of Series 2.	111
Figure 56. Stress-strain response of C-FRP reinforced wall panels of Series 2.	112
Figure 57. Summary of reinforced wall panels of Series 2.....	112
Figure 58. Comparison of strengthening techniques for panels of Series 2.	113
Figure 59. Comparison between panels of Series 1 and Series 2.	123
Figure 60. DIANA 9.6 elements used for modelling: a) Q8MEM, plane stress element and b) CL12I, interface element.	126
Figure 61. Interface model used in this study [2].	127
Figure 62. Division of the masonry elements into elements ready for modelling. ..	128

Figure 63. The finished model in midas FX+ for DIANA.	131
Figure 64. Comparison of Nxy stresses after linear analysis.	133
Figure 65. Comparison of Principal stresses S3 after nonlinear analysis.	134
Figure 66. Comparison of stress-strain response for Series 1.	135
Figure 67. Comparison of load displacement diagrams for Series 2.	135
Figure 68. Summary of stress-strain response of experimental and numerical results for Series 1.	136
Figure 69. Comparison between experimental and numerical results of plain, ferrocement and polypropylene strengthened panels for Series 1.	137
Figure 70. Summary of stress-strain response of experimental and numerical results for Series 2.	138
Figure 71. Comparison between experimental and numerical results of plain, ferrocement and polypropylene strengthened panels for Series 2.	139

LIST OF ABBREVIATIONS

URM	Unreinforced Masonry
TRM	Textile Reinforced Mortar
G-FRP	Glass Fibre Reinforced Polymer
C-FRP	Carbon Fibre Reinforced Polymer
FC	Ferrocement
PP	Polypropylene
ASTM	American Standards for Testing and Materials
FEM	Finite Element Modelling
SW	Severe Weathering
MW	Moderate Weathering
NW	Negligible Weathering
NDT	Non-Destructive Testing
$f_{t,axial}$	uniaxial tensile strength
f_{cb}	compressive strength of brick
f'_b	brick compressive strength
f'_j	mortar compressive strength
f'_m, f_m	masonry compressive strength
f_t	masonry tensile strength
τ_m	shear strength at the shear bond failure
τ_0	shear bond strength at zero normal stress
μ	internal friction coefficient between brick and mortar
σ_n	normal stress at bed joint
E_m	Modulus of Elasticity of masonry
τ_{max}	maximum shear stress
ν	Poisson's ratio
AMS	Artificial Mass Simulation
G_{II}^f	mode II fracture energy

G_f, G_c	the amount of energy that is necessary to create a crack with a unit area
KTP	Kodet Teknike te Projektimit, (Albanian Design Codes)
AFRP	Aramid Fibre Reinforced Polymer
ρ_h	the reinforcement ratio of FRP in the horizontal direction
E_{FRP}	modulus of elasticity of FRP
ε_{tu}	the ultimate strain of FRP
S	modulus of rupture of the specimen at the plane of failure
W	maximum load indicated by the testing machine
C	compressive strength of the specimen
A	average of the gross areas of the upper
W_d	dry weight of the specimen
W_s	saturated weight of the specimen after submersion in cold water
S_s	shear stress
P	load exerted along the compression diagonal
A_n	net area of the specimen
γ	shearing strain
ΔV	vertical shortening
ΔH	horizontal extension
g	vertical gage length
G	modulus of rigidity
Δu	diagonal displacement corresponding to the ultimate strength
δ_u	shearing strain corresponding to ultimate strength
δ_y	shearing strain near yielding strength
ε_{max}	maximum strain
D	elastic stiffness matrix
D_{11}	Linear normal stiffness
D_{12}	Linear tangential stiffness
D_{11}	Linear normal stiffness
D_{12}	Linear tangential stiffness

f_t	Tensile strength
G_f	Fracture energy
c	Cohesion
$\tan\varphi$	Friction angle
$\tan\psi$	Dilatancy angle
Φ	Residual friction coefficient
σ_u	Confining normal stress for ψ_0
δ	Exponential degradation coefficient
f_c	Cap critical compressive strength
C_s	Shear traction control factor
G_{fc}	Compressive fracture energy
K_p	Equivalent plastic relative displacement
b	Fracture energy factor

CHAPTER 1

INTRODUCTION

1.1 Problem Statement

Unreinforced masonry (URM) buildings are one of the most used construction type around the world, as well as in Southern Europe and around the Mediterranean basin. Although these regions are characterized with medium-to-high levels of seismic hazard, the URM buildings are vulnerable as they have been designed (often not designed at all) to only resist gravitational loads and have been realized by rules of common practice. Many of those structures have suffered from the combined effects of inadequate construction techniques, seismic and wind loads, foundation settlements and deterioration of construction materials [1]. Because of these reasons, there is a growing need to improve the overall structural response of these buildings in order to prevent damages due to earthquakes. This improvement could be achieved by using external shear strengthening techniques.

Even though URM strengthening and retrofitting of masonry walls has been subject of many researchers, and has been under investigation for a long time, due to the special characteristics of masonry constituents, and different intervention techniques, there is a lack of knowledge in comparative studies for the performance of damaged and undamaged URM wall before and after strengthening.

1.2 Thesis Objective

The main objective of this study is to investigate the structural behavior of masonry panels. Three main specimen types have been tested: unreinforced, strengthened and repaired masonry panels. Four different strengthening techniques such as ferrocement jacketing, textile reinforced mortar (TRM), glass fiber reinforced polymer (G-FRP)

mesh and carbon fiber reinforced polymer (C-FRP) wrap have been used and the structural performance of the panels made of two different types of mortar has been evaluated.

Additionally, improvement of structural performance of the pre-cracked panels using the aforementioned methods is investigated and compared among each other.

Lastly, finite element modelling of plain and ferrocement and polypropylene reinforced wall panels is done in DIANA 9.6 in order to simulate the behavior under horizontal forces.

1.3 Scope of work

For this study, 37 panels with nominal dimensions of 1.2 x 1.2 x 0.25m made of solid clay brick were constructed using two different mortar types ASTM Type “N” (Series 1) and type “O” mortar (Series 2). These two compositions were aimed at replicating the mortars used in existing new buildings (Series 1) and existing old buildings (Series 2).

A total of 52 diagonal compression test were conducted in order observe the structural behavior of three types of panels; plain, reinforced and pre-cracked and then repaired. Four strengthening techniques are investigated and comparisons of improvement of shear strength, drift and energy dissipation are done among these methods. The same tests are simulated in a FEM modelling of plain and reinforced panels (with ferrocement and polypropylene) in order to have better insights on the relationship between masonry assemblage components; clay brick, mortar and brick/mortar interface.

1.4 Organization of the thesis

The organization of this thesis is done as follows:

In Chapter 1, the problem statement, thesis objective and scope of works is presented.

In Chapter 2, a comprehensive literature review is conducted starting with the main intrinsic properties of bricks, mortar and masonry assemblage, followed by previous research done on unreinforced masonry (URM), analysis of masonry and the typical modes of failure under each loading type. Additionally, a review of traditional strengthening techniques with their advantages and disadvantages is presented. In order to have a more effective method to improve performance of URM, new strengthening techniques are presented. Lastly, a review of modelling strategies is presented.

In Chapter 3, the methodology followed in this study is presented. It consists of destructive tests on masonry panels in order to determine the main mechanical properties of bricks, mortar and masonry assemblage. The testing procedures are the ones defined in American Standards for Testing and Materials (ASTM) where are defined all the steps to be followed.

In Chapter 4, the experimental results are presented. Structural behavior of all wall specimens is presented.

In Chapter 5, modelling approach is described and the analysis results are presented. The FEM software used in this study was DIANA 9.6.

In Chapter 6, conclusions and recommendations for further research are stated.

CHAPTER 2

LITERATURE REVIEW


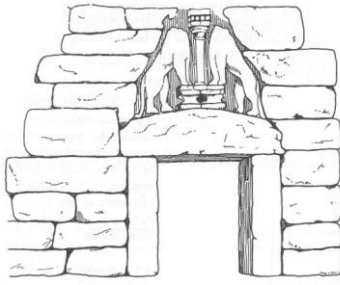






2.1. Introduction

Masonry, together with timber, is the oldest building material and one of the widely used construction method around the world. It is still used nowadays due to low material costs, good sound and heat insulation, locally availability, aesthetics and simplicity of construction. The construction technique which consists of assembling bricks, stone or block units on top of each other, laid dry or bonded with mortar, is essentially the same as thousands of years ago, making it an easy, simple, very effective and useful method of construction. The structures that have still remained today, have proven to be durable and were erected without the requirement of any special skill.

Masonry construction is closely associated with the earliest civilization about 10 000 years ago. The first masonry material to be used was stone. Some of the earliest examples of permanent dry-stone masonry houses are found in Israel and date back to 9000-8000 B.C. Nowadays, we are witness of great masonry structures which are inherited from the past such as Egyptian architecture with pyramids, 2800-2000 B.C., temples, palaces, bridges and aqueducts of Roman and Romanesque architecture 0-1200 A.D.; the 8800 km long Great Wall of China (14th century) Gothic architecture with cathedrals 1200-1600, etc. (Table 1) [2].

Archaeological excavations have uncovered evidences of sun-dried bricks which have been used thousands of years ago, used by indigenous people of North and South Americas, as well as Egypt, Middle East, etc. In arctic regions, ice blocks were used as a construction material to build igloos. In addition to utilitarian uses for creating shelter, masonry was also used to create great structures such as monuments, cathedrals, mosques and temples that have served for religious purpose, creating massive structures to emphasize the power and endurance of their beliefs [3].

Table 1. Examples of historic masonry constructions.

	
<p>Egyptian pyramids (2800-2000 B.C.)</p>	<p>Lion Gate at Mycenae (13th century B.C.) [4]</p>
	
<p>Parthenon of Athens (5th century B.C.)</p>	<p>Colosseum, Rome (1st century A.D.)</p>
	
<p>Pont Du Gard (1st century A.D.)</p>	<p>Hagia Sophia, Istanbul (6th century A.D.)</p>
	
<p>Notre Dame de Paris, (14th century A.D.)</p>	<p>Renaissance church domes, Florence Cathedral, (13 century A.D.)</p>

Brick masonry constructions date back to 8350-7350 B.C. at Jericho in Palestine, where many round and oval houses have been found. The first bricks were made of mud or clay, shaped in the desired form and dried in the sun. After sunburned, bricks

were laid on the walls using mud mortar. Some of the reasons why brick was used are: the ease of production, low weight, durability and fire resistance. The surrounding walls were made of roughly worked limestone with joints filled with earth and served as a military defense [5].

It was during 3000 B.C. that it was observed that baking of clay would produce stronger bricks. At the beginning, a fired brick took five years to natural dry under the sun, and it was molded by hand. In Egypt, sun dried bricks made of Nile mud has been the main construction material for building houses from 5000 B.C. - 50 A.D.

The widely spread of clay brick around the world was done only during Roman times. At the early ages, mortar was placed only to fill the cracks and help masonry units to lay better. During Roman Empire, it was observed that addition of volcanic ash to lime mortars had a considerable improvement on mortar strength and bonding properties.

Then, in 1858, invention of the Hoffman kiln, where all the stages of firing process could be carried out at the same time and continuously, made it possible the creation of more efficient bricks.

Nowadays, unreinforced masonry (URM) buildings are one of the most used construction type around the world, as well as in Southern Europe and around the Mediterranean basin. Although these regions are characterized with medium-to-high levels of seismic hazard, the URM buildings are vulnerable as they have been designed (often not designed at all) to only resist gravitational loads and have been realized by rules of common practice. A large number of the total population, due to lack of economic resources, lives in non-engineered, sub-standard dwellings which are extremely vulnerable to collapsing. Many of those structures have suffered from the combined effects of inadequate construction techniques, seismic and wind loads, foundation settlements and deterioration of construction materials [1]. Moderate or strong earthquakes may cause extensive damage or failure of these structures, killing many people and injuring thousands. Since demolishing is not a feasible option, strengthening and improving earthquake performance under cyclic ground shaking can be a good solution [6].

2.2. Material Properties

The overall behavior of a URM structure is closely dependent to the individual properties of masonry constituents. Thus, determination of the physical and mechanical parameters of brick units, mortar and masonry assemblage is of a vital importance for understanding the global behavior of a structure.

For example, if the masonry compressive strength is required, the brick compressive strength is used which then could be a useful parameter in determining other additional properties such as Modulus of Elasticity (E) and stress-strain behavior of masonry [7].

2.1.1 Bricks

Bricks are a principal structural component of URM buildings made of clay or silicates. The clay brick, as a building material, is made of pure clay, or clay with admixtures fired at a specific temperature (ranging between 700-1100°C) to prevent crumbling when in contact with water.

Brick production process started with the preparation stage, mining, when the topsoil layer was removed until a layer of clay or shale was reached. The digging process was done using either a hand shovel or a mechanical excavator (Figure 1 and Figure 2).

At the early stages, molding of bricks was done by hand, then wooden or metal molds were used. The next achievement in the production stage was the wire cut process which involved cutting by wires the bar of clay compressed by a pug mill or an auger machine. Then the drying process took place and the newly formed bricks were protected against rain, wind, sun and frost. Firing of bricks is performed in a kiln at a specified temperature [8].

The main factors affecting the brick physical properties are: (i) color, (ii) texture and (iii) the level of porosity. The mechanical properties are closely related to durability and compressive strength of bricks. There is no direct relationship between the brick color and mechanical properties. The classification of bricks based on their color is

valid only for the one made of the same clay material. A darker color indicates a higher firing temperature, consequently a higher compressive strength. The brick texture is a physical property which is affected by the degree of vitrification (formation of glassy layers during high temperatures, causing the clay particles to bond together) [9].



Figure 1. Brick-making process in a factory located in Fier, Albania.



Figure 2. Air-drying, firing of bricks and the finished product ready for transport (Location: Fier, Albania).

One of the main requirements for durability of brick units is the resistance to freeze-thaw cycles which is influenced by the size of pores in the brick, interaction of pore structure, and weathering [10].

The strength of the brick is closely dependent upon the purity of the clay material used, as well as the temperature at which it is fired; the higher the temperature, the higher degree of vitrification, thus clay elements are bonded more [9] [10].

Due to high porosity and brittleness, bricks are weak in tension, but very strong in compression. The compressive strength is also dependent on the level of porosity; the higher the level of porosity, the lower the strength [10]. The level of porosity decreases with increasing the firing temperature.

Bricks are classified as **solid** (when the net cross-sectional area in every plane parallel to bearing surface is 75% or more than its gross cross-sectional area), **perforated** (when the net cross-sectional area is between 25-75% of the gross cross-sectional area) and **hollow** (when the net area is less than 25% of the gross cross-sectional area of the brick).

According to the ASTM C 62-04 [11], the bricks should be manufactured from clay, shale or similar naturally occurring earthy substances, should be shaped during manufacturing process by molding, pressing or extrusion and should be subjected to firing process. When the brick is delivered to site, it should be subject to a visual inspection, and it should be provided that it is free of defects, deficiencies and other surface treatments that would impair the strength or the performance of the brick during construction process. The physical requirements are defined in (Table 2).

According to Sneek, the suction rate of the brick is the most important parameter affecting the fresh mortar and the hardened mortar and as a consequence the properties of the whole assemblage [12].

Table 2. Physical requirements for bricks, ASTM C 62-04 [11].

<i>Designation</i>	<i>Minimum Compressive Strength gross area (MPa)</i>		<i>Maximum Water Absorption by 5-h Boiling, (%)</i>		<i>Maximum Saturation Coefficient*</i>	
	Avg. of 5 Brick	Individual	Avg. of 5 Brick	Individual	Avg. of 5 Brick	Individual
Grade SW	20.7	17.2	17.0	20.0	0.78	0.80
Grade MW	17.2	15.2	22.0	25.0	0.88	0.90
Grade NW	10.3	8.6	no limit	no limit	no limit	no limit

*The saturation coefficient is the ratio of absorption by 24-h submersion in cold water to that after 5-h submersion in boiling water.

-Grade SW (Severe Weathering): Brick intended for use where high and uniform resistance to damage caused by cyclic freezing is desired and where the brick may be frozen when saturated with water.

-Grade MW (Moderate Weathering): Brick intended for use where moderate resistance to cyclic freezing damage is permissible or where the brick may be damp but not saturated with water when freezing occurs.

-Grade NW (Negligible Weathering): Brick with little resistance to cyclic freezing damage but which are acceptable for applications protected from water absorption and freezing.

The best way in determining the characteristic properties of bricks is to conduct direct tests, which consist of pushing the brick up to failure. However, in the case of vintage URM buildings sample extraction may not be an easy task to do. In order to predict in-situ material properties, NDT (non-destructive testing) may be used, when the following test could be performed: i) ultrasonic pulse velocity test; ii) Schmidt hammer test; iii) porosity test; iv) scratch test.

An important parameter to be determined is the tensile strength; the capacity of material to resist maximum tension. There are several tensile strengths calculations depending upon the applied load:

1. Flexural tensile strength (modulus of rupture) measured when masonry units are subjected to an axial load applied at the center between two end supports of the unit [13];
2. Splitting tensile strength measured when applying a line-load at both surfaces parallel to the length of the unit [14];
3. Direct tensile strength (axial tensile strength) measured on a cylindrical specimen where height/diameter ratio is 1.

According to Hilsdorf, 1967, in the absence of tests, the tensile strength may be calculated using the empirical formulas [15]:

$$f_{t,axial} = 0.26 \cdot f_{cb,cyl}^{0.67} \quad (\text{Equation 1})$$

$$f_{t,axial} = 0.72 \cdot f_{cb,splitting} \quad (\text{Equation 2})$$

$$f_{t,axial} = 0.50 \cdot f_{cb,flexural} \quad (\text{Equation 3})$$

where $f_{t,axial}$ is the uniaxial tensile strength and f_{cb} is the compressive strength of brick.

Sahlin 1971 suggested that the ratio of tensile strength to compressive strength is 1:20 for solid and 1:30 for hollow bricks. Modulus of rupture varies between 10-30% of the compressive strength, whereas the tensile strength is between 30-40% of modulus of rupture [16].

As all the wall panels used during this study were built in the laboratory, determining the mechanical properties of the material was carried out using destructive testing.

2.1.2 Mortar

Mortar is a construction material composed of a proportional mixture of water, sand and lime or cement which are used as binders. The characteristic properties of mortars are usually associated with the properties of the binder [17] [18] [19].

The mortars used nowadays are cement based and have a cement: lime: sand (c:l:s) volume ratio of 1:1:6. They are relatively stiff and have higher strengths than the lime-based mortars, with c:l:s of 1:2:9, which are characterised by very low strength but high ductility. The main types of mortar are:

1. **Lime mortar:** sand, water and quicklime (hydraulic or non-hydraulic) have low mechanical strength, high deformation capacity, high workability and self-repair ability.

2. **Cement mortar**: dry mix of Portland cement, sand and water sets quickly and has high mechanical strength and low porosity.
3. **Cement-lime mortar**: proportional mixture of lime, Portland cement, sand and water, is workable, creates good bonding, and has high deformation capacity and compressive strength as well as crack healing ability.
4. **Lime-pozzolan mortar**: a lime mortar containing pozzolanic materials, has higher mechanical strength, high porosity and low compressive strength when compared to cement mortars.

According to ASTM C 270-03 [20], classification of mortar is done according to the Table 3 below:

Table 3. Types of mortar ASTM C 270-03 [20].

<i>Mortar Type</i>	<i>Proportion by Volume</i>			<i>Binder: Aggregate ratio</i>	<i>28 Days Compressive strength</i>
	Cement	Lime	Sand		
M	4	2	15	1:3	17.2
S	2	2	9	1:3	12.4
N	1	2	6	1:3	5.2
O	1	2	9	1:3	2.4
K	1	3	12	1:3	0.5

The mortar conditions are highly affected by the following factors: i) freeze-thaw cycles, ii) water leaking, iii) salt crystallization, iv) chemical interaction, v) bio-deterioration, etc. The most important characteristics of mortar are: workability, plasticity, water retention capacity, compressive strength and bond strength developed between bricks and mortar.

Pure lime mortars' compressive strength ranges from 1.0 MPa to 2.0 MPa; for hydraulic mortar the strength increases up to 5 MPa, whereas for cement-mortar the compressive strength can reach up to 17 MPa.

The mortar's compressive strength depends on the quality of the bonding agent, as well as sand to cement or lime ratio. It is the ability of the mortar used to bond with

the bricks that governs the overall URM ability to resist the in-plane shear cracking during a seismic event.

2.1.3 Masonry assemblage

Nowadays, there are various types of masonry units produced by different raw materials such as clay, calcium silicate, stone and concrete in different production methods. Masonry assemblage is a composition two materials such as bricks and mortar which have quite different properties: stiffer bricks and softer mortar. It is considered to be a typically inelastic, highly inhomogeneous and anisotropic material. Masonry, due to mortar joints, can experience a significant loss of mortar due to combined chemical, physical and mechanical degradation.

Masonry is considered to be a quasi-brittle material with an unordered internal structure that contains a “large number of randomly oriented zones of potential failure in the form of grain boundaries” [21]. Quasi-brittle refers to the gradual decrease of resistive force after reaching the peak load when the micro-cracks are enlarging and become macro-cracks.

Several researchers have studied the masonry compression stress-strain characteristics and the relationships between masonry compressive strength and the constituent materials’ properties [7] [22] [23] [24]. All the tests were mainly focused on a laboratory based environment.

Brick/mortar bond development is an important factor that plays an important role in mechanical properties of masonry. Hendry and Khalaf, 2001, suggested that it is mainly influenced by: aggregate properties; water content and water retentivity of mortar; the surface roughness, pore structure and initial rate of absorption of bricks; quality of construction [25].

When water retentivity of mortar is high, the mortar would remain plastic and would retain sufficient amount of water for proper curing and brick/mortar bond would be developed properly.

The different arrangement of brick units forms the so-called "bond" which has aesthetics as well as structural functions. The most common types of bonds used worldwide are: (a) American or common bond; (b) English or cross bond; (c) Flemish bond; (d) stack bond; and (e) stretcher bond (Figure 3).

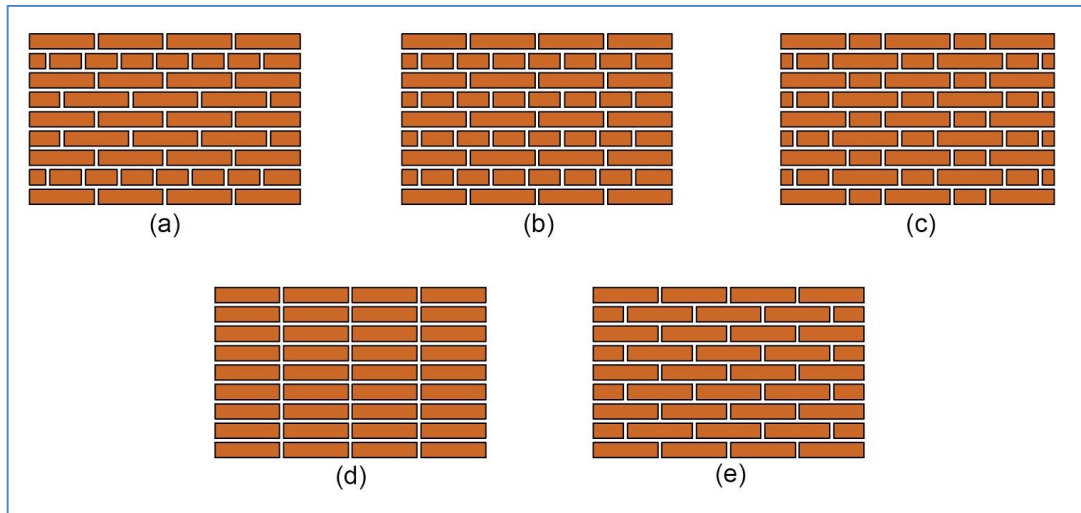


Figure 3. The most common types of bonds: (a) American or common bond; (b) English or cross bond; (c) Flemish bond; (d) stack bond; and (e) stretcher bond (reproduced after [26]).

English bond is one of the most popular types of arrangements of bricks as it is suitable for any wall thickness and is considered to be the strongest type of bond.

The material properties of masonry depend upon the following factors:

- i) age of masonry structure; ii) the quality of construction method; iii) presence of old cracks that have been sealed; iv) filling of the head joints; v) bricks (characteristic properties); vi) joints (mortar properties and dimensions); vii) properties of brick-mortar interface; viii) type of masonry bonds, etc. [8].

2.1.3.1 Masonry compressive strength

Masonry compressive strength defines the ability of the prism to resist compressive forces and varies to about 20-50% of the brick's compressive strength. Such a low value is as a result of low mortar strength; the higher mortar strength, the higher the

prism's strength [27] [28]. The compressive strength of masonry is affected by workmanship, properties of the masonry units, thickness of the mortar joints, age of mortar and the suction rate of bricks [16]. It is also influenced by mortar and brick thickness; the thicker the bricks in comparison to mortar, the higher the strength of masonry. The optimum joint thickness is suggested to be between 5-10 mm. Any value above would reduce the overall masonry strength in compression [22].

The failure of masonry in compression is caused due to the interaction between brick units and the mortar joints which have different deformation characteristics [29]. The compressive forces cause the prism (bricks and mortar joints together) to expand laterally. Generally, as the bricks are much stiffer than mortar, they do not expand laterally but constrain the mortar to be subjected under tri-axial compression. In order to maintain equilibrium, the confined mortar joints pull the brick units laterally, causing them to be under bi-lateral tension force in addition to the uniaxial compression. In this case, vertical splitting failure of bricks is observed [4] [30] [31].

According to Hilsdorf, [32], one of the main causes of failure of masonry, is the difference in the elastic properties of brick and mortar. Uniaxial compression perpendicular to bed joints leads to a triaxial compression of the mortar and compression-biaxial tension in the brick (Figure 4 a, b).

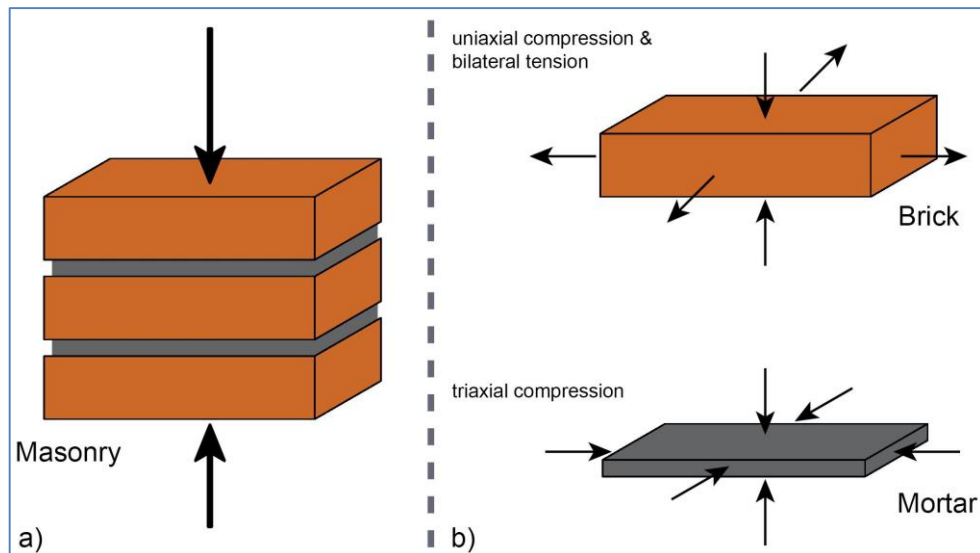


Figure 4. a) Compression of masonry prism, b) state of stresses of brick and mortar (reproduced after [32]).

The failure of the prism occurs due to the vertical splitting of brick rather than disintegration of mortar.

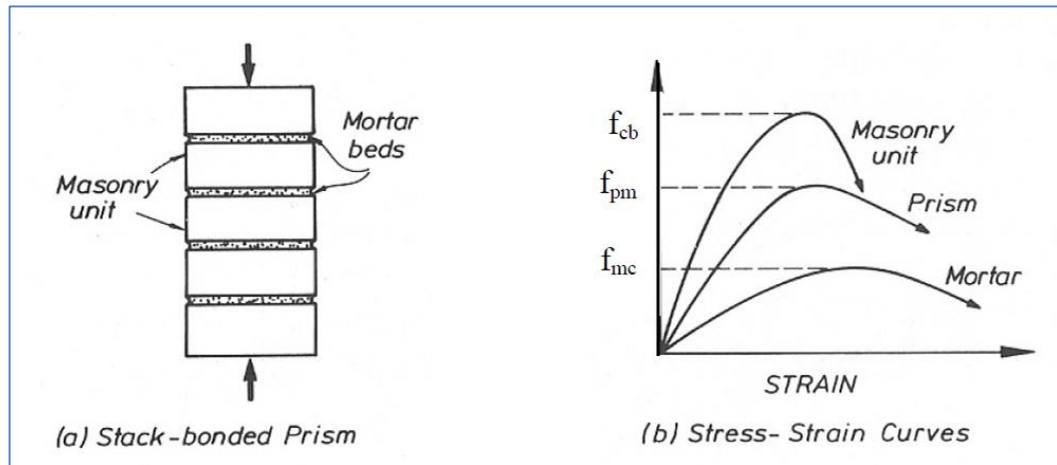


Figure 5. Correlation between stress-strain at masonry prism [27].

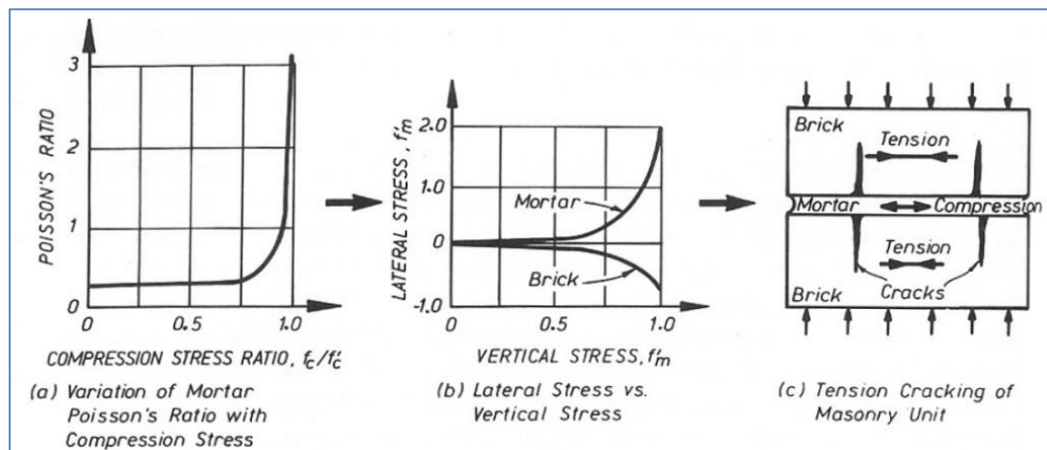


Figure 6. Mechanism of a collapse on the masonry prism [27].

The relationship between brick unit, mortar and masonry compressive strength is given by the following equation according to Eurocode 6 [33]:

$$f'_m = k \cdot f'_b{}^\alpha \cdot f'_j{}^b \quad \text{(Equation 4)}$$

where \mathbf{k} , α and β are constants and f'_b , f'_j and f'_m are brick, mortar and masonry compressive strength. The values of $\alpha = 0.7$ and $\beta = 0.3$, whereas α and β has a range of values.

From the equation, it is seen that the masonry compressive strength is influenced more by f'_b , the brick's compressive strength.

The Masonry Standards Joint Committee [34] proposed a new equation for determining the masonry compressive strength.

$$f'_m = \frac{A \cdot (400 + B \cdot f'_b)}{145} \quad (\text{Equation 5})$$

where $A=1.00$ and B is dependent upon mortar type; 0.2 for type "N" and 0.25 for type "S" and "M".

Lumantarna [8], using existing and laboratory constructed masonry prisms proposed the following formula for determining the compressive strength:

$$f'_m = 0.75 f_b^{0.75} \cdot f_j^{0.31} \quad (\text{Equation 6})$$

2.1.3.2 Masonry flexural tensile strength

Masonry flexural tensile strength is mainly governed by the bond between the brick units and the mortar type. As in the compressive strength, the tensile strength of masonry is lower than the individual tensile strength of its constituents. Generally, it is difficult to achieve a relationship between masonry tensile strength to its compressive strength due to different shapes, material and manufacture processes.

The tensile behavior is recognized in two main steps:

- Pre-peak stage: characterized by an elasto-plastic process when micro-crack development occurs at a regular trend, finalized with the reach of the peak strength, f_t .

- Post-peak stage: characterized by softening behavior around the fracture zone; conversion of micro-cracks to macro-cracks and instability of the cracking process.

The tensile strength of masonry can be estimated equal to the tensile bond strength between the joint and unit when bricks are much stiffer than mortar, and equal to the tensile strength of brick unit when the bricks are softer and high-strength mortar is used

The bond strength is affected by the connection between brick and mortar, water retentivity of mortar and the suction rate of bricks. In order to obtain a flexural failure of the prism, two methods may be adopted:

- (i) Flexural test with transverse loading; where masonry is tested as horizontal beam with a load applied vertically;
- (ii) Flexure test with eccentric loading; where the prism is tested vertically and the load would produce equal and opposite moment couple at each end.

Hendry et al., 1997, from their research, observed that the tensile strength of masonry varies between 0.2-0.8 MPa [35]. Tomazevič [36], proposed a correlation between tensile and compressive strength of masonry as follows:

$$0.03f_m \leq f_t \leq 0.09f_m \quad \text{(Equation 7)}$$

where f_m is masonry compressive strength and f_t is masonry tensile strength. Schubert 1988, suggested that the tensile strength of masonry is 0.03-0.1 times the compressive strength [37].

Backes, [38], conducted several experiments to investigate the tensile behavior of masonry in the direction parallel to the bed joints. During his experiments, it was observed that the failure modes resulted in: (a) a saw toothed crack pattern; (b) a straight crack that goes through the joints and the bricks.

The crack pattern depends on how much larger the tensile strength of the bricks is than the tensile strength of the mortar or the brick-mortar interface. Generally, the bricks are much stronger than mortar and crack pattern (a) is formed. On the other hand, when the bricks are relatively weak, the crack pattern (b) is formed.

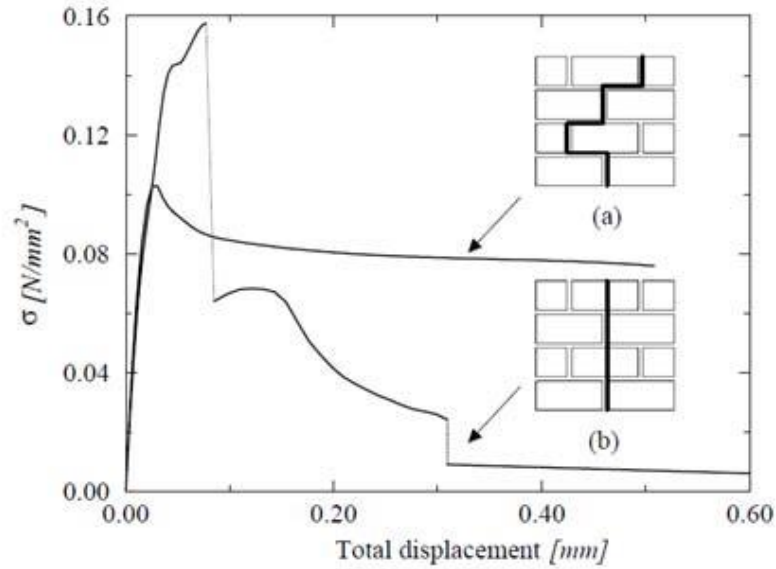


Figure 7. a) Saw-like failure and b) straight cracks failure [38].

2.1.3.3 Masonry shear strength

The shear strength under zero normal stress is one of the parameters required for prediction of numerical model for masonry; its exact definition plays a crucial role in the prediction of masonry behavior under seismic actions.

Crisafulli et al., [39] and Hendry et al. [35] suggest that the basic form of the shear strength of unreinforced masonry is based on the Mohr Coulomb shear friction expression:

$$\tau_m = \tau_0 + \mu\sigma_n \quad (\text{Equation 8})$$

where τ_m : shear strength at the shear bond failure; τ_0 : shear bond strength at zero normal stress due to adhesion strength of mortar; μ : internal friction coefficient between brick and mortar; σ_n : normal stress at bed joint.

In Figure 8 there are depicted several tests done in specimens subjected to combined shear axial loading.

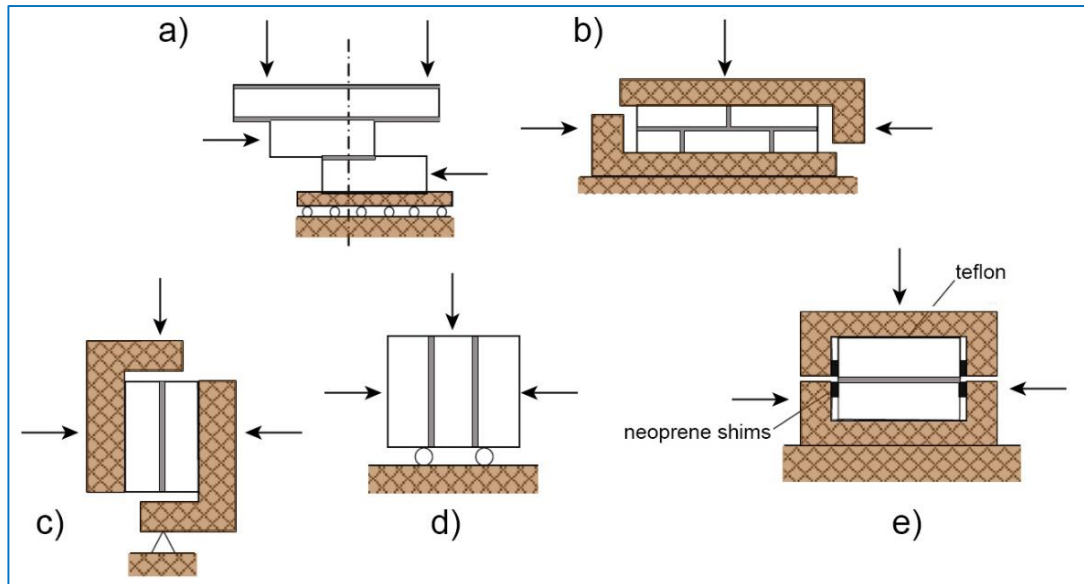


Figure 8. Different tests for masonry specimens subjected to combined shear and axial loading: (a) couplet test, [40], (b) direct shear test [41], (c) shear test [42], (d) triplet test [43] (e) Lourenço and Ramos [44].

However, the most common tests that are used to determine masonry shear strength are as follow:

- (i) **Couplet or Triplet Test:** used in order to quantify the shear strength parameters of horizontal bend joints. The triplet test, defined by EN 1052-3 [43], covers the determination of shear strength by testing at least six specimens constituted by brick unit and mortar joints. The test can be performed with or without lateral pre-compression.
- (ii) **Shear-compression test:** firstly, performed by Turnsek and Sheppard, in Slovenia [45]. The shear strength is evaluated as the average shear

stress of the wall panel subjected to in-plane loading by a horizontal force placed at mid-span of a masonry wall panel, with bed joints in horizontal direction, supported at the lower and upper sides. It is mainly performed on new masonry.

- (iii) **Diagonal compression test:** designed in order to evaluate the shear strength and the shear elastic modulus of masonry. Eurocode 8 [46] also suggests that the shear parameters of existing masonry walls to be calculated using diagonal compression test. This test is applicable to new masonry, too.

(a) The test according to ASTM E-519-02 [47] simulates a pure shear state of stress, positioning the Mohr circle of stress state at the origin of the σ - τ axes. The shear stress of masonry, S_s , is equal to the principal tensile stress, σ_1 :

$$S_s = \sigma_1 = \frac{0.707 \cdot P}{A_n} \quad (\text{Equation 9})$$

Additionally, the shear modulus, G , can be determined from:

$$\gamma = \frac{\Delta V + \Delta H}{g} \quad (\text{Equation 10})$$

The failure of the specimen usually occurs with the panel splitting apart parallel to the direction of the load. Development of cracks initially starts at the center and continues mainly along the mortar joints and, in some cases, through the bricks.

(b) RILEM LUM B6 [48] considers modeling of the masonry panel as it is an isotropic homogeneous material and running a linear analysis; but the stress state at the center of the specimen is not in a pure shear state:

$$\sigma_x = \sigma_y = -0.56 \cdot \frac{P}{A_n} \quad (\text{Equation 11})$$

$$\sigma_{xy} = 1.05 \cdot \frac{P}{A_n} \quad (\text{Equation 12})$$

The tensile strength is evaluated by:

$$f_t = 0.5 \cdot \frac{P}{A_n} \quad (\text{Equation 13})$$

Using the Turnašek and Cacovic, 1970 formulation, the shear strength τ_{OD} : [49]

$$\tau_{OD} = \frac{f_t}{1.5} = \frac{P}{3A_n} \quad (\text{Equation 14})$$

As it can be seen from the different methods above, determination of masonry shear strength is not a straightforward operation. The seismic behavior of URM walls can be experimentally simulated by two kinds of tests: shear-compression test and diagonal compression test [50].

The diagonal compression test is largely used by many researchers (Table 4). When comparing to shear-compression, Corradi et al. 2002, observed that the shear strength of the unreinforced structures struck by Umbria-Marche earthquake in 1997, the diagonal compression test gave more conservative results [51].

Table 4. Review of previous diagonal compression tests.

	<i>Author</i>	<i>Specimen types</i>	<i>Experiment type</i>	<i>Reinforcement Technique used</i>
1	Faella et al., [1]	9 yellow tuff masonry (120 x 120 x 40 cm)	Lab	Fiber Reinforced Cement Mortar
2	Corradi et al., 2003 [51]	5 roughly cut stone masonry (120 x 120 x 70 cm) 2 solid brick masonry	In-situ	-
3	Corradi et al., 2014 [52]	14 double leaf hewn stone (120 x 120 x 40 cm) 8 uncut rounded (pebble) stone masonry (120 x 120 x 40 cm)	In-situ	GFRP grid
4	Milosevic et al., 2013 [53]	4 roughly cut limestone masonry (120 x 120 x 70 cm)	Lab	-
5	Borri et al., 2011 [54]	12 triple leaf roughly cut stone masonry (120 x 120 x 45-62 cm)	In-situ	

				FRP jacketing
		8 double leaf roughly cut stone masonry (120 x 120 x 52-67 cm)		Retricolatus Deep repointing FRP jacketing
6	Alecci et al., 2013 [55]	3 solid brick masonry (120 x 120 x 12 cm) 15 solid brick masonry (40 x 40 x 5 cm)	Lab	-
7	Dizhur and Ingham, 2013 [56]	12 solid brick masonry (120 x 120 x 11-33 cm)	In-situ	-
8	Ismail et al., 2011 [57]	10 solid brick masonry (120 x 120 x 11 cm) 7 solid brick masonry (120 x 120 x 22 cm)	Lab	Twisted Stainless Steel Near Surface Mounted (TSNSM)
9	Kalali and Kabir, 2012 [58]	7 solid brick masonry (56 x 56 x 10.5 cm)	Lab	GFRP
10	Lin et al., 2014 [59]	4 solid brick masonry (120 x 120 x 10 cm) 11 solid brick masonry (120 x 120 x 22 cm) 4 solid brick masonry (120 x 120 x 35 cm) 4 solid brick masonry (120 x 120 x 47 cm)	Lab	Engineered Cementitious Composite (ECC)
11	Gattesco and Dudine, 2010 [60]	20 solid brick masonry (116 x 116 x 25 cm) 18 solid brick masonry (116 x 116 x 38 cm) 12 two-leaf solid brick masonry with rubble mound structure 12 rubble stone masonry (116 x 116 x 40 cm)	Lab	GFRP
12	Najafgholipour et al., 2013 [61]	27 single-leaf solid brick masonry (60 x 60 x 10 cm)	Lab	-
13	Yardim and Lalaj, 2016 [62]	2 solid brick masonry (120 x 120 x 25 cm) 10 solid brick masonry (65 x 65 x 25 cm)	Lab	Polypropylene and Ferrocement jacketing, GFRP
14	Gattesco and Boem, 2015 [63]	6 solid brick masonry (116 x 116 x 25cm) 8 cobble stone masonry (116 x 116 x 40 cm) 7 rubble stone masonry (116 x 116 x 40 cm) 6 rubble stone masonry (116 x 116 x 70)		-
15		16 solid brick masonry (117 x 117 x 22.5 cm)	Lab	

				GFRP
	Mahmood and Ingham, 2011 [64]	6 solid brick masonry (117 x 107.5 x 22.5 cm)		CFRP
				TSNSM
16	Corradi et al., 2008 [65]	2 roughly cut stone masonry (120 x 120 x 48 cm) 2 irregular stone masonry (120 x 120 x 67 cm)	In-situ	Deep repointing
17	Prota et al., 2006 [66]	12 tuff masonry (50 x 50 x 25 cm)	Lab	Cement based matrix-coated glass grid (CMG)
				GFRP
18	Valluzzi et al., 2002 [67]	33 solid clay brick masonry (51.5 x 51 x 12 cm)	Lab	CFRP
				PVAFRP (polyvinyl alcohol)
19	Borri et al., 2015 [68]	16 large stone masonry (120 x 120 x 48-180 cm) 15 large stone masonry	In-situ Lab	-

2.1.3.4 Elastic Modulus of masonry

One of the difficulties when calculating stiffness of masonry is the nonlinear behavior of it. Obtaining the Modulus of Elasticity from just the linear part of the stress-strain diagram is virtually impossible due to micro-cracks development at relatively low loads.

The Modulus of Elasticity of masonry (E_m) is calculated as the modulus of the chord of the linear part of the masonry compression stress-strain curve, typically defined to be between 5% and 33% of the ultimate masonry compressive strength (f_m^c) [20].

$$E_m = k \cdot f_m' \quad (\text{Equation 15})$$

$$E_m = k \cdot f_b^a \cdot f_m^c \quad (\text{Equation 16})$$

$$E_m = \frac{0.70f_m - 0.05f_m}{\varepsilon_{0.70f_m} - \varepsilon_{0.05f_m}} \quad (\text{Equation 17})$$

However, various design standards are using different formulas in order to calculate the modulus of elasticity (Table 5). For example:

Table 5. Various formulas for determining the modulus of elasticity.

<i>Author/Standard</i>	<i>Proposed equation</i>
Eurocode 6 [33]	$E_m = 1000 \cdot f'_m$
FEMA 273 [69]	$E_m = 550 \cdot f'_m$
NHERP [70]; Paulay and Prestley [27]	$E_m = 750 \cdot f'_m$
CSA [71]	$E_m = 850 \cdot f'_m$
Tomazević, [36]	$200f_{cb} \leq E_m \leq 2000f_{cb}$
MSJC [34]	$E_m = 700 \cdot f'_m$
Sahlin, [16]; Crisafulli et al. [39]	$E_m = 300 \cdot f'_m$
Drysdale et al., [28]	$E_m = 500 - 600 \cdot f'_m$
Lumantarna, [8]	$E_m = 294 \cdot f'_m$
ASCE, [72]	$E_m = 350 \cdot f'_m$

2.1.3.5 Shear Modulus of masonry

The shear modulus (also known as modulus of rigidity), G , is a parameter calculated by the ratio of the shear stress to shear strain, measured as the secant modulus between 5% and 70% of the maximum shear stress, τ_{max} , in the shear stress-horizontal drift, $\tau - \delta$, curve along the initial loading arm prior to τ_{max} [56] [59].

It may also be calculated by:

$$G = \frac{\tau_{1/3}}{\gamma_{1/3}} \quad (\text{Equation 18})$$

where $\tau_{1/3}$ is the shear stress for a load of 1/3 of the maximum load P_{max} and $\gamma_{1/3}$ is the corresponding shear strain [53].

The shear stiffness decreases substantially after cracking due to bed joint sliding or diagonal tension crack opening. The relationship between the Modulus of Elasticity and shear strength is given as follows:

$$E = 2G(1 + \nu) \quad (\text{Equation 19})$$

where: ν is the Poisson's ratio (adopted $\nu = 0.25$, as suggested by Harris, [73] and Pande et al., [74], for unreinforced masonry).

Nevertheless, in literature there are found various estimations of shear stiffness that relate Modulus of Elasticity, E_m , or the compressive strength of brick masonry, f'_m . (Table 6).

Table 6. Different shear modulus equations from various researchers.

<i>Author</i>	<i>Proposed formula</i>
Alcocer and Klinger, [75]	$G_m = 0.1E_m$ (for masonry with high-strength brick units); $G_m = 0.2E_m$ (for masonry with low-strength brick units) where G_m and E_m are shear and elastic modulus, respectively.
Paulay and Priestley [27]; Fattal and Cattaneo [76]	$G_m = 400f'_m$ where f'_m is the compressive strength of brick masonry
FEMA 273 [69]	$G_m = 0.4E_m$

2.2. Non-destructive testing (NDT) techniques

Non-destructive testing (NDT) methods can be used in cases when it is impossible to conduct laboratory experiments for an intended structure. Due to many reasons, extraction of the samples for the investigated structure may be not possible, and the only option to get the insights of the conditions of a structure is to use NDT.

NDT techniques are based on different theoretical principles and can provide various types of information related to physical properties of a structure. They mainly rely on compressional and shear wave velocities as well as electrical resistivity, which are interpreted in terms of the fabric of the structure, defining in this way the engineering properties. They may provide different types of information if used in different fields. For example, ground penetrating radar (GPR) may be used in both geological environment and/or in masonry or concrete structures [77].

In order to have a successful NDT survey, there are five major factors to be taken into consideration:

- the required depth of penetration into the structure;
- vertical and lateral resolution for the target;
- contrast in physical properties between the surroundings and the target;
- signal to noise ratio;

- historical information related to construction methods.

The NDT techniques may be categorized in four main groups:

1. ***Sonic/ Ultrasonic Methods***: Non-invasive based on transmission and reflection of stress waves through a medium at sonic or ultrasonic frequencies.

- a. Sonic transmission method
- b. Sonic/seismic tomography
- c. Sonic/seismic reflection method
- d. Impact-echo system
- e. Ultrasonic reflection method
- f. Sonic resonance method.

Tomographic Imaging method uses sonic and ultrasonic pulse velocity information to create 3-D reconstruction based on the velocities in order to locate and investigate materials' properties, cracks, voids, deteriorated materials as well as detection of the embedded steel reinforcement [78].

2. ***Electromagnetic methods***: commonly used to determine the location of reinforcing bars embedded in concrete, basically using the changes in the electromagnetic fields in the presence of steel.

- a. Impulse radar
- b. Conductivity measurements: used to assess moisture content in masonry, salt content, height of capillary rise, thickness of masonry wall, composite construction of masonry wall, multi-wythe nature of masonry wall, presence of voids, presence of metal reinforcements etc.
- c. Convergence meter.

3. ***Electrical methods***

- a. Resistivity measurements
- b. Half-cell potential measurements
- c. Infra-red thermography: usage of scanning cameras to produce a thermal image by heat at any temperature. The defects and other structural problems

hidden within the masonry or concrete element produce a different thermal image by emitting different amounts of infra-red radiation.

4. Radiography: usage of very short wavelength electromagnetic radiation by penetrating through the medium (masonry or concrete).

- a. X-ray radiation
- b. Gamma ray systems
- c. Neutron radiography.

Nevertheless, in order to achieve satisfactory results, it is of a high importance to understand the methodology, capabilities and limitations of every NDT technique. It is not a straightforward operation as there should be a calibration of the equipment as well as several assumptions to be made.

2.3. Scaling of masonry

Testing of an entire structure of large dimensions at a full scale is virtually impossible, thus, the experimental tests are either done only on certain parts of the investigated structure, or on the model structure scaled down at a reasonable size that can be accommodated at a testing facility. As a result, determination of the required size for the test unit is of a high importance.

In literature, there can be found many studies related to the scaling of solid brick masonry. There are two different results presented: scaling of URM provided good similitudes of the reduced scale and the full scale structure [79], [80] and scaling that provided undesirable similitude regarding strength, stiffness and failure mechanisms [81] [82].

Tomazević concluded that for a model to properly represent a full-scale structure must have three main similarities:

1. Similar failure mechanism;
2. Similarities in stresses;
3. Similarities in mass and stiffness.

In order to obtain acceptable reduced-scale models for masonry structures, the Artificial Mass Simulation (AMS) scaling law is applied [83], provided that the

reduced-scale model has the same parameters (density, stiffness, strength, drift capacity, etc.) as the full scale structure.

AMS scaling law provides multiplication factors in order to relate the properties of the reduced-scale models; i.e. if the length is reduced by a factor of “ S_l ”, the area will be reduced by “ S_l^2 ”. Other factors are summarized in Table 7.

Mohammed, 2006 and Mohammed and Hughes, observed that the best representation of the compressive strength of masonry could be achieved at a 1/2-scale [84] [85]. As a matter of fact, it is the same scale used by the ASTM to determine the brick compressive strength.

Table 7. Scaling laws for AMS [83].

Variable	Scaling	Variable	Scaling
Length	S_l	Strain	1
Time	$\sqrt{S_l}$	Stress	1
Frequency	$1/\sqrt{S_l}$	Strength	1
Velocity	1	Elastic modulus	1
Gravity	1	Displacement	S_l
Acceleration	1	Force	S_l^2
Mass density	1	Moment	S_l^3

2.4. Previous research on masonry

In recent years, considerable research has been carried out in determining the structural behavior of masonry buildings subjected to seismic forces. It has led towards development of new codes for masonry construction and design such as Eurocode 6- Design of masonry structures [33].

Tomazević investigated the diagonal shear strength and compared the results with the equations suggested by Eurocode 6 [86]. Other researchers have investigated brick-mortar bond strength and the response of URM under in-plane direct shear forces [41] [87] [88] [89].

Maheri et al., suggested that the mortar head joints have a considerable influence on the in-plane shear strength [90]. Grim and Tucker derived a relationship between the out-of-plane strength of brick wall and the flexural strength of masonry prisms [91]. Rao et al. [92], Pavia and Hanley, [93], investigated the mortar type and moisture content of masonry units that influence the flexural strength of prisms.

Most of the researches conducted so far, have been considering separately the behavior of URM walls under in-plane or out-of-plane loading. Najafgholipour et al., suggested that the wall aspect ratio has a high influence on the interaction level. They noticed an interaction between in-plane shear and out-of-plane bending capacities of the brick walls. This interaction becomes stronger when one of the loading types is near the wall's ultimate capacity in any of the loading directions [94].

The feasibility of in-situ testing is limited due to the highly destructive nature, high cost and time consuming due to preparations required and test duration. In order to overcome these disadvantages, ASCE-41 suggests a simplified model that allows prediction of the diagonal tension strength to be made based on the wall's material constituents and simplified in-situ testing procedure [72].

Due to many constraints regarding in-situ testing, a good solution is replicating the wall components in laboratory based setting. In this way, a larger number of test specimen with a lower cost could be obtained in a shorter time. However, in order for the study to be relevant, the material characteristic properties must be the same.

Dizhur and Ingham, in their study, tested two existing vintage unreinforced clay brick masonry under diagonal compression loading, in order to induce diagonal failure mode for the URM wall. The main aims of their experimental program were to establish the diagonal tensile strength of URM walls and validate the accuracy of the existing ASCE-41 model, as well as establishing a benchmark mortar mix suitable for use when manufacturing replicas of clay bricks for restoration and repair purposes [56]. In this experimental program panels were obtained from two existing vintage URM (unreinforced clay brick masonry) buildings and subjected to a diagonal compression loading in order to induce diagonal tension failure. The main aim was to calculate the diagonal tension strength of the vintage clay brick URM.

Based on the observations on the behavior of the URM walls during seismic shaking, the most relevant in-plane shear failure mode of URM is the diagonal shear cracking, characterized by a diagonal cracks perpendicular to the maximum tensile stress in the wall panel [94].

When researching for similar tests on masonry, Brignola et al., reported that the diagonal tension strength of vintage rubble stone masonry which generally has a chaotic pattern, is not representative of the diagonal tension strength of solid clay masonry due to the latter's elderly bond pattern and regular use of header brick for inter-connection of the masonry leafs [95].

It was observed that, as expected, the diagonal tension strength of URM panel increases when increasing mortar compressive strength. Sathiparan et al., 2005, conducted a series of diagonal compression test as well as out-of-plane test on plain and Polypropylene (PP) retrofitted wallets. It was observed that this technique improved the strength by 2.5 times and the deformation capacity by 45 times [96].

Badoux et al., investigated the dynamic in-plane behavior of URM walls by using half-scale hollow clay masonry walls subjected to a series of simulated seismic earthquake motions before reinforcing with GFRP. The presence of GFRP prevented the development of cracks through the wall panel until masonry crushing at the bottom corners occurred resulting in a "balanced" upgraded wall reinforcement [97].

Turco et al., 2006, analyzed retrofitted walls with glass and carbon FRP and observed two types of modes of failure: debonding of FRP reinforcement and shear failure of masonry at the support, when specimens were loaded diagonally. The strength was increased up to 2.5 times in shear strengthening and 4.5-26 times in case of flexural strengthening. Even though it has a lower modulus of elasticity, GFRP performed better than CFRP [98].

Fam et al., used the combination of injection and GFRP strengthening techniques in order to repair deteriorated walls. It was observed that this combination recovered and even improved the capacity of the walls [99].

Wang et al., carried out experiments on eight brick masonry walls reinforced with GFRP, and observed that this method increased the load carrying capacity of masonry subjected to in-plane shear loading [100].

Kalali and Kabir, presented an experimental study focused on the in-plane behavior of unreinforced brick (URB) walls before and after retrofitting, using glass fiber reinforced polymers (GFRPs) aiming to investigate the efficiency of shear reinforcing technique. The test specimens were built in such a way to simulate the traditional masonry walls built in Iran [58].

Corradi et al., carried out in-situ tests on masonry panels on the structures damaged during the Umbria-Marche earthquake of 1997-1998. The main aim was to suggest a technique for seismic upgrade against in-plane mechanisms of collapse using lime based mix injection over layers of CFRP and GFRP meshes [51].

Corradi et al., carried out experimental tests on historic masonry wall panels reinforced with GFRP jacketing inserted into inorganic matrix. In-situ tests were done on panels from two different sites in Italy; 2 double leaf rubble stone masonry and one solid brick masonry. The panel shear strength was determined before and after reinforcement by means of diagonal compression test and shear-compression tests. It was observed that the panels reinforced with GFRP exhibited a significant improvement in lateral load-carrying capacity up to 1060% when compared with control panels [52].

Many researchers have studied the feasibility of usage of GFRP reinforcement techniques as a good method to improve shear resistance of URM walls [99] [100] [101] [102].

2.5. Performance of URM walls

The analysis of masonry structures is a rather complex task due to the particular nature and the mechanical behavior of masonry due to the lack of homogeneity and standardization. Understanding the mechanical behavior of URM buildings is one of the most complex and challenging issues of structural engineering.

When analyzing masonry, a prominent feature to be considered is the softening behavior, which is typical of quasi-brittle materials. Softening is a gradual decrease of mechanical resistance under a continuous increase of deformation, caused by progressive internal crack growth, generally attributed to the heterogeneity of the material, due to the presence of different phases and material defects, like flaws and voids.

Usually, the bond between brick unit and mortar is considered to be the weakest link in masonry assemblage. The nonlinear response of the mortar joints is associated with two types of failure modes: tensile failure (mode I) and shear failure (mode II).

In Figure 9, it is presented the characteristic stress-displacement diagrams for quasi-brittle materials in uniaxial tension, uniaxial compression and pure shear.

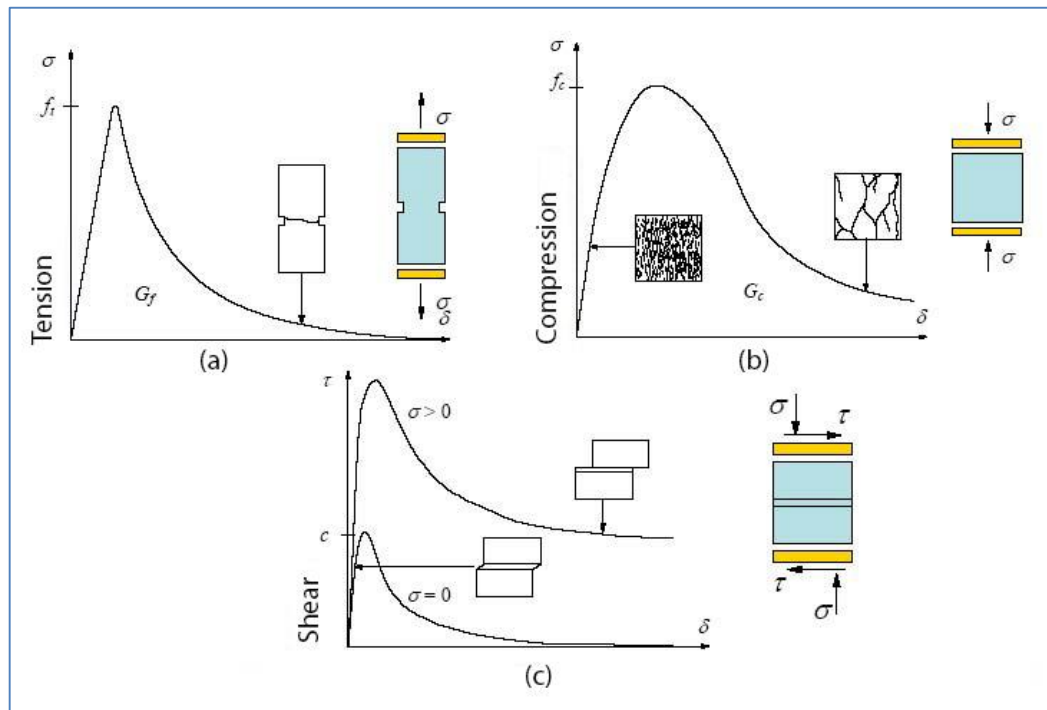


Figure 9. Typical behavior of quasi-brittle materials and definition of fracture energy: uniaxial tensile loading (a); uniaxial compressive loading (b); pure shear (c) [103].

Tensile behavior (Figure 9, a) begins linearly until the tensile strength is reached and first cracking occurs. After that point softening is observed associated with a decrease

of the stiffness of the material and a decrease of the load applied to the material specimen. The failure of material is considered when the strength and stiffness are equal to zero.

Compressive behavior Figure 9, b) also begins linearly until the yielding strength is reached and first micro-cracks appear. After that point, the hardening starts, when the stiffness of the material decreases but the load can still increase. It continues until the ultimate strength is reached and when multiple micro-cracks connect and result in bigger macro-cracks. Then, the softening stage occurs, where the size and number of cracks increases. At the final stage, regardless of the amount of cracks that have developed, a small amount of strength remains.

The shear behavior is (Figure 9, c) begins linearly until the critical shear stress is reached. Depending on the level of confining stress, shear behavior can result in slip of the unit-mortar interface. The inelastic shear behavior in shear can be described by the mode II fracture energy G_f^{II} .

The total fracture energy (the amount of energy that is necessary to create a crack with a unit area), denoted by G_f or G_c , for tension and compression, respectively, is obtained by integrating the stress-displacement (σ - δ) curve.

The fact that the mechanical response of masonry exhibits significant nonlinear, irreversible and dissipative phenomena, requires that the structural predictive model should not neglect it when considering the URM response when subjected to cyclic loading. However, the relevant phenomena such as crack nucleation and growth within the mortar layers or brick-mortar interfaces; frictional sliding at the contact point between opposite cracks' faces; rocking of cracks edges, occur at a very small scale. It is indeed, the global overall response, affected by geometrical and morphological configuration that governs the overall behavior of the structure [104].

Masonry is a material that exhibits distinct directional properties due to the mortar joints that act as a plane of weakness. The structural response of URM structures is governed by the complex interaction between brick units and the mortar joints. When subjected to earthquake ground motion, the structural system vibrates as a result of the

generated inertia forces that are proportional to the mass of the building and induced accelerations. Vibration causes the development of additional bending and shear stresses that often exceed the resistive capacity of materials and cause the failure of the structural elements, leading to collapse as masonry does not have good bending and shear resistive capacities.

Old buildings of all types represent an important part of the building stock that are highly vulnerable to earthquakes. The necessity of conducting more research and experiments is strengthened by the fact that masonry has orthotropic behavior, and it is built up of two different materials each of which has a wide range of property values.

Page [105] [106] observed that the strength and the failure mode change when different inclinations of bed joints are considered due to the anisotropic nature of masonry. The experimental set-up consisted of parts of URM walls 300x300 mm to be loaded in bi-axial compression, bi-axial tension-compression, uni-axial compression and uni-axial tension until the failure of masonry (Figure 11).

For tensile loading perpendicular to bed joints, the failure is caused by the debonding between bed joint and the brick unit. It can be estimated that the masonry tensile strength is equal to the bond strength between brick and mortar.

For tensile loading parallel to bed joints, according to Backes, 1985, the failure is affected by both, bricks and mortar strengths. In bi-axial compression, the failure occurs due to the splitting of the specimen at mid-thickness in the plane parallel to its free surface.

Exceptional events such as earthquakes, are one of the major cause of damage of URM buildings, often even for their collapse. During an earthquake, the walls are subjected to a combination of lateral seismic forces, induced by the earthquake, that are in the form of out-of-plane or in-plane loading depending on the orientation of the building with respect to the earthquake epicenter. They manifest a brittle behavior and are very weak when subjected to such types of loads. Both in-plane and out-of-plane earthquake loading can cause significant damage to URM; it is the wall characteristics in the in-plane direction of the wall that govern the structural integrity of the complete building.

The overall seismic performance of URM buildings depends on the capacity of in-plane walls to safely transfer the lateral loads to foundations. In this way, the masonry walls provide the post-earthquake stability necessary to avoid collapse of the entire structure.

Among those two, the out-of-plane failure is considered to be more critical but it is impeded (inhibited) through adequate wall-diaphragm connections and other supplementary structural elements. Of the most important failure modes, diagonal cracking failure mode is regarded to be the most dangerous that can seriously affect the vertical load capacity of a URM wall [107].

As a result, it is the response of in-plane loaded wall that governs the global seismic performance of a URM building. The principal in-plane failure mechanisms of URM walls subjected to earthquake actions can be summarized as shown in Figure 10 [108].

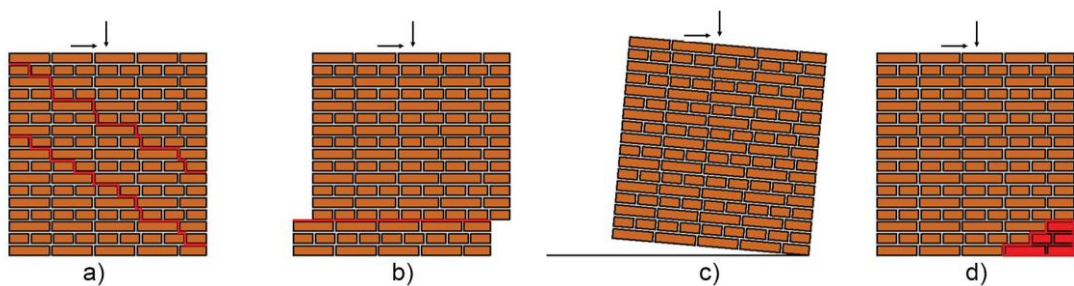


Figure 10. Failure modes of in-plane loaded URM walls: (a) shear failure; (b) sliding failure; (c) rocking failure; and (d) toe crushing failure (Reproduced after [108]).

Failure of URM structures can be categorized as either flexural or shear controlled. The flexural failure mode is identified by rocking directly related with masonry crushing, whereas the shear failure mode is identified by two main mechanisms: horizontal bed joint sliding and diagonal shear (tension) cracking [108].

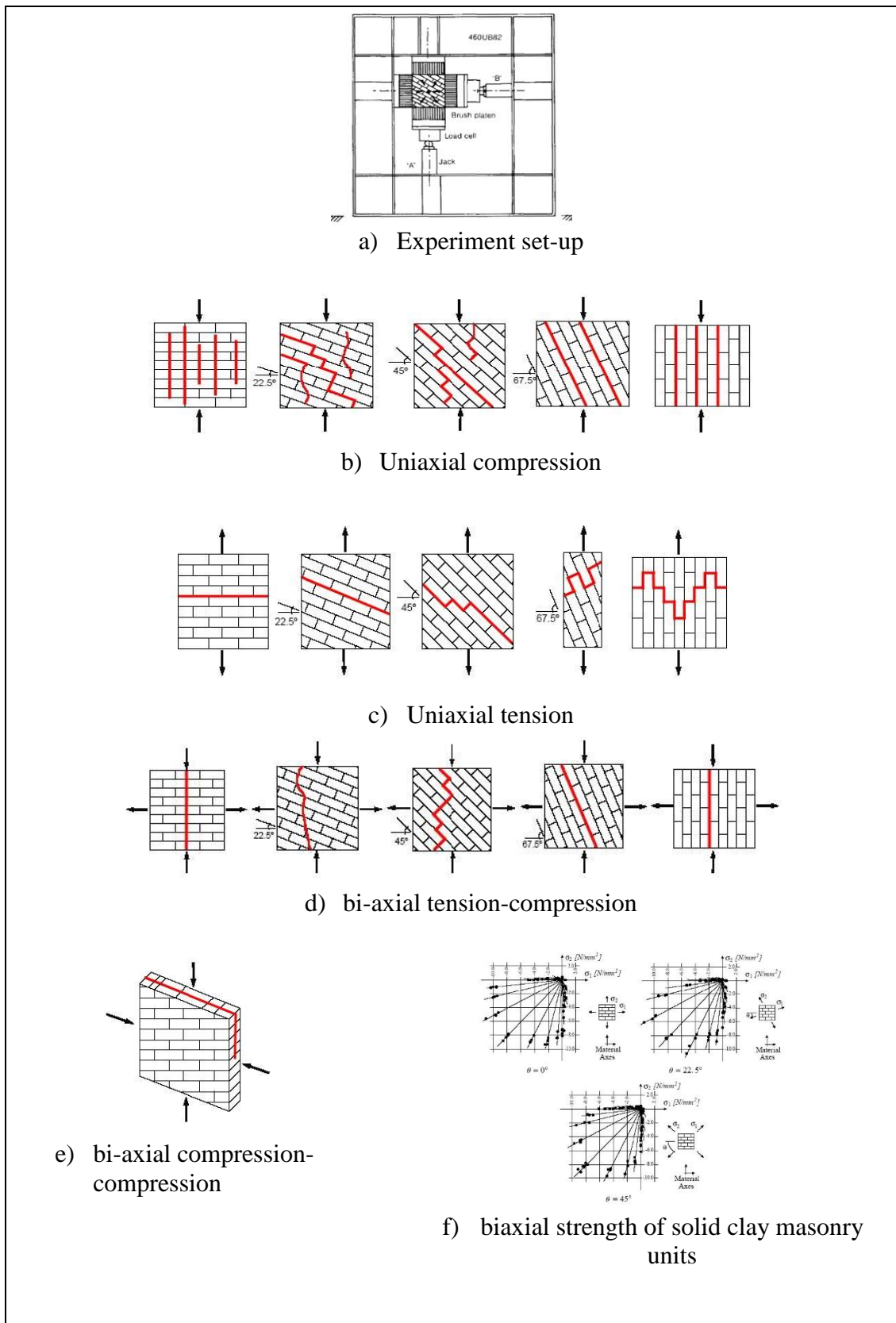


Figure 11. a) Experiment set-up, b, c, d, e) Modes of failure of solid clay masonry units under uniaxial compression, f) bi-axial strength by Page [105] [106].

Shear failure: occurs when the generated tension stresses due to the combination of vertical and lateral loads, exceed the tensile strength of the masonry. Generally, since bricks are much stiffer than mortar, the cracks follow a diagonal pattern along the vertical and horizontal mortar joints.

Sliding failure: occurs due to poor mortar quality, when cracks are initially formed in horizontal joints generating sliding planes that are extended along the complete length of the wall, causing displacement of the upper part of the wall from the bottom part.

Flexural failure: occurs due to the crushing of the compressed zones, when the wall has high flexural/shear ratio that cause the overturning of the wall.

The occurrence of these different failure modes depends on several parameters [108] [109] [49] [110] [111]; [112] [113]:

i) wall aspect ratio; ii) wall boundary conditions; iii) the size and the geometry of wall; iv) the magnitude of the axial compressive force; v) the material characteristics of the wall constituents (mortar, brick unit and interfaces); vi) cross-section of masonry pattern.

When masonry is subjected to tensile forces, two types of failure modes may occur, depending upon its mechanical properties. Firstly, the cracks may be formed vertically through the head joints and bricks, with a brittle behavior with a sudden decrease in strength, or in a stepped path through the head and bed joints [2]. When the stepped path failure mode occurs, the strength reduction due to cracking is small, and the element exhibits a ductile behavior.

When masonry is subjected to shear forces, shear cracks appear on the element; nonlinear shear displacement and crack opening occur in the surface, pushing the crack surfaces to touch each other, transferring the shear and normal compressive stresses among them. The roughness of the crack surface has a strong influence on the transferred stresses and the direction of contact stresses [114]. The most common failure modes of masonry are depicted in Figure 12.

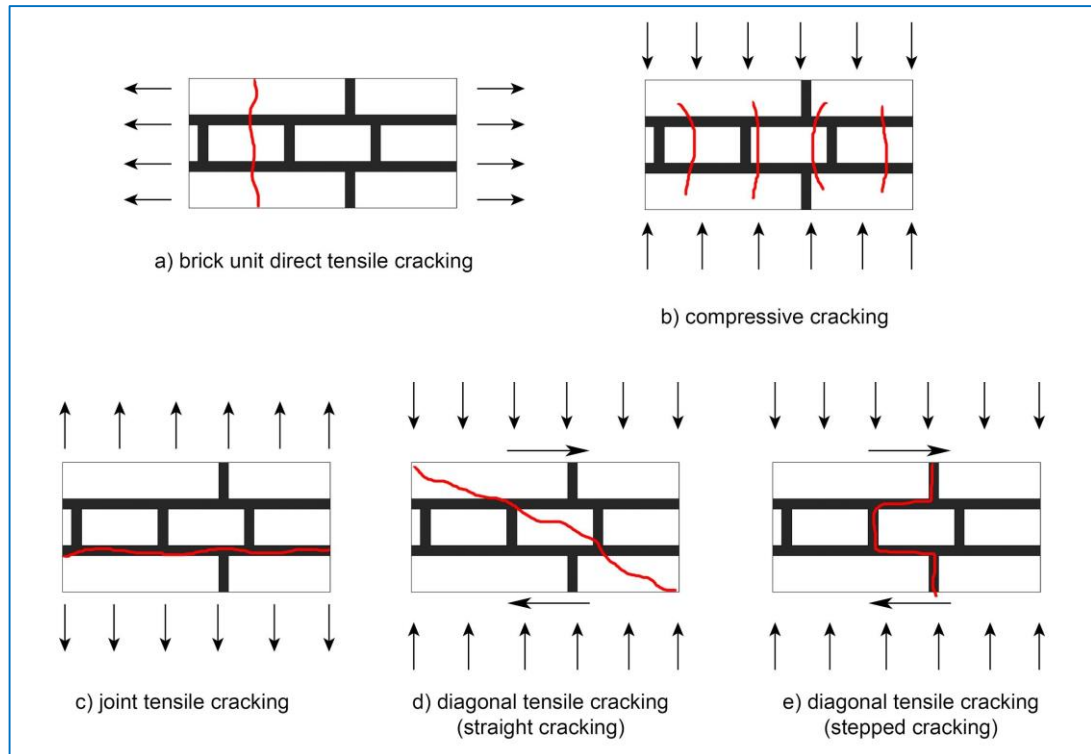


Figure 12. Failure modes of masonry.

The masonry prism failure in compression can be initiated by [23]:

- i) tensile splitting of mortar joints;
- ii) shear failure at brick/mortar interface due to debonding of brick and mortar followed by tensile splitting of bricks;
- iii) inconsistency of brick manufacturing process, where some bricks are very weak and result in local crushing of masonry.

The factors that affect the lateral load carrying capacity of a URM building are: the layout and the geometric properties of the walls in plan; types of bricks used, quality and age; mortar mix.

Diagonal tension cracking may result in two failure types depending on the ratio of mortar strength to brick strength. The first failure mode is diagonally inclined cracks through brick units, which is considered to be a brittle failure mode, where the

initiation of visible diagonal cracking is associated with the peak lateral force capacity immediately followed by a rapid strength degradation.

The second failure mode is diagonally inclined stepped pattern through the mortar bed and head joints due to the formation of tensile horizontal cracks in the bed joints which have the potential to act as sliding planes when subjected to reverse earthquake loading. In the event as earthquakes, sliding and rocking failure modes cause the wall components to exhibit considerable displacements [56].

The out-of-plane resistance deficiency is a common feature for historical URM buildings due to several factors, among which, the masonry texture plays an important role. The out-of-plane response of the URM building is dependent upon [51] shape and the arrangement of the building units (blocks, bricks, or stones) and the organization and the layout of the units within the thickness of the section of the wall.

It was observed that after an earthquake, the multi-leaf masonry walls were highly vulnerable against out-of-plane failure as the outer leaf was poorly connected along the thickness [115].

The load bearing capacity of URM walls is strongly dependent upon their slenderness ratio (height to thickness ratio) as well as the effective eccentricities of the loads applied. At a smaller scale, it is also dependent on the components' properties such as compressive strength of brick and mortar and the tensile strength of brick-mortar interface [116]. For short elements, with low slenderness ratio, the failure occurs due to material crushing, whereas for the element with higher slenderness ratio, the failure occurs due to lateral instability (buckling failure).

One of the most important failure modes that need to particularly assessed in the diagonal shear failure mode of in-plane URM walls is commonly observed during seismic shaking of the earthquakes [107] [117].

However, obtaining a diagonal shear failure mode of a wall experimentally, was found to be difficult due to the tendency of isolated walls to rock. Thus, in some cases, diagonal shear failure was obtained by restraining the wall from rocking or by pre-compressing the wall with a large axial load that is improbable in common URM

buildings [118]. In order to overcome this problem, as it was suggested by ASTM E 519 [47], the force can be applied along a panel diagonal to obtain a diagonal crack in a so-called diagonal compression test, which has been standardized for URM panels measuring 120 cm x 120 cm.

Due to the aforementioned constraints associated with in situ testing, the effectiveness of various improvement techniques that enhance the performance of seismically deficient URM wall components is typically evaluated using replicated wall components in a laboratory based setting. Such studies allow experimental evaluation of a large number of test specimens to be conducted in a cost effective manner and in a controlled environment. However, replicated wall components must have strength characteristics that are adequately representative of those present in existing vintage URM buildings in order for the laboratory study to have relevance.

2.5.1. Typical failure modes of adobe masonry

Houben and Guillard, estimated that about 30% of the world's population lives in adobe dwellings, accounting for 20% of the world's urban/suburban population [119]. Adobe buildings are vulnerable to collapse due to heavy walls which produce large inertia forces during an earthquake. Additionally, these type of structure lack ductility. The most common failure modes are due to separation of walls at corners, roof from the walls or due to excessive cracking (Figure 13).

Brick masonry structures are also vulnerable to collapse during an earthquake. The earthquake in China, in 1976, caused the loss of 240000 lives as a result of collapse of brick masonry buildings [120].

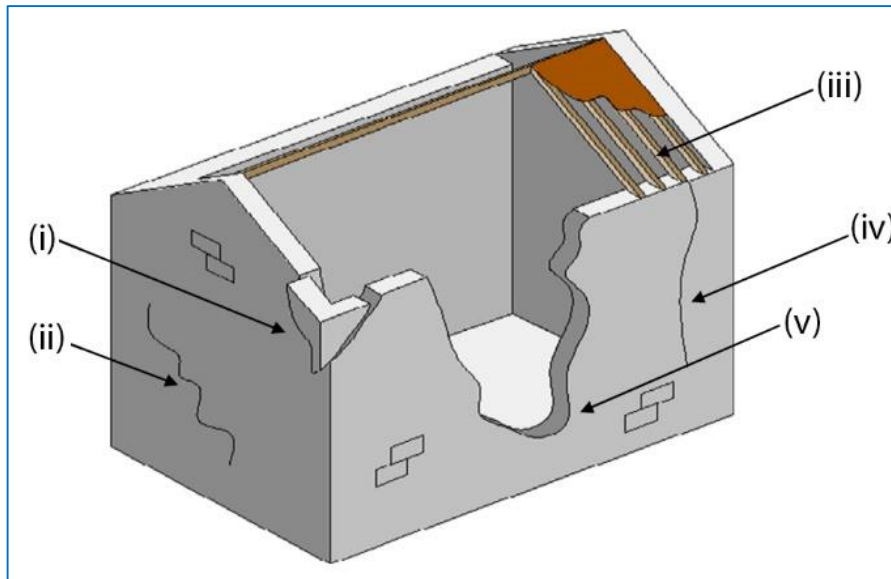


Figure 13. Common failure mechanisms for adobe structures: (i) separation of walls at corners; (ii) diagonal cracking in walls; (iii) separation of roofing from walls; (iv) vertical cracking in walls; (v) out-of-plane wall failure, (extracted from [121]).

2.5.2. Typical failure modes of stone masonry

Stone masonry buildings are a common type of construction in developing regions especially around the Mediterranean, North Africa, the Middle East, India, Nepal and other parts of Asia. It is a useful type of construction as it provides low-cost housing due to local availability of stone materials.

It is observed that stone masonry buildings have a very poor performance due to the low strength of the bond between stone and mortar as well as inadequate wall connections. The most common failure modes of stone masonry structures during an earthquake are:

- i) delamination: two layers of stone wall that are connected with loose rubble infill detach and crack during lateral motion induced by the earthquake;
- ii) overturning due to out-of-plane failure of long-span walls;
- iii) in-plane failure due to development of shear cracks;
- iv) connection failure leading to an out-of-plane failure.

2.6. Overview of URM buildings in Albania

The common buildings in Albania may be categorized as the ones built before World War II, mainly small 3-storey residential buildings, and the ones built after WWII, multi-story and condominium. Both types of buildings have suffered extensive damage during past earthquakes.

The first national building codes were published in 1978-79 and revised second edition in 1989, KTP (Kodet Teknike të Projektimit), Albanian Design Codes. KTP-2/1978 and KTP-N2/1989 are related to earthquake resistant design (Equivalent of Eurocode 8, EN-1998-1-1). KTP-9/1978 is related to Design of Masonry Structures (equivalent of Eurocode 6, EN-1996-1-1).

Most of the unreinforced masonry buildings were built before 1978, therefore they can be assumed not to comply with KTPs.

During 1950-1990, manufacturing of construction materials, especially clay and silicate bricks of standard dimension 250 x 120 x 65 mm, was mainly concentrated in four big factories located in Tiranë, Vlorë, Shkodër and Lushnje [122].

A large portion of the Albanian building inventory, more precisely, about 62% is composed of URM structures built before 1990s based on KTP-89 provisions or with no compliance to any codes at all, if built before 1978 [123].

2.6.1. Seismic Risk in Albania

Albania and the Balkan Peninsula are part of the Alpine Mediterranean seismic belt. The released energy from the earthquakes of this belt is estimated to be about 15 % of the total amount of the overall energy released from the earthquakes around the world [124]. The recorded earthquakes that have hit Albania through history are of a variable intensities and magnitudes. According to the statistical records of the seismic centers in Albania and the neighboring countries, during 1900–2005, Albania was hit by 234 earthquakes with a magnitude of greater than 5 on the Richter scale. In Table 8 it is

presented a summary of the recorded earthquakes with an intensity $I_0=6$ and above that hit Albania during 19th and 20th centuries.

As a result of this high activity, together with the relatively high number of URM structures, emphasize the need of this structures to be strengthened in order to be able to safely resist a future disastrous event such as an earthquake.

Table 8. Earthquake occurrence during 19th and 20th century.

<i>City</i>	<i>Year of occurrence</i>	<i>Casualties</i>
Shkoder	1855	Magnitude 6.6, $I_0>VIII$, destroyed 3 villages
	1905	1500 houses destroyed completely
	1948	N.A
	1979	17122 buildings were almost destroyed, affected Lezha, too.
Leskovik	1919	N.A
Tepelene	1920	250 housed destroyed or heavily damaged
	1969	N.A
Elbasan	1920	173 houses destroyed completely
Diber	1931	N.A
	1942	495 houses destroyed completely, 929 buildings were heavily damaged, 2200 were affected
	1967	534 houses destroyed, 1623 heavily damaged
	1926	most of the houses destroyed, the portal of the city castle was demolished
Vlore	1833	N.A
	1851	Magnitude 6.6, $I_0=IX$, 2000 killed
	1859	N.A
	1866	N.A
	1930	almost destroyed 3 villages, 494 houses
	1963	N.A
Librazhd	1935	N.A
	1967	N.A
Lushnje	1959	761 houses collapsed
	1982	N.A
Korce	1960	103 houses collapsed, 878 were heavily damaged
Fier	1962	about 1000 houses were destroyed or heavily damaged
	1969	$I_0=VIII$ destroyed or heavily damaged 842 buildings, affecting cities nearby too.
	1982	278 houses collapsed, 2186 were heavily damaged, affected the cities of Lushnje and Berat
Tirane	1988	magnitude 5.4, $I_0=VII$, $PGA=0,4048g$

2.7. Strengthening techniques used in existing URM structures

In order to improve deficiencies related to poor structural performance of URM structures under seismic actions, various strengthening techniques have been developed and applied throughout history of construction. The main aim of the strengthening techniques is to increase low parameters of masonry such as tensile and shear strength. As discussed in Section 2.5, URM structures are highly vulnerable against lateral loads. For this reason, this deficiency is to be overcome by strengthening techniques. Depending upon the method and materials used, these techniques are categorized as: traditional and modern techniques.

2.7.1. Traditional Retrofitting Techniques

Traditional techniques such as: i) filling cracks and voids by grouting; ii) stitching of large cracks and weak areas with metallic or brick elements; iii) external or internal post-tensioning with steel ties; iv) shotcrete jacketing; v) ferrocement and vi) center core are available for retrofitting of existing masonry structures [58] [125].

- **Surface Treatment:** It is a technique that covers the exterior face of masonry by affecting the architectural appearance of the structure. It consists on constructing a steel or polymer mesh, coated by high strength mortar, around the exterior of the structure. This system confines the masonry after cracking and increases the ultimate load resistance. The surface treatment improves the out-of-plane resistance and reduces any “arching action”. However, application of this technique seriously affects the architectural properties and the lack of “breathing” of the wall may accelerate degradation.
- **Ferrocement jacketing:** This technique is applied by embedding closely spaced meshes of fine rods with reinforcement ratio of 3-8% in high strength (15-30 MPa) cement-mortar layer of 10-50 mm thickness. The typical mortar mix consists of cement: sand ratios of 1: (1.5-3) with a w/c ratio of 0.4 [126]. It causes considerable increase in stiffness. Strengthening of pre-damaged URM walls can restore the

original capacity and stiffness. Ferrocement can control crack formation as it has high flexural and shear strength.

It has been subject of many studies for both unreinforced masonry as well as concrete structures [127] [128] [129] [130]. Kaushik et al. [131], observed that ferrocement provided an increase of strength and ductility for columns in both axial and eccentric loading conditions, improvement of cracking resistance [132], increased stiffness and ultimate load carrying capacity [133].

Some of the advantages of ferrocement such as considerably low price and ability to be completed with unskilled workers, make it an ideal solution for low cost housing.

It has been observed that the mesh helps to confine the masonry unit after cracking and it improves in-plane elastic deformation capacity. Abrams et al. [134], observed that the in-plane lateral resistance was increased 1.5 times during a static cyclic test. The out-of-plane behavior (arching action and out-of-plane stability) is improved too, as the ferrocement increases the wall height-to-thickness ratio [135] [136].

- **Reinforced Plaster:** This technique is achieved by applying a thin layer of cement plaster over a high strength steel reinforcement (diagonal bars or horizontal mesh). It was observed that in diagonal tension tests and static cyclic test, the in-plane resistance was increase by 1.25-3 times [137].
- **Shotcrete:** It is achieved by spraying overlays on to the surface of masonry wall over a mesh of reinforcing bars. The thickness of the shotcrete layer can be adopted to the seismic demand.
- **Grout and epoxy injection:** It is applied by injecting grout into pre-drilled holes on the wall. The main purpose is to restore original integrity and to fill the voids and cracks which are present in the wall. Injection is sustainable and may also be able to restore the initial strength of masonry. However, the success of this technique lies on the fact that the mechanical properties of the grout mix are compatible with the physical and chemical properties of the masonry that is to be retrofitted.

- **External Reinforcement:** It is achieved by attaching steel plates or tubes as an external reinforcement for an existing URM building.
- **Confining using RC tie columns:** This method consists of addition of tie columns and tie beams along the walls connected together at floor levels that confine the URM walls at corners and wall intersections.
- **Post-tensioning:** It is achieved by applying a compressive force on the masonry wall in order to counteract the tension stresses resulting from the lateral loads. It is mainly used for structures of high importance such as monuments.
- **Center core technique:** It consists on creating a reinforced grouted core inside the existing URM wall by drilling a vertical hole from the top to the basement of the wall, placing the reinforcement (50-125 mm) and pumping filler material from top to the bottom of the wall.

2.7.2. Summary of Traditional Strengthening Techniques

Traditional strengthening techniques offer a suitable method for improving the structural behavior of URM buildings, but there are some limitations such as: time consuming to be applied, reduction of available space, occupancy disturbance, building operation disruption and affecting the aesthetics of the existing wall. Furthermore, the added mass can also increase the earthquake induced inertial forces and may require strengthening of the foundations as well.

2.7.3. Modern Strengthening techniques

Development of new materials and techniques came as a consequence of the need to overcome the limitations of traditional strengthening techniques. Many of those disadvantages could be repressed by using modern techniques for retrofitting. The polymer reinforced polymers are an efficient alternative, as they improve the behavior of masonry elements under monotonic, seismic and explosive loads. Additionally,

since the added mass and stiffness are negligible, the dynamic properties of the reinforced structure will not be altered.

2.7.3.1. TRM (Textile reinforced mortar)

It is a technique that combines the essential properties of both conventional and modern materials by using textile grids externally embedded in mortars. The grid is made of long fiber rovings (made of carbon, glass or aramid) arranged in two orthogonal directions. Instead of polymer resins, cement or lime-based mortars are used. The composite action of TRM is achieved through the mechanical interlock of the grid structure and the mortar [138]. It increases shear strength, stiffness and ductility

Some of the advantages of usage of TRM and replacement of organic resins with an inorganic binder are the improvement of the following:

- i) poor behavior at high temperatures;
- ii) high cost;
- iii) vapor impermeability;
- iv) incompatibility with masonry substrates;
- v) irreversibility and lack of recyclability.

2.7.3.2. Fiber Reinforced Mortar (FRM)

It is a reinforcing technique that consist of microfibers made of steel, glass, synthetic fibers (acrylic, aramid, carbon, nylon, polyester, polyethylene and polypropylene) and natural fibers (straw, coconut, bamboo, etc.) embedded in mortar.

Polypropylene fibers are chemically inert fibers that bond mechanically with the mortar through contact area.

2.7.3.3. Fiber Reinforce Polymer (FRP) reinforcement

A fiber reinforced polymer (FRP) system consists of two main materials: resin and fibers. These FRP composites are made of carbon (CFRP), glass (GFRP) or aramid (AFRP) fibers bonded together in an inorganic polymeric matrix (such as putty fillers, saturants and adhesives like epoxy, polyester or vinylester) that offer many advantages such as high strength and stiffness in the direction of the fibers, immunity to corrosion, low weight, availability in various forms as laminates, fabrics and tendons of unlimited lengths, exceptional durability in many environments, cost effectiveness. Fiber is made of very thin filaments and is the most important element which provides the system strength and stiffness. FRP systems exhibit linear-elastic stress-strain relationship. Neither sudden failure, nor plastic behavior is observed when subjected to tensile forces. The FRP systems' characteristics are defined by: type of fiber volume, orientation and thickness and type of resin. One of the most important characteristics of FRP composites is that when a structural member is reinforced with FRP, stresses are transferred from substrate to the FRP through shear and epoxy interface. Among other advantages, some of the most useful properties of FRP materials are: i) easy implementation; ii) requirement of minor preparation works, iii) well preservation of the material integrity of the masonry wall.

On the other hand, some of the possible disadvantages of FRP could be: the difficulty on removal of FRP, the used resins are highly flammable and give off toxic vapors when burned; additional fire protection measures must be taken when implementing such a system; when exposed to ultraviolet light the resin slowly becomes brittle; the long-term reliability of FRPs is largely unproven; and FRPs are impermeable to moisture transport.

In order for a successful application of FRPs, surface preparation is required as unfilled cracks or unsmoothed irregularities can cause premature debonding.

In many cases, FRP retrofitting techniques may be inadequate for heritage or historic constructions because of lack of compliance with conservation principles resulting from excessive invasivity and non-removability. It may be advisable to use a technique

composed of traditional materials such as wood or ceramics glued on the wall surface and anchored with mechanical devices [139].

Retrofitting of URM wall with FRP is a promising technique as it was observed that FRP improves the in-plane lateral resistance by 1.1-3 times and the out-of-plane resistance by more than 7 times.

Triantafillou proposed that the shear resistance of the FRP retrofitted URM is equal to the shear resistance of the FRP material itself, plus the shear resistance of the URM [125].

$$F_{FRP} = \rho_h \cdot E_{FRP} \cdot \varepsilon_{tu} \cdot k \cdot t \cdot L \quad (\text{Equation 20})$$

where:

F_{FRP} : the contribution of the FRP in the lateral resistance of URM specimen; ρ_h : the reinforcement ratio of FRP in the horizontal direction; E_{FRP} : modulus of elasticity of FRP; ε_{tu} : the ultimate strain of FRP; k : efficiency factor; t : wall thickness; L : wall length.

Nanni and Tumialan, [140], proposed a value of k as 0.3, whereas Zhao et al., [141] proposed a value of 0.2 for pre-cracked specimens and 0.3 for uncracked specimens.

The main types of in-plane failure of URM-FRP walls are:

- a) **shear failure**: step-like cracks that pass through either head or bed joint;
- b) **sliding failure**: complete separation at bed joints with a fracture of fiber material;
- c) **flexural failure**: complete separation at bed joints with a fracture of fiber material;
- d) **anchorage failure**.

In order to improve out-of-plane failure, the research was mainly focused on monotonic and static cyclic loading. These experiments showed that FRP increased the URM flexural strength. The modes of failure of the tested FRP-strengthened specimens are as follows [125] [140] [141] [142] [143]:

- a) sliding shear: complete separation at mortar joints in the shear region with a fracture in fiber material;

- b) flexural failure: caused by masonry compression failure or the rupture of the fibers;
- c) combination shear-flexural failure: cracks started at the maximum bending region and continue 45° as a shear crack;
- d) delamination;
- e) combination of delamination and pullout of face shell;
- f) interface shear failure in multiple wall leaf.

One important factor that has a big influence in the behavior of FRP reinforced URM is the reinforcement ratio. It was observed that the increase in the thickness of reinforcing fibers slightly increases the load carrying capacity of the masonry wall. However, this fact is valid up to a certain level of thickness [144].

FRP composite strips were used by Gabor et al, to reinforce masonry panels and test them in diagonal compression. There were used 3 types of them; unidirectional glass fiber (RFV), unidirectional carbon fiber (RFC) and bi-directional glass fiber (RFW). It was observed that the failure strength was governed by shear strength induced by the interaction of mortar with the internal walledes at the brick/mortar interface. It was observed that the seismic behavior was improved as the deformations corresponding to the maximum loads of the reinforced walls were three times higher than the ones of URM walls [145].

Valluzzi et al., investigated the efficiency of an alternative shear reinforcement technique, such as strengthening of brick masonry panels with by Fiber Reinforced Polymer (FRP) laminates using different reinforcement configurations. They conducted experiments in order to study the shear behavior of masonry panels reinforced with FRP laminates by testing in diagonal compression a series of nine unreinforced masonry (URM) panels and 24 strengthened panels were subjected to diagonal compression tests. As it was seen from the results, double-side configurations provided a less brittle failure and a noticeable ultimate capacity increase [67].

According to the modern codes, safety evaluations of URM structures is clearly based on quantitative assessment of performances. In this study, the main focus was on the shear behavior of masonry panels subjected to in situ diagonal compression tests on

both unreinforced (mainly focused on diagonal cracking failure mode) and reinforced panels. The reinforced panels were tested in order to investigate the effectiveness of the methods of repair by comparing the traditional methods (deep repointing and FRP jacketing) with the innovative seismic-upgrading techniques (“Reticolatus” method, embedding a continuous steel mesh cord in mortar joints whose nodes are anchored to the wall by means of transversal metal bars) [54].

Some of the problems that require special attention when considering FRP retrofitting technique are [139]:

- i) possible peeling of the brick surface;
- ii) the brittle behavior of FRP in both shear and tension;
- iii) the effective resistive response of the reinforcement compared to its theoretical capacity;
- iv) the influence of friction and dilatancy in brick-mortar interface on the response of strengthening;
- v) the coupling effect of the different strength mechanisms activated after strengthening.

Additionally, before implementing, it should be clearly known that application of FRP requires fire resistant measures when epoxy-based materials are used as bonding material (they are highly flammable) and addition of the FRP layer may cause undesired water proofing effect that may disturb the natural perspiration of ceramic materials.

2.8. Review of the Computational Modelling of Masonry Structures

Finite Element Modeling of URM structures is a complex and a challenging task for engineers. It requires the simulation of structural behavior of a heterogeneous composite where are present many uncertainties. This modelling strategy consists of representing the material properties, boundary conditions as well as the loading cases in a proper way.

There are several alternatives that should be selected upon the related requirements for analysis such as:

i) the selected information: failure mechanism, damage pattern, collapse mechanisms, serviceability level; ii) the level of accuracy: local or global behavior of the structure; iii) the necessity of the input data: detailed or rough information about material characteristics; iv) the cost: the available time to conduct analysis.

In order to capture all the possible failure modes of masonry (tensile cracking, shear sliding and diagonal tension cracking) a suitable predictive model should be adopted in modelling [106] [146] [147].

2.8.1. Macro-modelling (Simplified Method via Macro-elements)

In this modelling approach, the structure is represented as a combination of structural elements such as: truss, beam, plate or shell elements. It is a more practice-oriented, less time consuming, requires less computational memory as the macro-elements represent an entire wall or panel, reducing the number of degrees of freedom. Macro-modelling approach treats masonry as a homogeneous anisotropic continuum. It is used when the structure is composed of solid walls with sufficiently large dimension so that the stresses should be uniform across or along the macro-length. It is also characterized by generating of user-friendly meshes. This method does not take into account the interaction between units and mortar. The material is assumed as a homogeneous orthotropic continuum taking into account the average masonry stresses

and strains. The concept “Equivalent Frame Method” introduced by Magenes and Della Fontana, [148]; Roca et al. etc. Usually, macro-elements provide a coarse description of the real element behavior.

Ghiassi et al, in their study, presented a macro-modelling computational framework for nonlinear analysis of URM under combined in-plane loads. This strategy was based on modelling of the behavior of masonry and extending it to the overall wall behavior. The model considers shear and flexural deformations in global behavior and could predict all possible failure modes in masonry such as: crushing from compression, bed-joint sliding, rocking, diagonal tension cracking and diagonal stepped cracking [114].

2.8.2. Micro-modelling

It is accepted to be the best tool to analyze the real behavior, in particular, the local response of the structural element. In this approach, each element such as brick unit, mortar and mortar-unit interface is represented separately. The earliest attempts for micro-modelling were done by Page, [149] and has continued by other authors [150] [151] [152] [153], etc.

2.8.2.1. Detailed Micro-modeling

In detailed micro-modeling, the units and the mortar joint are represented by a continuum element, whereas the unit-mortar interface is represented by a discontinuous element, taking into account both elastic and inelastic properties of unit and mortar. The characteristic properties of materials such as: Modulus of Elasticity, Poisson’s ratio and optionally, inelastic properties of both brick unit and mortar need to be defined as input values.

Moreover, in order to avoid interpretation of continuum, the interface represents a potential crack/slip plane with initial dummy stiffness, leading to very accurate results but requiring a lot of computational efforts.

2.8.2.2. Simplified micro-modeling

Simplified micro-modeling [154] [155] [150] [156] avoids the huge computational efforts by representing the joint consisting of mortar and two unit-mortar interfaces is lumped into an “average” interface lumped in discontinuous elements and brick units by continuum elements are expanded in order to keep the geometry unchanged. In this way, masonry is considered as a set of elastic blocks bonded by potential fracture/slip lines at the joints. This technique is suitable for small structural elements in order to understand the heterogeneous states of stress and strain. It requires experimental data to obtain input values for modeling. In this approach it is seen a reduced degree of accuracy since the Poisson’s effect of mortar is not included.

2.8.2.3. Homogenized Modelling

This technique consists of identifying an elementary cell which generates the entire panel by regular repetition [157] [156] [158] [159] [160] [161]. It replaces the complex geometry of the basic cell by a simplified geometry.

For large scale simulations, homogenization could be an appropriate solution as it accounts the complex geometry of the basic cell and constituent material properties at meso-scale, provided that a repetitive unit cell is defined.

Since the mortar joints act as planes of weakness, the structural response of masonry is closely dependent upon the orientation of the bed joints.

The most relevant property, is the structural material behavior of the uniaxial compressive strength of masonry in the direction perpendicular to bed joints.

Some of the modern modelling approaches consists of enriching the continuous models with a very deep micromechanical insight, best described as “multiscale”. According to Phillips, 1998, “multiscale” refers to algorithms in which different scales of observations of the same physical phenomenon interact and exchange information [162].

2.8.3. Structural Analysis

Modelling of the investigated structure requires assumptions related to mechanical behavior of materials, geometry of structural elements, Boundary conditions and the applied loading conditions. There are three different modelling assumptions to be carried out:

- a) Mechanical modelling: constituents' materials are defined through strength, stress-strain relationships and deformation parameters;
- b) Geometrical and constraints modelling: dimensions of the elements and constraints are defined;
- c) Load modelling: accurate definition of environmental and man-made actions is defined.

Based on the abovementioned assumptions, a linear or nonlinear analysis can be performed. The selection of either methods is dependent on the target performance level and target value of the reference parameters to be controlled as a reference based on stress-strain relationship at material level or force-displacement relationship at global level.

Linear and nonlinear analyses are complementary of each other; when assessment of safety levels against pre-defined serviceability conditions for masonry structures is required, linear analysis is used; when the ultimate capacity of the structure is required to be assessed, nonlinear analysis is used instead.

Generally, nonlinearities may be grouped in three main categories:

- a) Mechanical nonlinearity: defined by nonlinear constitutive laws where stresses are not proportional to their relevant strains (σ - ϵ or τ - γ relationships);
- b) Geometrical nonlinearity: induced by large strains or deformations;
- c) Constraint nonlinearity: when the boundary conditions of the structure change depending on the load pattern.

The solution of the linear analysis is only one as the structure's configuration is not dependent upon previous states.

On the other hand, in nonlinear analysis, the solution may not exist, or may not be unique as the current state of structure must also consider the predecessor configuration and the principle of superposition is not applicable [163].

2.9. Summary of Literature Review

From the literature survey, it was observed that one of the main obstacles in analyzing the structural behavior of URM structures lies in the heterogeneity of the composite material (masonry assemblage) and the variability of mechanical parameters of masonry constituents (brick and mortar).

Masonry properties are strongly related to brick's and mortar's properties, but it is the mortar layer the weakest link of masonry assemblage.

The most important property to be observed is the performance of the URM during earthquakes. The simulation of this type of structural behavior can be achieved by inducing a diagonal compression force on a representative masonry wall panel of a standard dimension of 1.2m x 1.2m x 0.25m. As it is inferred in Section 2, the diagonal compression test has been a widely used procedure to determine masonry shear strength and other shear related parameters for masonry.

It was seen that most of the researches were mainly focused on the undamaged state of the wall panels, considering only two types of specimen: either plain (unstrengthened) or strengthened.

The implementation of the abovementioned techniques was done accordingly either on laboratory constructed panels or on existing vintage masonry.

The studies were mainly focused on panels made of the same mortar mix and the comparisons were done only based on the applied techniques.

There was limited information related to any study where the pre-cracked plain panels were repaired and re-tested in diagonal compression.

CHAPTER 3

METHODOLOGY

3.1. Introduction

The methodology followed in this study consists of destructive tests on masonry panels in order to determine the main mechanical properties of bricks, mortar and masonry assemblage. The testing procedures are the ones defined in American Society for Testing and Materials (ASTM) where are defined all the steps to be followed. These standards have been used by many researchers who have experimented with unreinforced clay brick masonry all over the world [1] [53] [56] [63] [68] [95] [57].

3.2. Determination of bricks parameters

Determination of bricks' required physical and mechanical parameters is presented in this section. All the testing procedures such as: physical requirements, sampling and testing procedure, determination of weight and water absorption, compressive and tensile strength and dimensioning are computed following the ASTM provisions.

3.2.1. Physical requirements

According to the ASTM C 62-04 [11], the bricks should be manufactured from clay, shale or similar naturally occurring earthy substances, should be shaped during the manufacturing process by molding, pressing or extrusion and should be subjected to firing process. When the brick is delivered to site, it should be subject to a visual inspection, and it should be provided that it is free of defects, deficiencies and other surface treatments that would impair the strength or the performance of the brick during construction process. The physical requirements are defined in Table 2.

3.2.2. Sampling and testing procedure

These test methods cover procedures for the sampling and testing of brick and structural clay tile by defining the standard procedure in order to determine the characteristic properties of clay bricks such as: modulus of rupture, compressive strength, and water absorption, initial rate of absorption and determination of weight, size and void area, ASTM C67-04 [13].

3.2.2.1. Sampling

For the purpose of the tests, full-size bricks were selected on the condition to be representative of the lot of units from which they are selected and shall include specimens' representative of the complete range of colors, textures, and sizes and shall be free of or brushed to remove dirt, mud, mortar, or other foreign materials unassociated with the manufacturing process. For the determination of modulus of rupture, compressive strength, and absorption determinations, (based on the ASTM criteria) least ten individual random bricks were selected being marked with an individual unique number.

3.2.2.2. Weight Determination

This process consists of firstly drying the test specimens in a ventilated oven at 110 to 115°C for not less than 24 h. After drying, the specimens were cooled at a temperature of 24°C. Then, five dry full size specimens were weighted on a balance having a capacity of not less than 3000 g and sensitive to 0.5 g. The results of the weight of the specimen were reported separately and the average of the five was obtained to the nearest 0.1 g.

3.2.2.3. Modulus of Rupture (Flexure Test)

Five whole dry full-size units were tested. The testing procedure consists of supporting the test specimen flatwise (the load is applied in the direction of the depth of the unit) on a span approximately 25.4 mm. The modulus of rupture is calculated as the average of each specimen reported to the nearest 0.01 MPa.

$$S = \frac{3W(l/2-x)}{bd^2} \quad (\text{Equation 21})$$

S = modulus of rupture of the specimen at the plane of failure, Pa;

W = maximum load indicated by the testing machine, N;

l = distance between the supports, mm;

b = net width, (face to face minus voids), of the specimen at the plane of failure, mm;

d = depth, (bed surface to bed surface), of the specimen at the plane of failure, mm;

x = average distance from the mid-span of the specimen to the plane of failure measured in the direction of the span along the centerline of the bed surface subjected to tension, mm.

3.2.2.4. Compressive Strength

Five test specimens of dry half brick cut obtained by any method that will produce, without shattering or cracking, a specimen with approximately plane and parallel ends having the full height and width of the unit, with a length equal to one half the full length of the unit 25.4 mm. The brick specimens are tested flatwise; (the load is applied in the direction of the depth of the brick). The compressive strength is calculated as the average of the specimens to the nearest 0.01 MPa as follows:

$$C = \frac{W}{A} \quad (\text{Equation 22})$$

C = compressive strength of the specimen, kg/cm²;

W = maximum load, N, indicated by the testing machine;

A = average of the gross areas of the upper and lower bearing surfaces of the specimen, cm².

3.2.2.5. Water Absorption

Five half brick specimens were used for testing. Dry and cool the test specimens. Submerge the dry, cooled specimen, without preliminary partial immersion, in clean water for 5 and 24 hours. Then the specimens were removed, wiped off the surface water with a damp cloth and weighted using a balance of a capacity of not less than 2000 g, sensitive to 0.5 g.

Calculation of the cold water absorption of each specimen to the nearest 0.1 % was done as follows:

$$\text{Absorption, \%} = \frac{100(W_s - W_d)}{W_d} \quad (\text{Equation 23})$$

where:

W_d = dry weight of the specimen;

W_s = saturated weight of the specimen after submersion in cold water.

3.2.2.6. Measurement of Size

Ten whole dry full-size units' representative of the lot, including the extremes of color range and size determined by visual inspection, were tested using a steel rules graduated in 1-mm divisions. The average width, length, and height of each specimen tested is calculated to the nearest 0.8 mm.

3.3. Specifications of mortar properties

According to ASTM C 270-03, the classification of standard mortars to be used in construction is described in Table 3 [20].

3.3.1. Determination of mortar compressive strength

50-mm test cubes are compacted by tamping in two layers. The cubes are cured one day in the molds and stripped and immersed in lime water until tested. The specimens are tested immediately after their removal from storage water. The load to specimen faces is applied on those faces that were in contact with the true plane surfaces of the mold. The total maximum load indicated by the testing machine is recorded, and the compressive strength is calculated as follows:

$$f_m = \frac{P}{A} \quad (\text{Equation 24})$$

f_m = compressive strength in MPa;

P = total maximum load in N;

A = area of loaded surface in mm²

The average compressive strength of all acceptable test specimens made from the same sample and tested at the same period, was calculated to the nearest 0.1 MPa.

3.4. Determination of masonry assemblage compressive strength

This test method covers procedures for masonry prism construction and testing, and procedures for determining the compressive strength of masonry, f_{mt} , used to determine compliance with the specified compressive strength of masonry, f'_m . Firstly, the length and width at the edges of the top and bottom faces of the prisms are measured to the nearest 1.3 mm [164]. The failure mode of the assemblage is depicted in Figure 14.

The compressive strength of each masonry prism is calculated by dividing each prism's maximum compressive load sustained by the net cross-sectional area of that prism. Additionally, the h_p/t_p ratio for each prism using the height and the least lateral dimension of that prism is calculated. Then, the correction factor from Table 9 is determined.

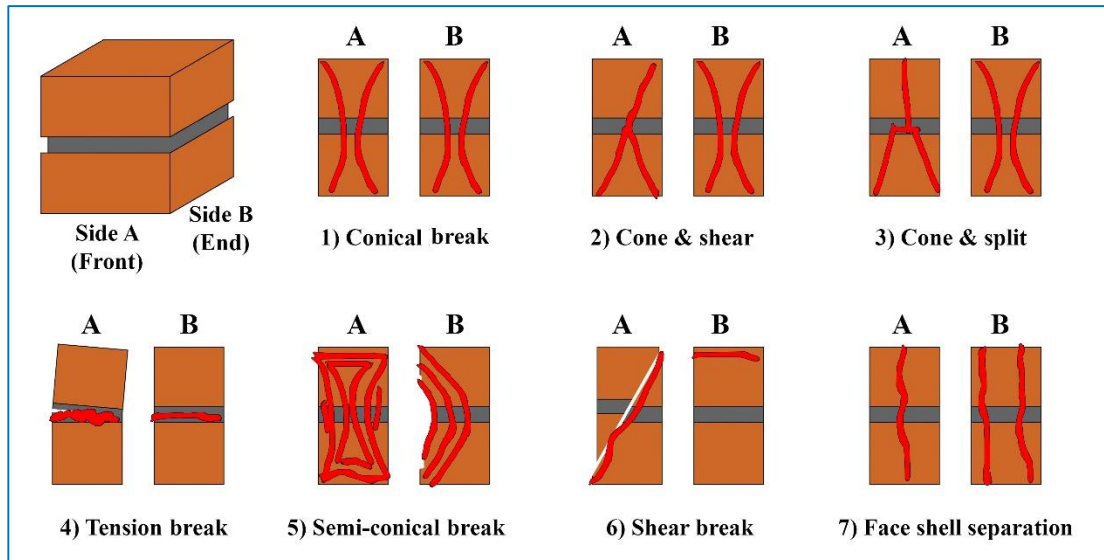


Figure 14. Failure modes of masonry prisms (reproduced after [164]).

Table 9. Height to Thickness Correction Factors for Masonry Prism Compressive Strength [164].

h_p/t_p *	1.3	1.5	2.0	2.5	3.0	4.0	5.0
Correction factor	0.75	0.86	1.0	1.04	1.07	1.15	1.22

* h_p/t_p – Ratio of prism height to least lateral dimension of prism

The compressive strength of masonry, f_{mt} , is calculated by multiplying the masonry prism strength by the correction factor for the respective prism and by averaging the values obtained from them.

3.5. Determination of diagonal tensile strength (shear strength)

ASTM E 519-02 [47], the standard testing procedure requires rotation of the tested specimen by 45° and vertical loading along one of the wall's diagonals. However, due to low masonry bond strength of the wall, as well as the risk of disturbing the overall state of stresses by involuntarily adding extra stress, the test set-up was modified such

that the wall specimen remained vertical on its original position and the loading mechanism was rotated as in the Figure 16. The movable test set-up consists of two loading shoes placed on two diagonally opposite corners of the panel connected by four high strength steel rods positioned along the compressed diagonal (Figure 15). The 50-tonne-capacity hydraulic jack was incorporated between the top loading shoe and a metallic plate connected to the steel rods, which when loaded, developed tension forces on the four steel rods connecting the loading shoes, compressing the wall diagonally, providing the desired failure mode; diagonal cracking and/or bed joint sliding failure. The applied load was gradually increased until failure occurred. The deformations of the wall specimen (compression and elongation of diagonals) was recorded by two diagonally positioned displacement gauges attached on every wall panel over a gauge length of 1000 mm that were oriented parallel and perpendicular to the loading direction.

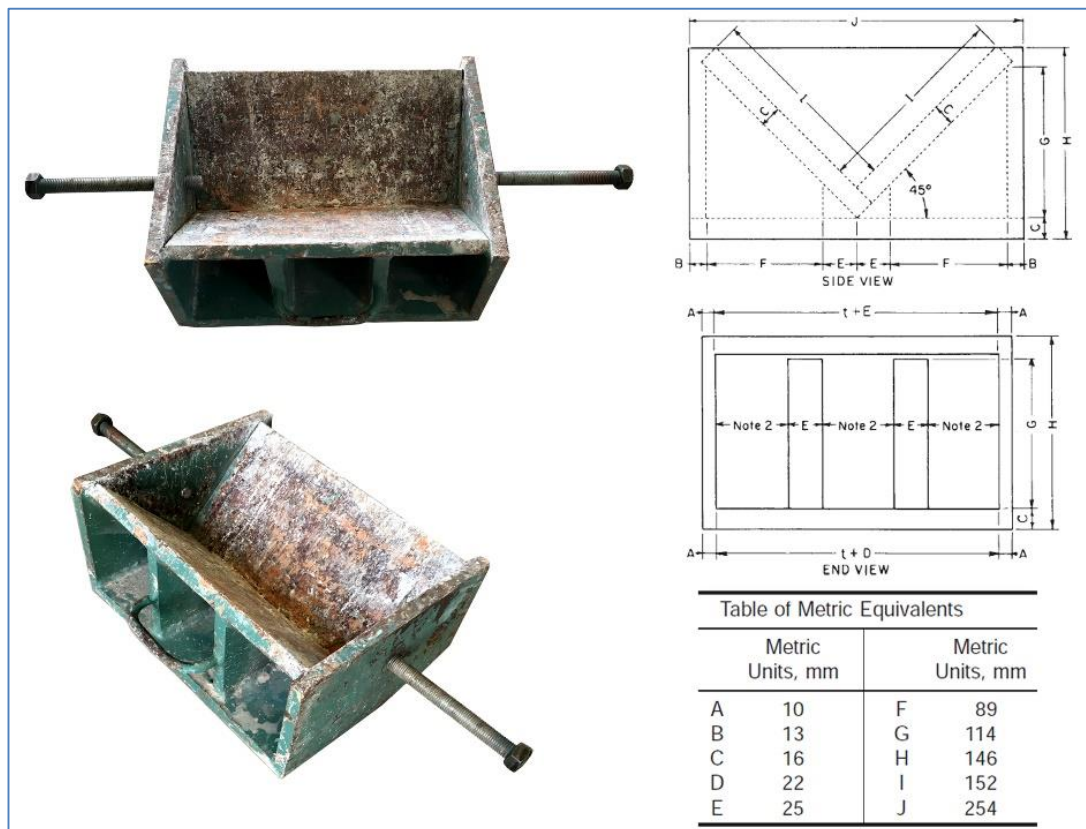


Figure 15. Loading shoes used for diagonal compression test.

One of the issues which was carefully taken into consideration during the application of diagonal compression test was the load distribution along the corners of the wall panels in order to avoid an excessive concentration of compressive stresses at the surface of metallic plates.

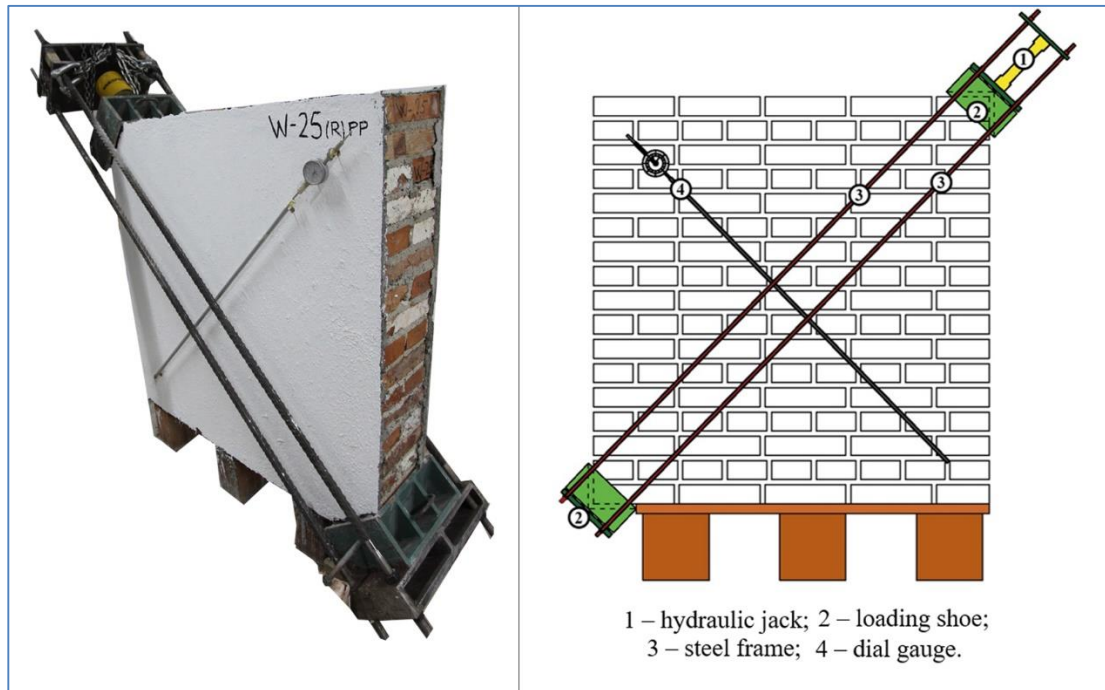


Figure 16. Diagonal compression test set-up (example from W-25-R-PP and the schematic view of the system set-up).

This test method is used to determine the diagonal tensile or shear strength of 1.2 by 1.2-m masonry assemblages by loading them in compression along one diagonal, thus causing a diagonal tension failure with the specimen splitting apart parallel to the direction of load (Figure 16). According to this procedure, the test should be carried out on at least three specimens constructed with the same size and type of masonry units, mortar, and workmanship. In order to achieve adequate curing, the specimens should not be moved for at least 7 days and should be stored in the laboratory for not less than 28 days.

The calculation procedure is as follows:

$$S_s = \frac{0.707P}{A_n} \quad (\text{Equation 25})$$

where:

S_s – shear stress (MPa); P – load exerted along the compression diagonal (N); A_n – net area of the specimen (mm²);

$$A_n = \frac{w+h}{2} t \cdot n \quad (\text{Equation 26})$$

where:

w – width of specimen (mm); h – height of specimen (mm); t – total thickness of specimen (mm); n - percent of the gross area of the unit that is solid, expressed as a decimal.

$$\gamma = \frac{\Delta V + \Delta H}{g} \quad (\text{Equation 27})$$

where:

γ - shearing strain (mm/mm); ΔV – vertical shortening (mm); ΔH – horizontal extension; g – vertical gage length;

$$G = \frac{S_n}{\gamma} \quad (\text{Equation 28})$$

where:

G - modulus of rigidity, MPa

3.6. Stiffness

Material stiffness can be measured by the Shear Modulus, G , which is calculated as the ratio of the shear stress to shear strain. The shear modulus can be determined as the secant modulus of $0.05\tau_{max}$ and $0.70\tau_{max}$ of the stress-strain response curve.

The stiffness of a wall specimen can be quantified by the Modulus of Elasticity, E , which is related to shear modulus by the following Equation 19, where $\nu = 0.25$ adopted by [74]:

$$E = 2G \cdot (1 + \nu) \quad (\text{Equation 19})$$

3.7. Ductility

Another parameter to be taken into consideration while analyzing the behavior of URM is the ultimate drift and ductility. As mentioned in previous chapters, in case of an earthquake, due to seismic shaking, URM buildings are subjected to lateral loads which impose the structure lateral deformation. Ductility is defined as the ability of a material to deform without rupture, or in case of URM buildings, the ability of the structure to deform without collapsing.

In order to quantify the ductility of the tested wall panels, a drift ratio was defined as:

$$\gamma_u = \frac{\Delta u}{H} \quad (\text{Equation 29})$$

where Δu , is the diagonal displacement corresponding to the ultimate strength and H is the height of the wall panel.

From the experimental campaign, as well as similar experiments reported in literature ([1] [53] [56] [63] [68] [95] [57] etc.), as the wall panels did not have a distinct yield point, pseudo-ductility using bilinear approximation was used. The pseudo-ductility, μ , was determined using the following equation

$$\mu = \frac{\delta_u}{\delta_y} \quad (\text{Equation 30})$$

where δ_u , is the shearing strain corresponding to ultimate strength and δ_y , is the shearing strain near yielding strength. Nevertheless, in the comparisons of the wall panels, δ_u values are used as comparisons.

3.8 Experimental Campaign

The experimental campaign used for this study consists of two series of wall panels: Type “N” mortar (W-01 until W-19) grouped in Series 1 and Type “O” mortar (W-20 until W-37), grouped in Series 2. Within each series there are unreinforced walls (plain specimens), reinforced ones and retrofitted (pre-cracked and repaired) walls. Wall panels of mortar type “N” and “O” characteristics are summarized in Table 10 and Table 11, respectively.

The solid clay bricks used for this project were obtained in the city of Fier, Albania. The clay bricks were manufactured on site using the quarries of the clay nearby the factory. All the bricks were backed at the same time, and have similar to identical characteristics.

The remaining materials were obtained from Fushe-Kruje, a place well-known for cement and lime production. Cement was selected CEM II/B-L 32.5 R, suitable for lower water demand and improved workability, delivered in 50 kg bags.

Table 10. Wall panels of Series 1.

<i>Specimen type</i>	<i>Wall Panel</i>	<i>Dimension</i>			<i>Reinforcement type</i>
		<i>H (mm)</i>	<i>L (mm)</i>	<i>t (mm)</i>	
Series 1 (Type "N" mortar)	W-01	1200	1200	250	-
	W-02	1200	1200	250	-
	W-03	1200	1200	250	-
	W-04	1200	1200	250	-
	W-05	1200	1200	250	-
	W-06	1200	1200	250	-
	W-07	1200	1200	250	-
	W-08	1200	1200	250	-
	W-09	1200	1200	250	-
	W-10-FC	1200	1200	250	ferrocement reinforcement
	W-11-FC	1200	1200	250	
	W-12-FC	1200	1200	250	
	W-13-PP	1200	1200	250	polypropylene reinforcement
	W-14-PP	1200	1200	250	
	W-15-PP	1200	1200	250	
	W-16-GFRP	1200	1200	250	glass FRP reinforcement
	W-17-GFRP	1200	1200	250	
	W-18-GFRP	1200	1200	250	
W-03-R-PP	1200	1200	250	repair with polypropylene	
W-05-R-PP	1200	1200	250		
W-09-R-PP	1200	1200	250		
W-06-R-FC	1200	1200	250	repair with ferrocement	
W-07-R-FC	1200	1200	250		
W-08-R-FC	1200	1200	250		

Table 11. Wall panels of Series 2.

<i>Specimen type</i>	<i>Wall Panel</i>	<i>Dimension</i>			<i>Reinforcement type</i>
		<i>H (mm)</i>	<i>L (mm)</i>	<i>t (mm)</i>	
Series 2 (Type "O" mortar)	W-19	1200	1200	250	-
	W-24	1200	1200	250	-
	W-25	1200	1200	250	-
	W-26	1200	1200	250	-
	W-27	1200	1200	250	-
	W-28	1200	1200	250	-
	W-29	1200	1200	250	-
	W-33	1200	1200	250	-
	W-34	1200	1200	250	-
	W-35	1200	1200	250	-
	W-36	1200	1200	250	-
	W-20-FC	1200	1200	250	ferrocement reinforcement
	W-22-FC	1200	1200	250	
	W-23-FC	1200	1200	250	
	W-21-PP	1200	1200	250	polypropylene reinforcement
	W-30-PP	1200	1200	250	
	W-31-PP	1200	1200	250	
	W-32-CFRP	1200	1200	250	carbon FRP reinforcement
	W-37-CFRP	1200	1200	250	
	W-24-R-PP	1200	1200	250	repair with polypropylene
	W-25-R-PP	1200	1200	250	
	W-26-R-PP	1200	1200	250	
	W-27-R-FC	1200	1200	250	repair with ferrocement
	W-28-R-FC	1200	1200	250	
W-29-R-FC	1200	1200	250		
W-34-R-CFRP	1200	1200	250	repair with carbon FRP	
W-35-R-CFRP	1200	1200	250		
W-36-R-CFRP	1200	1200	250		

3.9 Construction of Plain Wall Panels (Unstrengthened specimens)

The wall panels were built of solid clay brick and tested in two series. For the mortar, two different compositions were used; type “N” mortar (Series 1) (Table 10) and type “O” mortar (Series 2) (Table 11). These two compositions were aimed at replicating the mortars used in existing new buildings (Series 1) and existing old buildings (Series 2).



Figure 17. Construction process of plain walls.

The wall panels of Series 1 were built using two leaf, English bond and new clay bricks with typical nominal dimensions of 243.4 mm x 118.9 mm x 56.8 mm with 15 mm thick mortar joints made of hydraulic cement mortar with a volumetric mix ratio of cement: lime: sand, 1:1:6, which is found to be a good representative of modern brick constructions.

The wall panels of Series 2 were built in the same manner as Series 1 but the hydraulic cement mortar had a volumetric mix ratio of cement: lime: sand, 1:2:9.

All the wall panels were built in laboratory by experienced masons using the English bond which is the prevalent bond of URM buildings in the world and in Albania, too. They were left to cure for 28 days prior to either testing or reinforcing. After that time, a layer of white lime paint was applied in order to provide a better medium for analyzing the crack formation.

For Series 1, a total of eighteen (18) wall panels were tested out of which, three (3) were plain walls, six (6) were pre-cracked and then repaired with ferrocement or polypropylene and other nine (9) were strengthened with ferrocement, polypropylene or glass fiber reinforced polymer prior to testing.

For Series 2, a total of nineteen (19) wall panels were tested, out of which two (2) were plain walls, nine (9) were pre-cracked and then repaired with ferrocement, polypropylene and carbon fiber reinforced polymer and eight (8) were strengthened with ferrocement, polypropylene or carbon fiber reinforced polymer prior to testing.

In total, 52 diagonal compression tests were performed on 38 specimens with nominal dimensions of 1.2m x 1.2m x 0.25m.

All the wall panels were built in laboratory and were also tested in their own place. The testing system was designed in such a way that no disturbance would be caused to the walls. The experiment set-up is described in details in Section 3.5.

The testing continued until the wall panels failed; when after the main diagonal crack was seen sudden drop of the ultimate load (it reached to zero up to a few tones).

The full testing configuration is seen in Table 10 and Table 11, where the naming of the specimens was done in the following manner: “W” is designated for the standard sized wall panel of 1.2 x 1.2 x 0.25 m, “R” represents the initially cracked repaired wall panel, whereas FC, PP, G-FRP and C-FRP represent plastering method of the specimens with ferrocement, polypropylene, glass and carbon fiber reinforced

polymers, respectively. For example, W-07-R-FC represents a pre-cracked panel, more specifically, W-07, which is then repaired with ferrocement jacketing.

3.10 Reinforcing techniques

The aim of strengthening of URM is to increase resistive capacity of the masonry under combined tensile and compressive forces. As discussed in Section 2.7, there is a variety of techniques that may be implemented in order to mitigate the associated hazards coming from natural disasters and deterioration of structure during time, and improve load resisting capacity and overall structural performance, extending the service life of the URM structures. The selected strengthening techniques are presented in the following sections.

3.10.1 Ferrocement jacketing (W-X-FC)

Ferrocement jacketing consists of attaching a double-layered galvanized steel mesh on both sides of the plain wall (Figure 18). The technical specifications of the mesh are presented in Table 12. The mesh is fixed to the wall by means of mechanical anchors and common mortar. The dimensions of the steel mesh are equal to the plain wall (1.2 m x 1.2 m). Allowance of 1.5-2 cm on each side shall be made in order to have a proper jacketing of the wall. The galvanized steel mesh is fixed using anchors (threaded bolts of diameter 8 mm and length 70 mm with washers, mounted on previously drilled holes, having 10-mm wall plugs on the bricks at a distance of 30 cm). The spacing of the connections was slightly changed depending on the brick arrangements, in order to make sure that the connection was done on the brick and not on the mortar joint. The process of mounting the steel mesh on the faces of the wall should be done carefully in order to lay the layers properly, as well as to provide a 5-10 mm allowance between mesh and the bricks for plaster mortar. The mortar mix is prepared using cement: sand 1:4, by volume and water/cement ratio of 0.4.



Figure 18. Plastering process with ferrocement jacketing (FC).

Table 12. Technical specifications for ferrocement mesh.

Mesh type	galvanized welded
Mesh size (mm)	12 x 12
Thickness (mm)	1
Weight (kg/m²)	0.3
Modulus of Elasticity, E (GPa)	170
Yield strength, σ_y	200
Ultimate strength, σ_u	550

3.10.2 Textile Reinforced Mortar (TRM) – plastering with polypropylene fibers (W-X-PP)

Strengthening with polypropylene fibers consists on plastering the plain walls with a 25 mm thick layer of fiber reinforced mortar on both sides (Figure 19). The mortar mix is composed of sand and cement ratio of 1:1 and adding 1.5% fibers in volume and a water/cement ratio of 0.5, as it has been found to be the proper amount not to affect workability. The fibers improve cracking and shear capacity, as well as toughness. The fibers' technical specifications are summarized in Table 13. However, they do not have a considerable effect of the compressive strength of the matrix (mortar).

Preparation of the mix consists on dry mixing the fibers with the sand and the cement, and addition of the water at the end, producing a plater mix with medium workability.

Table 13. Technical specifications of polypropylene fibers.

Chemical base	100% polypropylene fibre
Specific gravity	0.91g / cm ³
Fibre length	12mm
Fibre diameter	18 micron-nominal
Melt point	160°C
Ignition point	365°C
Thermal conductivity	Low
Electrical conductivity	Low
Specific surface area of fibre	250m ² / kg
Acid resistance	High
Alkali resistance	100%
Tensile strength	300 - 400 N / mm ²
Module elasticity	~ 4000 N / mm ²



Figure 19. Plastering process with polypropylene fibres (PP).

3.10.3 G-FRP jacketing reinforcement (W-X-GFRP)

G-FRP jacketing reinforcement consists of attaching a single-layered G-FRP mesh on both sides of the plain wall covered by a plaster layer of 25 mm thick (Figure 20). The technical specifications of G-FRP mesh are presented in Table 14. The mesh is fixed to the wall by means of mechanical anchors and hydraulic cement mortar of cement: sand volumetric ratio of 1:1. The dimensions of the G-FRP mesh are equal to the plain

wall (1.2 m x 1.2 m). The mesh is fixed using anchors (threaded bolts of diameter 8 mm and length 70 mm with washers, mounted on previously drilled holes, having 10-mm wall plugs on the bricks at a distance of 30 cm). The process of mounting the mesh on the faces of the wall should be done carefully and to provide a 5-10 mm allowance between mesh and the bricks for plaster mortar.

Table 14. Technical specification for G-FRP mesh (SikaWrap® Hex 106G).

Primary Fiber Direction	0°/90° (bi-directional)
Weight	325 g/m ²
Weight Ratio (Warp: Weft)	1:1
<i>Cured Laminate Properties (0° & 90°) Design Values</i>	
Tensile Strength	244 MPa
Modulus of Elasticity	16215 N/mm ²
Elongation at Break	1.43%
Thickness	0.33 mm
Strength per cm width	2.53 kN
<i>Fiber Properties</i>	
Tensile Strength	2,276 MPa
Tensile Modulus	72,390 MPa
Elongation	4%
Density	2.54 g/cc



Figure 20. Plastering process with glass fibre reinforced polymer (G-FRP).

3.10.4 C-FRP reinforcement (W-X-CFRP)

Reinforcement pattern of C-FRP strengthened specimens consists was application of a 300 mm thick carbon reinforced polymeric wrap which is attached to a previously smoothly grinded surface using Epoxy along the non-compressed diagonal (Figure 21). In order to improve connection, glass fiber anchorages are applied every 350 mm on previously drilled holes passing through both sides of the wall panel.

Table 15. Technical specification for C-FRP and epoxy.

Fiber Type	Mid strength carbon fibers.
Fabric Construction	Fiber orientation: 0° (unidirectional). Warp: black carbon fibers (99% of total areal weight). Weft: white thermoplastic heat-set fibers (1% of total areal weight).
Areal Weight	230 g/m ² + 10 g/m ²
Fabric Design Thickness	0.131 mm (based on fiber content).
Fiber Density	1.76 g/cm ³
<i>Dry Fiber Properties</i>	
Tensile strength	4300 N/mm ² (nominal).
Tensile E-modulus	238000 N/mm ² (nominal).
Elongation at break	1.8% (nominal).
<i>Laminate Properties</i>	
Laminate thickness:	1.0 mm per layer (impregnated with Sikadur®-330).
Ultimate load:	350 kN/m width per layer (at typical laminate thickness of 1.0 mm).
Tensile E-modulus:	28.0 kN/mm ² (based on typical laminate thickness of 1.0 mm).
<i>Adhesive material</i>	
Adhesive material	2-Part Epoxy Impregnation Resin
Tensile Strength	30 N/mm ² (7 days at +23°C)
Flexural elastic modulus	3800 N/mm ² (7 days at +23°C)
Tensile elastic modulus	4500 N/mm ² (7 days at +23°C)
Elongation at Break	0.9% (7 days at +23°C)



Figure 21. Application of carbon fibre reinforced polymer (G-FRP).

Installation of C-FRP is done after drilling the holes for anchorage and smoothing the diagonal surface, a layer of epoxy is applied on the wall diagonal using Sikadur 330. Then the C-FRP wrap is attached to the wall specimens and another layer of epoxy is applied over the wrap ensuring that the anchorages are properly attached. The technical specifications of C-FRP and epoxy are presented in Table 15.

3.11 Repairing Strategy

The procedure of repairing of the damaged walls consists of application of a plastering layer of 25 mm thickness together with the reinforcing materials. In this way, the reinforcing layer will absorb all tensile stresses and will limit crack propagation as well as will increase the panels' deformation capacities, resulting in a more ductile behavior.

3.11.1 Repair with Ferrocement jacketing (W-X-R-FC)

The procedure of repairing of the damaged walls with ferrocement is the same as strengthening of the plain wall (Section 3.10.1). The only difference is application of an extra layer of galvanized steel mesh along the diagonal cracks of the damaged wall (Figure 22). This layer is fixed using extra anchors drilled every 30 cm along the diagonal. Its main function is to restrain crack propagation and “stitch” the diagonal crack, in order to make the panel behave as a whole.



Figure 22. Repairing of the damaged walls with ferrocement jacketing (W-X-R-FC).

3.11.2 Repair with Polypropylene fibers (W-X-R-PP)

The procedure of repairing of the damaged walls with polypropylene fibers is the same as strengthening of the plain wall (Section 3.10.2). The only difference is application of a thin layer of mortar over the big cracks where dislocation and missing of mortar joints is observed (Figure 23).



Figure 23. Repairing of the damaged walls with polypropylene fibers (W-X-R-PP).

3.11.3 Repair with C-FRP (W-X-R-CFRP)

Repairing of the cracked walls with C-FRP consists of a similar procedure with the reinforcement (Section 3.10.4) with one C-FRP wrap bonded to the uncompressed diagonal. Additionally, parallel to the main wrap, smaller sized wraps are bonded perpendicular to the cracked diagonal, stitching the main diagonal crack (Figure 24).



Figure 24. Repairing of the damaged walls with C-FRP (W-X-R-CFRP)

3.12 Summary of methodology

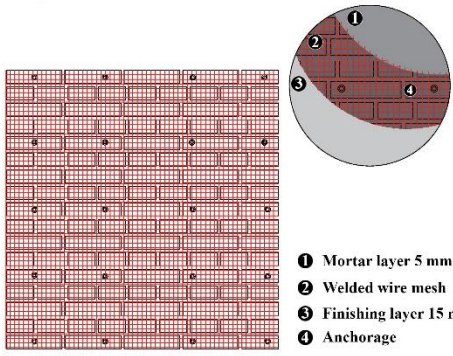
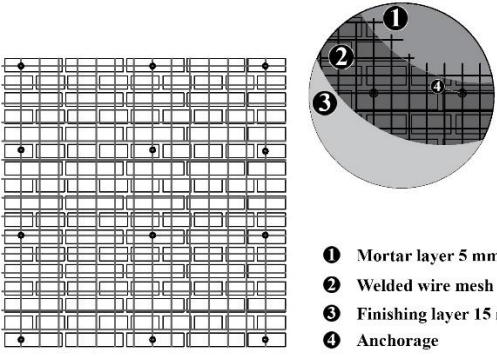
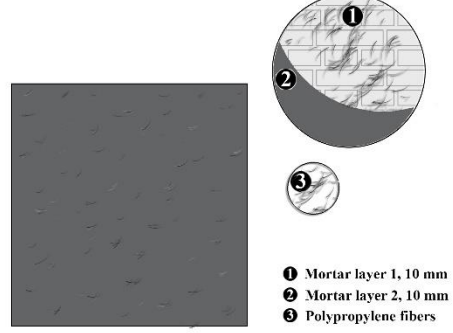
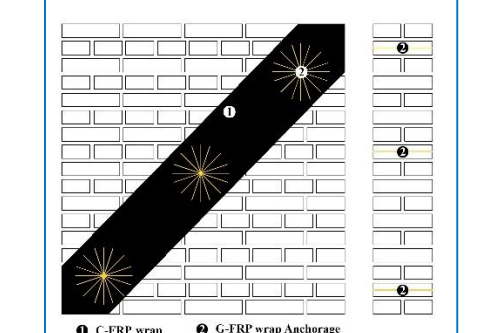
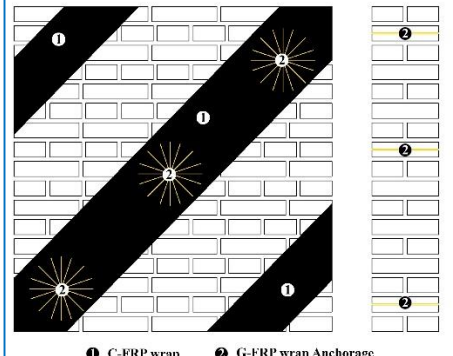
The testing methods and procedures used in this experimental campaign were in accordance to ASTM standards. All the experimental tests were done in order to simulate the behavior of URM buildings made high strength mortar, type “N” (Series 1 panels) and of low strength mortar, type “O” (Series 2).

The selected strengthening techniques (Table 16) were chosen as the ones which are easily available and were selected from the extensive literature survey that other researchers had obtained satisfactory results. Another important consideration related

to strengthening is that in all cases, all the reinforcing layers were applied on both sides. Single-sided strengthening was proven to be inefficient and would not provide satisfactory results [50] [67].

Determination of bricks' and mortar's mechanical properties as well as masonry prism properties was of a fundamental importance before testing the wall panels in diagonal compression.

Table 16. Summary of schematic views of strengthening techniques

 <ul style="list-style-type: none"> ❶ Mortar layer 5 mm ❷ Welded wire mesh ❸ Finishing layer 15 mm ❹ Anchorage 	 <ul style="list-style-type: none"> ❶ Mortar layer 5 mm ❷ Welded wire mesh ❸ Finishing layer 15 mm ❹ Anchorage
<p>a) Ferrocement jacketing</p>	<p>b) G-FRP jacketing</p>
 <ul style="list-style-type: none"> ❶ Mortar layer 1, 10 mm ❷ Mortar layer 2, 10 mm ❸ Polypropylene fibers 	 <ul style="list-style-type: none"> ❶ C-FRP wrap ❷ G-FRP wrap Anchorage
<p>c) Polypropylene plastering</p>	<p>d) C-FRP reinforcement</p>
 <ul style="list-style-type: none"> ❶ C-FRP wrap ❷ G-FRP wrap Anchorage 	
<p>e) C-FRP repair</p>	

CHAPTER 4

EXPERIMENTAL RESULTS

4.1. Introduction

The experimental testing program was implemented in order to investigate the structural performance of URM, in particular the in-plane performance of diagonal shear cracking and/or bed joint sliding mode of failure, strengthened by means of ferrocement jacketing, polypropylene reinforced mortar, glass and carbon reinforced polymers.

The wall panel behavior was investigated during diagonal compression test (ASTM E 519-02), where important parameters such as: types of failure modes, shear strength, elastic and shear moduli and drift were determined. A special attention was paid for in-plane performance governed by diagonal shear cracking mode of failure. As specified in the ASTM regulation, at least 3 wall specimens for each type of strengthening or repair technique were tested.

The diagonal compression test was performed according to the procedure explained in Section 3.5. In total, 52 diagonal compression tests were performed on 38 specimens of 1.2m x 1.2m x 0.25m dimensions, made of type “N” and type “O” mortars.

Prior to testing of wall panels, material characteristics of brick, mortar and masonry assemblage were determined as explained in Section 3.2 and 3.3.

4.2. Brick Properties

Determination of brick parameters was done according the ASTM C 62-04, explained in details in Section 3.2.

4.2.1. Brick Dimensioning

The method of measuring is described in Figure 25, and the results of brick dimensioning are presented in Table 17.



Figure 25. Determining brick dimensions.

Table 17. Dimensioning of the bricks.

<i>Sample Name</i>	<i>Length (l) (mm)</i>	<i>Width (w) (mm)</i>	<i>Thickness (t) (mm)</i>	<i>Area (mm²)</i>	<i>Weight (g)</i>
BR-1	245	118	58	28910	2713.00
BR-2	238	117	56	27846	2707.50
BR-3	245	119	54	29155	2788.50
BR-4	242	122	57	29524	2758.00
BR-5	246	120	59	29520	2822.00
BR-6	246	120	58	29520	2937.00
BR-7	241	119	55	28679	2764.00
BR-8	242	119	56	28798	2707.00
BR-9	246	117	57	28782	2785.00
BR-10	243	118	58	28674	2846.50
Average Brick (BR-X)	243.4	118.9	56.8	28940.3	2782.85
Standard Deviation					72.01
C.O.V (%)					2.59

Table 18. Determination of weight per unit area of the bricks.

<i>Sample Name</i>	<i>Dry Weight (g)</i>	<i>Area (mm²)</i>	<i>Weight per unit area (g/mm²)</i>
BR-1	1286.50	14455.00	0.09
BR-2	1350.50	13923.00	0.10
BR-3	1374.00	14577.50	0.09
BR-4	1426.50	14762.00	0.10
BR-5	1338.50	14760.00	0.09
Average Brick (BR-X)	1355.20	14495.50	0.09
Standard deviation			0.0036
C.O.V (%)			0.04

4.2.2. Water Absorption

The procedure of determining the water absorption is described in details in the Figure 26 and the results are tabulated in Table 19.



Figure 26. Determination of brick water absorption.

Table 19. Determination of water absorption.

<i>Sample Name</i>	<i>Dry Weight (g)</i>	<i>Fully Saturated Weight (g)</i>	<i>Water Absorption (%)</i>
BR-1	1286.50	1544.00	20.02
BR-2	1350.50	1618.00	19.81
BR-3	1374.00	1649.00	20.01
BR-4	1426.50	1714.00	20.15
BR-5	1338.50	1608.00	20.13
Average Brick (BR-X)	1355.20	1626.60	20.03
Standard deviation			0.0014
C.O.V (%)			0.0069

4.2.3. Compressive strength

Bricks' compressive strength was determined using the test procedure explained in Section 3.2.2.4. The results the compression test of 10 randomly selected clay bricks are presented in Table 20.

Table 20. Determination of compressive strength.

<i>Sample Name</i>	<i>Length (l) (mm)</i>	<i>Width (w) (mm)</i>	<i>Area (mm²)</i>	<i>Ultimate Load (kN)</i>	<i>Compressive Strength (MPa)</i>
BR-1	122.5	118	14455	305.8	21.16
BR-2	119	117	13923	317.4	22.80
BR-3	122.5	119	14577.5	338.7	23.23
BR-4	121	122	14762	376.8	25.52
BR-5	123	120	14760	355.5	24.09
BR-6	123	120	14760	321.9	21.81
BR-7	120.5	119	14339.5	360.8	25.16
BR-8	121	119	14399	329.5	22.88
BR-9	123	117	14391	388.4	26.99
BR-10	121.5	118	14337	382.5	26.68
Average Brick (BR-X)	121.7	118.9	14470.13	347.73	24.03
Standard Deviation					2.00
C.O.V (%)					8.32

4.2.4. Flexural Strength

The results of flexural strength of 5 clay bricks is summarized in Table 21. Testing procedure is done according to Section 3.2.2.3. The average flexural strength of the bricks was calculated as 4.53 MPa.

Table 21. Determination of flexural strength.

<i>Sample Name</i>	<i>Width (mm)</i>	<i>Thickness (mm)</i>	<i>Section modulus (W) (mm³)</i>	<i>Ultimate Load (kN)</i>	<i>Bending Moment (N*mm)</i>	<i>Tensile Strength (MPa)</i>
BR-1	118	58	66158.67	21.3	266250	4.02
BR-2	117	56	61152.00	22.6	282500	4.62
BR-3	119	54	57834.00	23.7	296250	5.12
BR-4	122	57	66063.00	25.6	320000	4.84
BR-5	120	59	69620.00	22.5	281250	4.04
Average Brick (BR-X)	119.2	56.8	64094.63	23.14	289250	4.53
Standard Deviation						0.49
C.O.V (%)						10.78

4.2.5 Summary of mechanical properties of bricks

The mechanical properties of bricks are presented in Table 22. As it can be seen from the table, the average compressive and tensile strengths of bricks are 23.76 MPa and 4.53 MPa, respectively.

Table 22. Summary of brick's mechanical properties.

<i>Sample Name</i>	<i>Water Absorption (%)</i>	<i>Porosity (%)</i>	<i>Specific Gravity</i>	<i>Tensile Strength</i>	<i>Compressive Strength</i>
BR-1	20.01	32.6781	2.5433	4.02	21.16
BR-2	19.80	33.0356	2.5753	4.62	22.80
BR-3	20.01	31.6643	2.5932	5.12	23.23
BR-4	20.15	30.4567	2.5840	4.84	25.52
BR-5	20.13	32.8217	2.6224	4.04	24.09
Average Brick (BR-X)	20.02	32.1313	2.5837	4.53	24.03
Standard Deviation	0.14	1.07	0.03	0.49	2.00
C.O.V (%)	0.70	3.34	1.11	10.78	8.32

After determination of most of the main mechanical and physical properties, the bricks are categorized as adequate for severe weathering conditions, SW, according to ASTM C 62-04 [11].

4.3 Mortar Properties

The main characteristics of mortar to be determined were compressive and flexural strength. The testing procedure was done as explained in Section 3.3. In Figure 27 it is shown the flexural and compressive test on mortar. The results are presented in Table 23 and Table 24 where mortar samples were obtained for every wall specimen.



Figure 27. Determination of mortar's flexural and compressive strength.

As it may be seen from the Table 23 and Table 24, the average compressive and tensile strengths of mortars are 5.676 MPa (Series 1), 2.856 MPa (Series 2) and 0.551 MPa (Series 1) and 0.272 MPa (Series 2), respectively. Based on the test results, the types of mortar can be categorized as Type "N" and Type "O" according to ASTM C 270-03 [20].

Table 23. Results of the compressive and flexural strength of mortars from wall panels of Series 1.

<i>Specimen Name</i>	<i>Mean Compressive Strength of Mortar (MPa)</i>	<i>Mean Flexural Strength of Mortar (MPa)</i>
W-01	5.28	0.53
W-02	5.48	0.54
W-03	5.20	0.58
W-04	5.64	0.55
W-05	5.65	0.56
W-06	5.79	0.57
W-07	5.84	0.56
W-08	5.92	0.54
W-09	5.80	0.55
W-10	5.90	0.55
W-11	5.75	0.55
W-12	5.92	0.56
W-13	5.60	0.55
W-14	5.82	0.56
W-15	5.97	0.57
W-16	5.69	0.53
W-17	5.01	0.49
W-18	5.90	0.57
Average	5.676	0.551
Standard Deviation	0.26	0.02
C.O.V (%)	4.66	3.61

Table 24. Results of the compressive and flexural strength of mortars from wall panels of Series 2.

<i>Specimen Name</i>	<i>Mean Compressive Strength of Mortar (MPa)</i>	<i>Mean Flexural Strength of Mortar (MPa)</i>
W-19	3.68	0.36
W-20	2.95	0.29
W-21	2.90	0.28
W-22	2.95	0.28
W-23	2.95	0.28
W-24	3.06	0.29
W-25	3.06	0.29
W-26	2.61	0.25
W-27	2.81	0.27
W-28	2.81	0.27
W-29	2.80	0.26
W-30	2.80	0.26
W-31	2.81	0.27
W-32	2.76	0.26
W-33	2.65	0.25
W-34	2.44	0.23
W-35	2.33	0.22
W-36	2.88	0.27
W-37	3.02	0.29
Average	2.856	0.272
Standard Deviation	0.27	0.03
C.O.V (%)	9.48	10.37

4.4 Masonry Compressive Strength Results

Determination of masonry assemblage compression strength was done according to Section 3.4. As it can be seen from Figure 28, the cracks have propagated in both mortar joints and bricks. The average compressive strength of the prism was found to be 10.68 MPa. As expected, the masonry assemblage compressive strength was greater than the mortar's and smaller than the bricks' individual compressive strength. The results of 13 tested prisms are presented in Table 25.



Figure 28. Determination of masonry assemblage compressive strength.

Table 25. Results of the compressive strength of masonry assemblage.

<i>Prism Name</i>	<i>Length (mm)</i>	<i>Width (mm)</i>	<i>Height (mm)</i>	<i>Load (kN)</i>	<i>h_p/t_p</i>	<i>Correction Factor</i>	<i>Compressive Strength (MPa)</i>
P-1	245	251	208	523.9	0.83	1.5	12.779
P-2	238	249	202	458.3	0.81	1.5	11.600
P-3	245	253	196	409.7	0.77	1.3	8.593
P-4	242	259	205	408.9	0.79	1.3	8.481
P-5	246	255	211	513.6	0.83	1.5	12.281
P-6	246	255	208	472.1	0.82	1.5	11.289
P-7	241	253	199	432.9	0.79	1.3	9.230
P-8	242	253	202	417.9	0.80	1.5	10.238
P-9	246	249	205	453.6	0.82	1.5	11.108
P-10	243	251	208	434.6	0.83	1.5	10.688
P-11	242	259	205	516.3	0.79	1.3	10.709
P-12	243	249	205	408.6	0.82	1.5	10.113
P-13	241	253	199	548.6	0.79	1.3	11.697
Average (P-X)	243	253	204	461.46			10.68
Standard Deviation							1.330
C.O.V (%)							12.45

4.5 Diagonal Compression Tests Results

The diagonal compression test was performed according to the procedure explained in Section 3.5. In total, 52 diagonal compression tests were performed on 38 specimens of 1.2m x 1.2m x 0.25m dimensions, made of type “N” and type “O” mortars.

It was observed that the strengthened wall failed in a more ductile manner in comparison to the control specimen. Hair-like cracks started at the strengthening layer, which is the first element that absorbs all the loads at the beginning. After the jacket has yielded, cracks formation becomes evident, widening of the cracks is seen and the load is carried by the brick masonry wall.

The cracks developed in the unreinforced wall panels were exclusively in the mortar joints including the entire thickness along the compressed diagonal. On the other hand, in the panels which were tested prior or after cracking, this reinforcing technique showed a substantial effectiveness.

4.6 Failure modes (crack pattern)

The exact crack pattern of a heterogeneous structure can be hardly predicted. As described in Section 2.5, the failure mode is closely dependent upon mortar and bricks' properties. As the mortar joints happen to be weakest link in masonry assemblage, and as the load is applied diagonally, the crack propagation may be predicted to occur diagonally along the mortar layers. Nevertheless, predicting exactly at which course of mortar layer is almost impossible.

In this section, all the failure modes of the tested specimens are presented. The experimental results showed that all the tested specimens presented a similar failure mode, mainly characterized by a step-like crack along one of the diagonals. Nevertheless, crack propagation, maximum deformation as well as ultimate load carrying capacity of the panel was observed to be closely dependent upon the mortar type and reinforcing or repairing technique.

4.6.1 Plain walls (W-X)

The unstrengthened wall panels had a similar failure mode; it was observed that cracking occurred along the compressed diagonal, predominantly through the mortar joints in a diagonal step pattern. Nevertheless, in some cases, sliding along the mortar bed joints, following by diagonally extended cracks was observed (Figure 29). The overall failure mode can be categorized as tension failure followed by shear-sliding along the compressed diagonal in a step-like pattern.

The panels of Series 1, W-01, W-03, W-05 and W-19 exhibited similar failure modes. Shear sliding started at the third course from top of the panel, continued horizontally along the bed joint at an approximate length of 500 mm, and then propagated in a diagonal step-like pattern exclusively through the mortar joints.

The remaining plain panels exhibited a step-like pattern along the compressed diagonal. Even in those cases, the cracks occurred in the mortar joints.

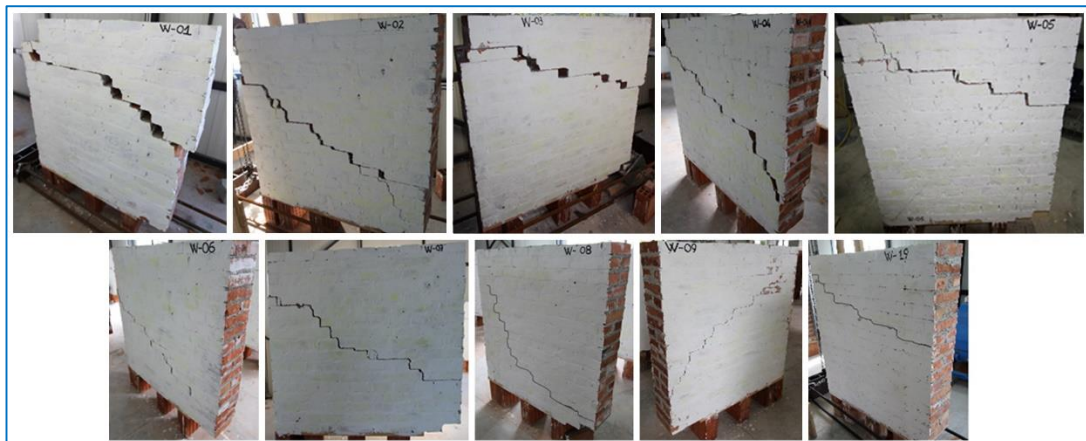


Figure 29. Failure mode of Plain walls of Series 1.

As it may be seen from Figure 30, all the plain wall panels of Series 2, made of type “O” mortar, exhibited a step-like diagonal crack, with a failure in the mortar joints, mainly due to the considerably low strength of the mortar.



Figure 30. Failure mode of Plain walls of Series 2.

4.6.2 Ferrocement jacketing reinforced panels (W-X-FC)

The W-X-FC panels while loading, hair-like cracks were observed, mainly in the compressed diagonal. From the tests, it was observed no splitting in the head or bed joints. The total failure of the wall after the reinforcing ferrocement-plastering layer yielded, is attributed to the loss of bond between the plastering layer and the wall (Figure 31). The connection failure is the main cause of loss of adhesion of the strengthening layer that caused the overall failure of the panels.

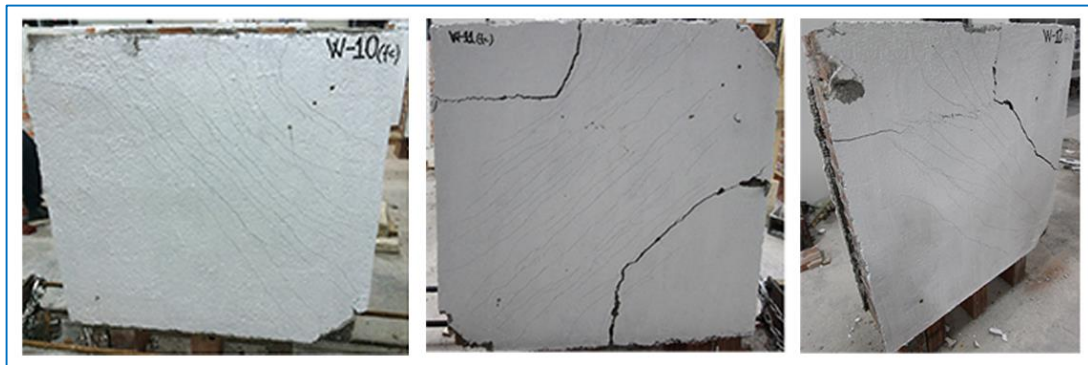


Figure 31. Failure mode of Ferrocement jacketing strengthened wall panels of Series 1.

In W-11-FC apart from the diagonal and hair-like cracks that were developed in the plaster layer, after exceeding the materials' resisting capacities, due to high tensile stresses, connection failure was observed, which resulted in thick radial cracks around

the unloaded upper and bottom edges of the panel. In W-12-FC panel, connection failure resulted in debonding of the mesh reinforced plaster layer.

The crack pattern for the reinforced panels of Series 2 is very similar to Series 1 (Figure 32).



Figure 32. Failure mode of Ferrocement jacketing strengthened wall panels of Series2.

Despite the various final cracks of the panels, it was observed that the reinforcing layer had quite a satisfactory behavior with respect to the strengthened panel. Until the ultimate strength was reached, no debonding of the mesh and wall panel was observed. For such a composite structure, made of heterogeneous and anisotropic material, the most important properties are ductility and shear strength (discussed in detail in Section 4.8), thus, in such a case, the performance of this technique is deemed successful.

4.6.3 Polypropylene reinforced wall panels (W-X-PP)

All the wall panels of Series 1 and Series 2 exhibited the same failure mode characterized by a deep crack along the compressed diagonal, followed by some other cracks parallel to it (Figure 33 and Figure 34).



Figure 33. Failure mode of polypropylene reinforced mortar strengthened wall panels of Series 1.

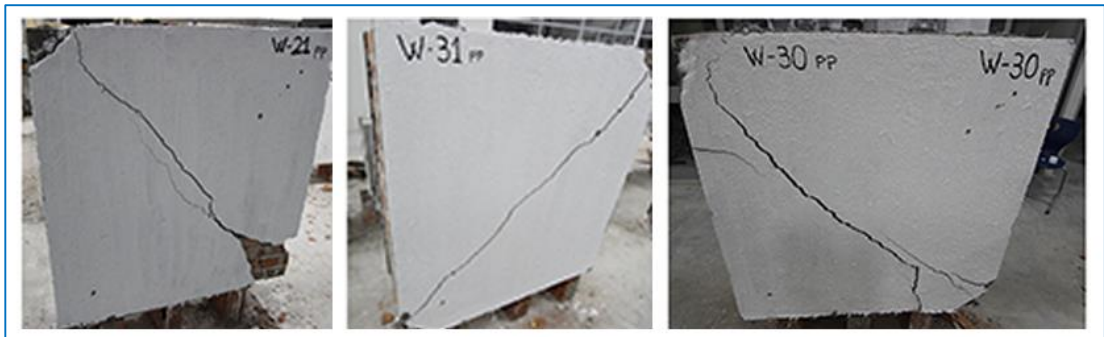


Figure 34. Failure mode of polypropylene reinforced mortar strengthened wall panels of Series 2.

4.6.4 G-FRP reinforced panels (W-X-GFRP)

In G-FRP reinforced wall panels, a clear splitting crack along the compressed diagonal was observed in all three specimens (Figure 35). The mesh yielded in all these cases indicating that this technique was properly applied. The first crack developed in the compressed diagonal. With increasing of the load, the cracks grew bigger until yielding strength of mesh is reached.



Figure 35. Failure mode of GFRP strengthened wall panels of Series 1.

4.6.5 C-FRP reinforced panels (W-X-CFRP)

The crack pattern of the C-FRP reinforced panels consisted of a step-like pattern along the compressed diagonal. Near the edges of the panel (at the top corner in W-32-CFRP and bottom corner of W-37-CFRP), rupture of C-FRP strip was observed. Additionally, delamination of the reinforcing material due to poor mechanical quality of clay material is observed locally (Figure 36).



Figure 36. Failure mode of C-FRP strengthened wall panels of Series 2.

Occurrence of this phenomena is due to stress distribution after yielding of the panel is achieved; after linear stage, the stress along the compressed diagonal will be distributed in an alternative way, still following the weakest local mortar joint. As a result, a different failure mode may be observed.

4.6.6 Repaired walls with Ferrocement jacketing (W-X-R-FC)

The crack pattern of the ferrocement jacketing repaired panels of both series were similar to the corresponding W-FC reinforced panels. Before failure, after unloading, the diagonal cracks were not visible to the naked eye. Because of this reason, during testing stage, all the developed cracks were marked with a graphite pencil at various loading stages. Apart from the usual cracking mode, debonding of the repairing plaster layer was observed. In Figure 37 and Figure 38 it is presented the failure modes of repaired wall panels of both series.



Figure 37. Failure mode of ferrocement jacketing repaired wall panels of Series 1.



Figure 38. Failure mode of ferrocement jacketing repaired wall panels of Series 2.

4.6.7 Repaired walls with polypropylene (W-X-R-PP)

The cracked panels which were repaired with polypropylene reinforced mortar exhibited similar crack patterns as their homologous polypropylene reinforced panels; a deep diagonal crack along the compressed diagonal followed by smaller parallel cracks (Figure 39 and Figure 40).



Figure 39. Failure mode of polypropylene reinforced mortar repaired wall panels of Series 1.

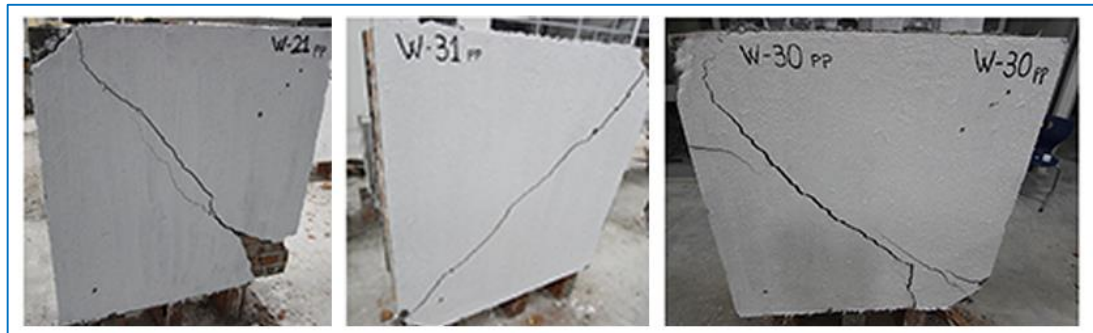


Figure 40. Failure mode of polypropylene reinforced mortar repaired wall panels of Series 2.

4.6.8 C-FRP Repaired panels (W-X-R-CFRP)

The panels repaired with C-FRP failed in a similar pattern as their homologous reinforced panels. Due to excessive tensile stresses, rupture of the wrap attached along the unloaded diagonal was observed (Figure 41). Additionally, delamination of the C-FRP strips was seen. The cracks propagated diagonally and only some locally crushed brick were observed.



Figure 41. Failure mode of C-FRP repaired wall panels of Series 2.

4.6.9 Summary of failure modes

All the tested specimen exhibited similar failure modes; cracking occurred predominately through the mortar joints, and the failure was associated with the development a stair-like crack along the diagonal. The overall response of the panels can be categorized as a diagonal tension failure followed by shear sliding along the cracked diagonal stepped joints.

4.7 Shear stress-strain response

The shear stress-strain response is presented in Figure 42 - Figure 53. For all the wall panels, the experimental curve was approximately linear prior to crack initiation, followed by a nonlinear portion of the curve up to the maximum strength. This similar behavior was also observed in other studies [51] [54] [68] [95].

The curves are plotted to a scale of a maximum strain, ϵ_{max} , 0.005 which corresponds to a drift of 0.5% (which is the allowable drift limit for design of masonry structures, as it is explained in details in Section 0 where the maximum allowable drift ranges between 0.5-0.6%) considered to be an optimum value where the comparisons of all 52 experiments may be presented.

4.7.1 Series 1

The plain wall panels of both series are very brittle, and the stress-strain response is very short. The plain panels of each series are grouped according to their latter usage; three plain panels (used as control panels), three pre-cracked panels that were repaired using polypropylene and three pre-cracked panels that were repaired using ferrocement (Figure 42).

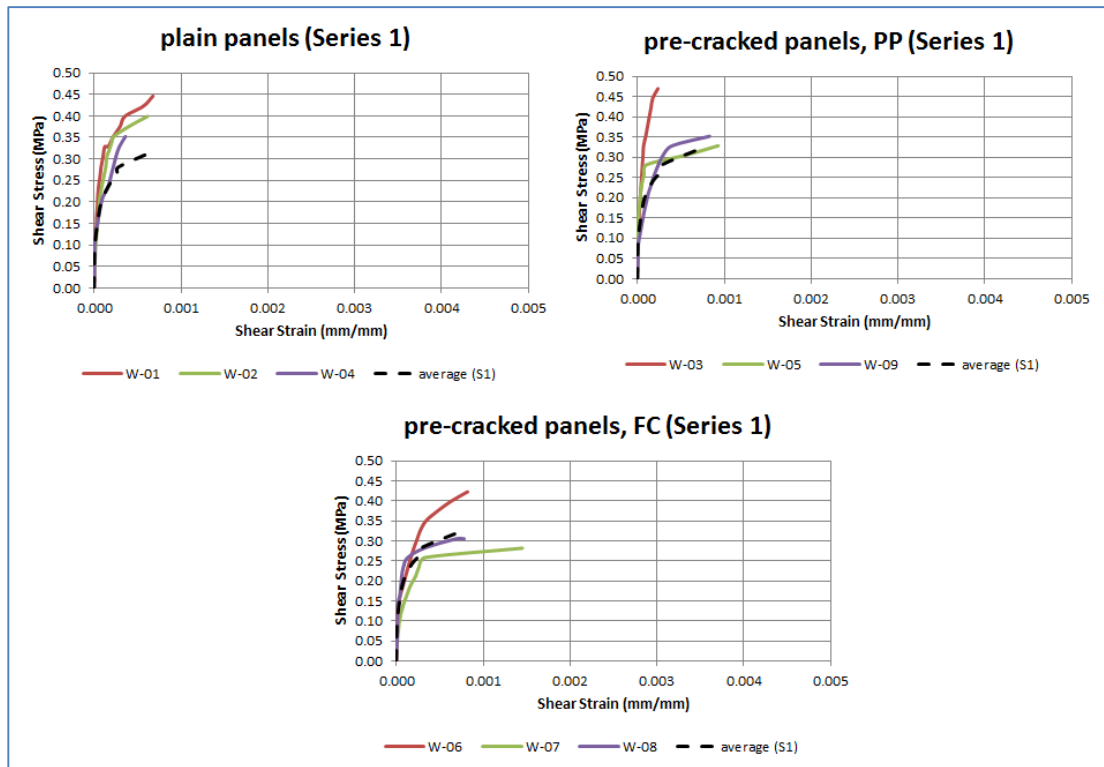


Figure 42. Stress-strain response of plain wall panels of Series 1.

As it may be seen from Figure 43, the repaired panel, W-03, if compared to other cases, exhibited inconsiderable improvement in both shear strength and deformation capacity. This fact may be explained by the inhomogeneous and anisotropic nature of masonry. The effect of the pre-damaged cracks may have caused loss of integrity of the units not only along the main diagonal but also in the mortar joints parallel to it. In Figure 29, it may be seen that the failure of W-03 was done at the third course of the bricks also characterized by a sliding failure.

Nevertheless, the capacity of W-03(R)-PP was still increased, even though not at a considerable amount when compared to other panels.

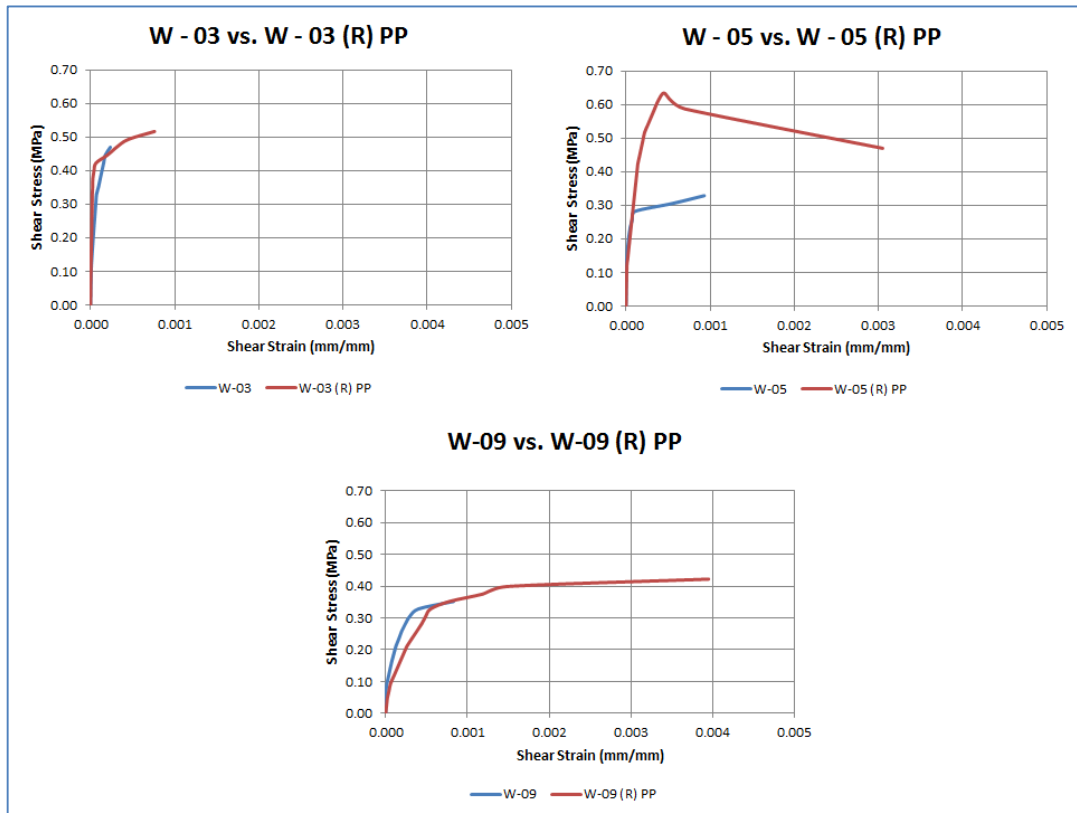


Figure 43. Stress-strain response of polypropylene repaired panels vs. plain wall panels of Series 1.

In Figure 44 are presented the stress-strain diagrams of the ferrocement jacketing repaired panels compared to their homologous pre-cracked panel. As it may be seen from the graphs, after repair, there is a considerable improvement of ductility and shear strength of the repaired panels.

The stress-strain response of the panels strengthened with ferrocement jacketing is presented in Figure 45. All the three walls exhibited higher shear stress and deformation capacities when compared to the plain panels indicating a more ductile behavior. The plastic deformation has extended and can be clearly seen.

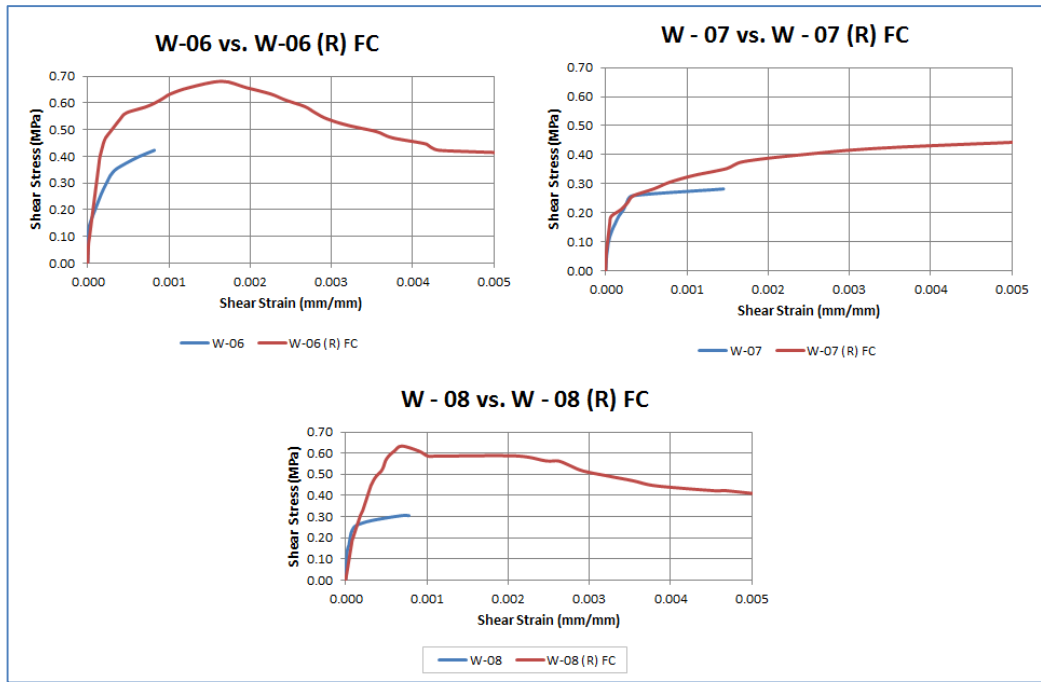


Figure 44. Stress-strain response of ferrocement jacketing repaired panels vs. plain wall panels of Series 1.

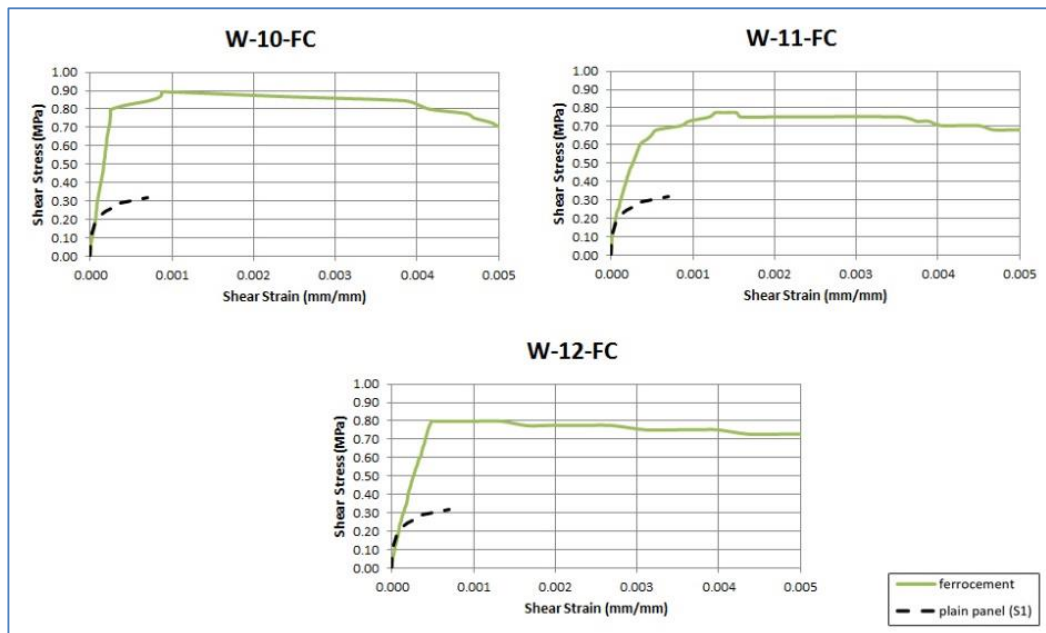


Figure 45. Stress-strain response of ferrocement jacketing reinforced wall panels of Series 1.

The stress-strain response of polypropylene strengthened panels is short (Figure 46), indicating a very brittle behavior of the panels. Nevertheless, the shear strength is observed to be considerably higher when compared to the plain panels of the same group.

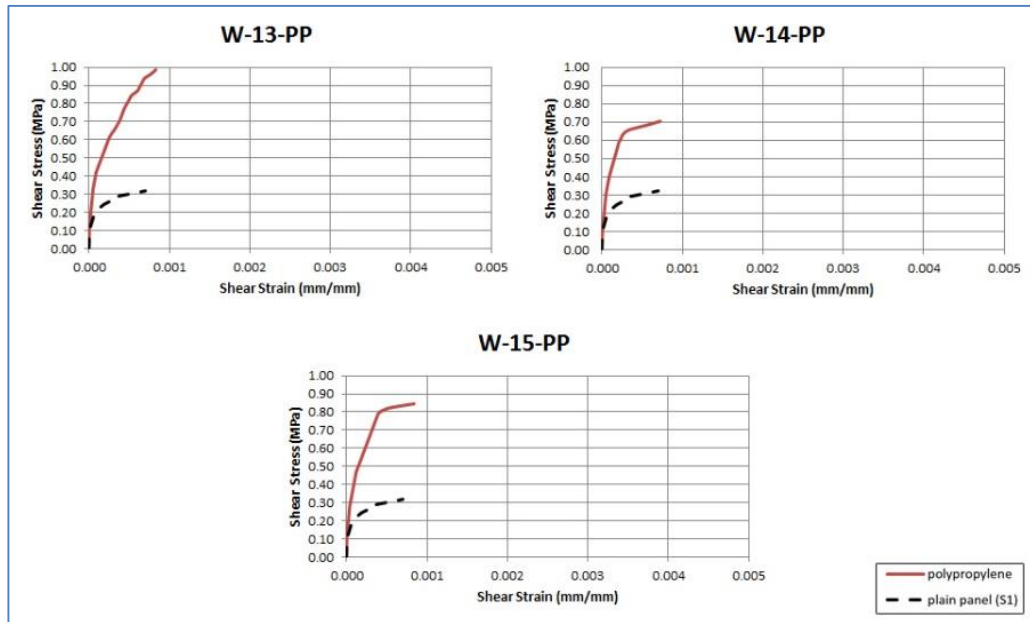


Figure 46. Stress-strain response of polypropylene reinforced wall panels of Series 1.

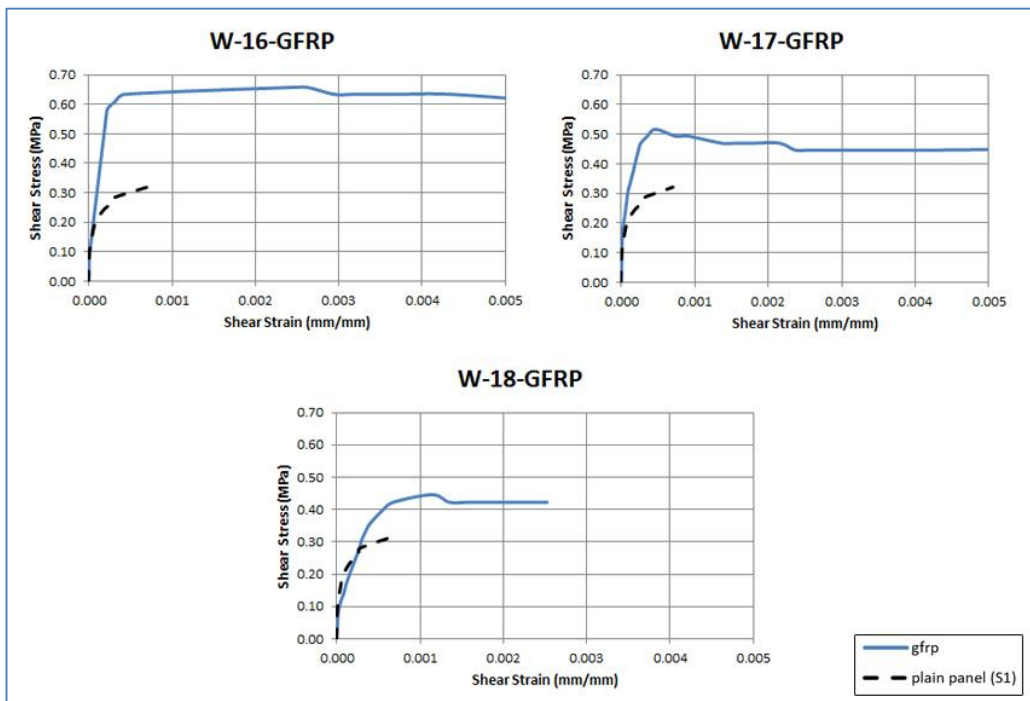


Figure 47. Stress-strain response of G-FRP reinforced wall panels of Series 1.

As it can be seen from Figure 47, the G-FRP reinforced panels, W-16 and W-17 exhibited considerably higher shear stresses and strains, whereas W-18, had an increase but at a lower rate.

In Figure 48, it is presented a summary of the stress-strain diagrams of the reinforced panels of Series 1 having as a reference the diagram of the average of the plain panels. Every group of the reinforced panels exhibits a similar trend among each other, considerably higher than the plain panels.

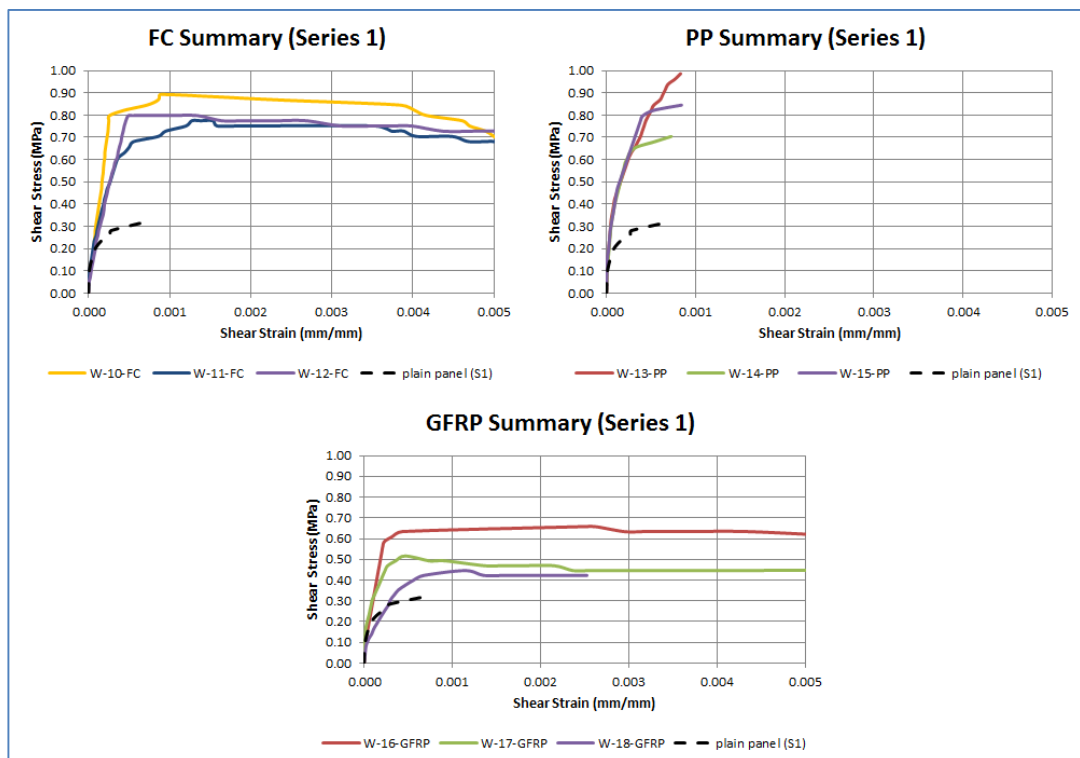


Figure 48. Summary of reinforced wall panels of Series 1.

As it may be seen from Figure 49, from all the wall panels of Series 1, ferrocement jacketing reinforced panels exhibited the highest stress and strain increase. Polypropylene reinforced panels showed a considerably high strength, but lacked ductility. The brittle failure mode can be easily seen from the graph, where the maximum strain, 0.005, does not even exceed the plain wall panels, which on the other hand, as expected, exhibited the lowest strength. G-FRP reinforced panels showed lower strength, but larger deformation ability when compared to polypropylene.

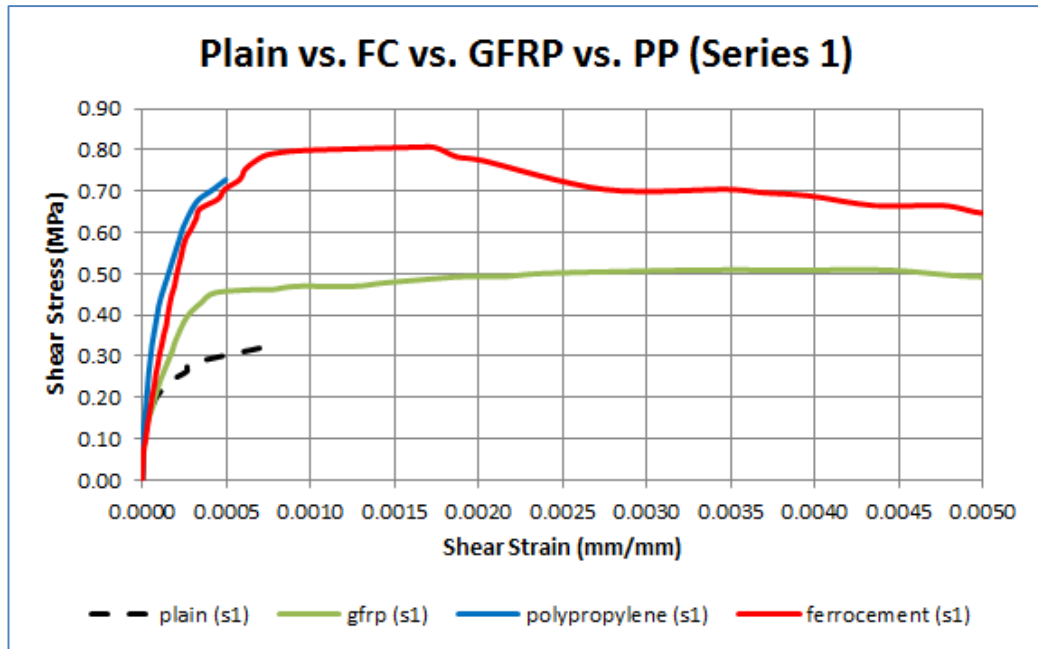


Figure 49. Comparison of strengthening techniques for panels of Series 1.

4.7.2 Series 2

The plain panels of Series 2 exhibited similar behavior with the ones of Series 1. Nevertheless, as it may be seen from Figure 50, they were more ductile, but had a lower ultimate shear strength.

For all the panels of Series 2, due to higher ductility, the limiting strain value was selected to be 0.012 (instead of 0.005 that was for Series 1).

The panels repaired with polypropylene exhibited similar behavior. The stress-strain diagram of W-25 (R)-PP has a shorter extension along the strain axis when compared to the other two panels. The main reason of this behavior may be the limited deformation capacity of the pre-cracked panel which was almost two times lower than the other two plain panels (W-24 and W-26) (Figure 51).

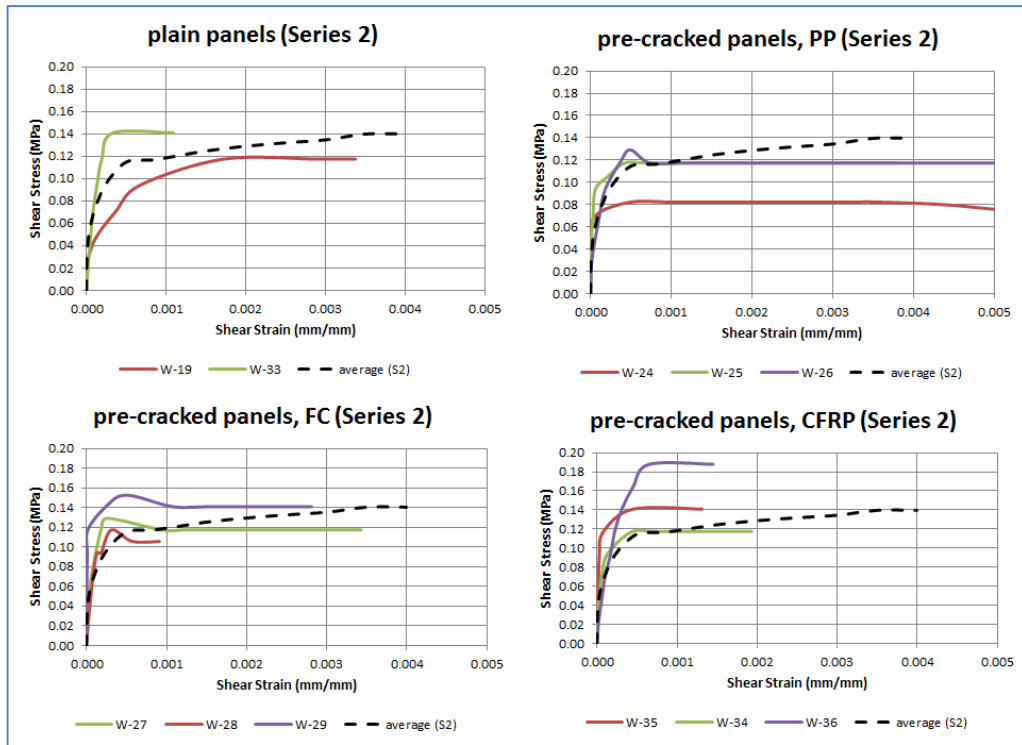


Figure 50. Stress-strain response of plain wall panels of Series 2.

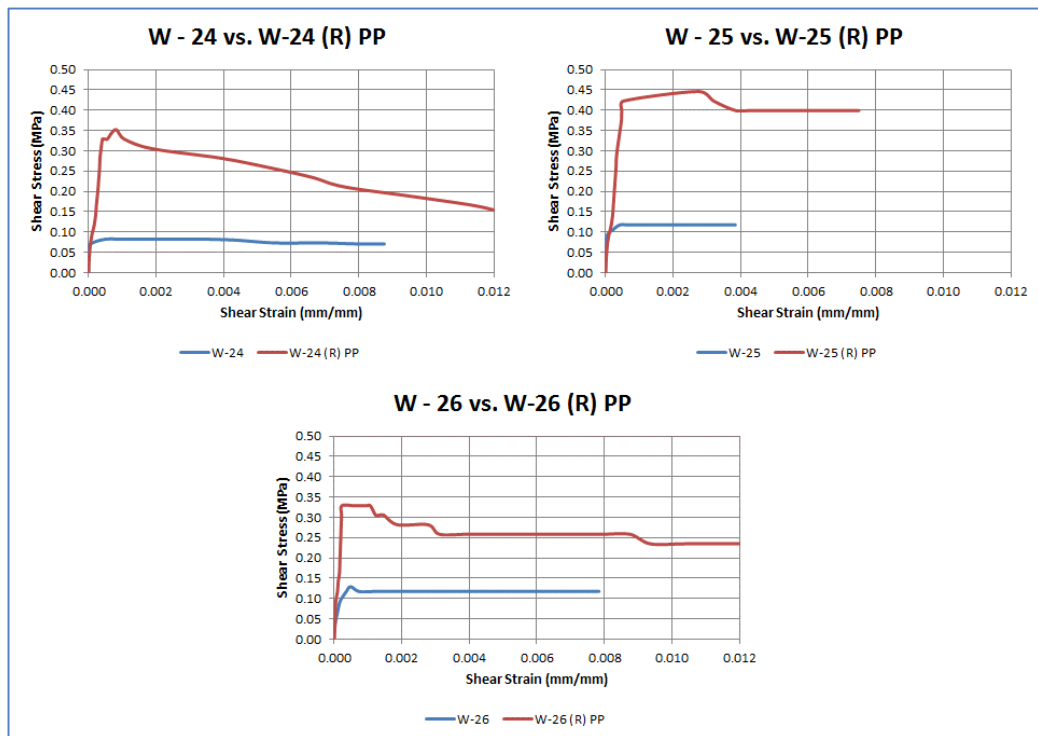


Figure 51. Stress-strain response of polypropylene repaired wall panels of Series 2.

The stress-strain diagrams of the panels repaired using ferrocement jacketing were similar, too. When compared to the plain specimen, increase of shear resistance and maximum strain was noticeable. From this group, W-28 (R)-FC had the smallest improvement. From the graph, it is seen that the strain was 0.008 which is smaller than the other two panels. This phenomenon may be explained due to the very brittle behavior of the pre-cracked panel W-28 (Figure 52).

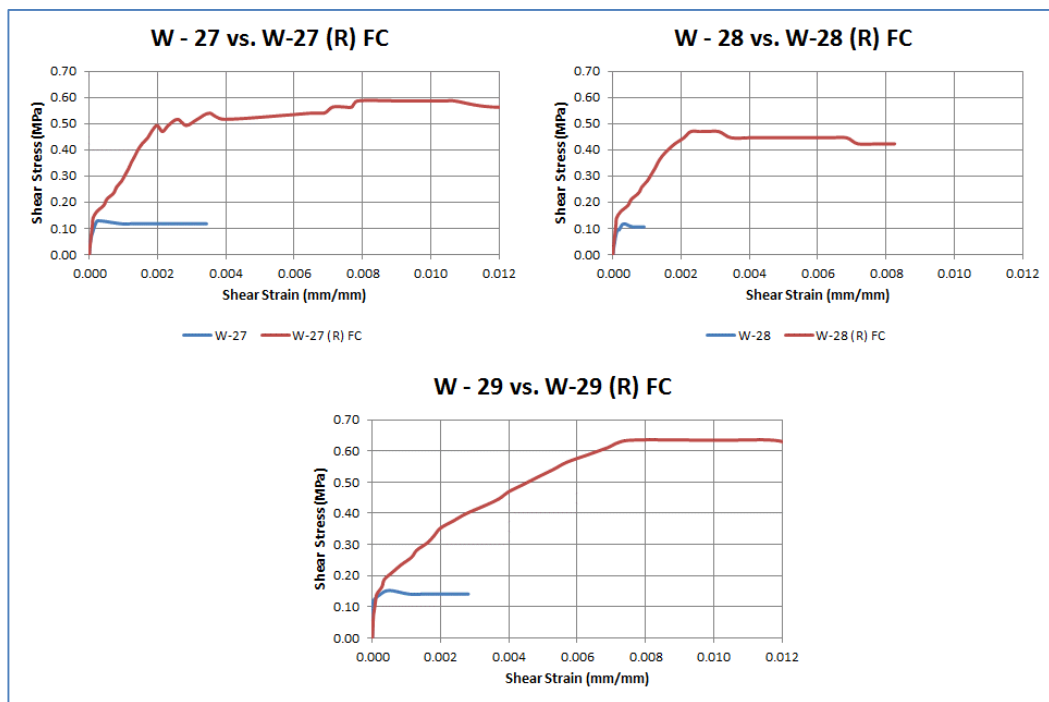


Figure 52. Stress-strain response of ferrocement jacketing repaired wall panels of Series 2.

The stress-strain diagrams of the group of the repaired panels using C-FRP is summarized in Figure 53. All the three panels' mechanical parameters are increased at a similar rate.

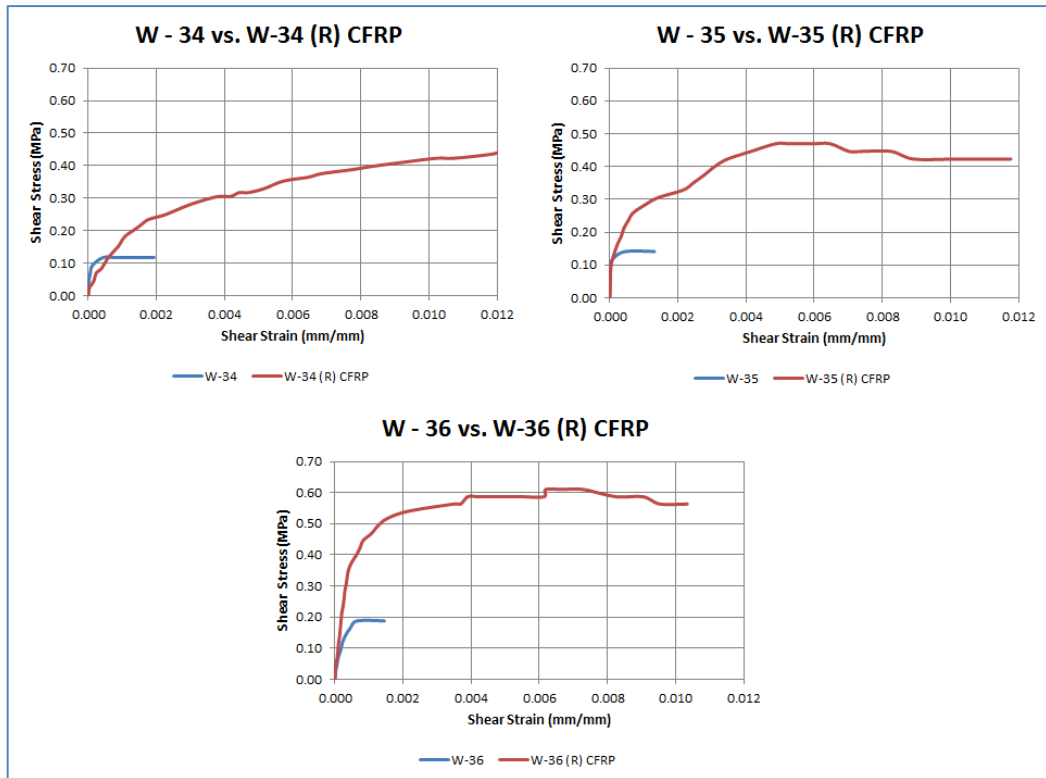


Figure 53. Stress-strain response of C-FRP repaired reinforced wall panels of Series 2.

All the three ferrocement jacketing reinforced panels exhibited both shear stress and strain increase. As it may be seen from Figure 54, deformation capacity of these panels is increased considerably.

As it can be seen from Figure 55, all the three reinforced panels exhibit higher shear strength, but the shear strain of W-30-PP and W-31-PP is smaller than the average strain of the plain wall panels of Series 2. This phenomenon can be explained by the brittle failure of all these three specimens.

The stress-strain diagrams of C-FRP reinforced panels presented in Figure 56, describes a similar trend of both panels; increased ductility and shear strength when compared to the average of the plain panels.

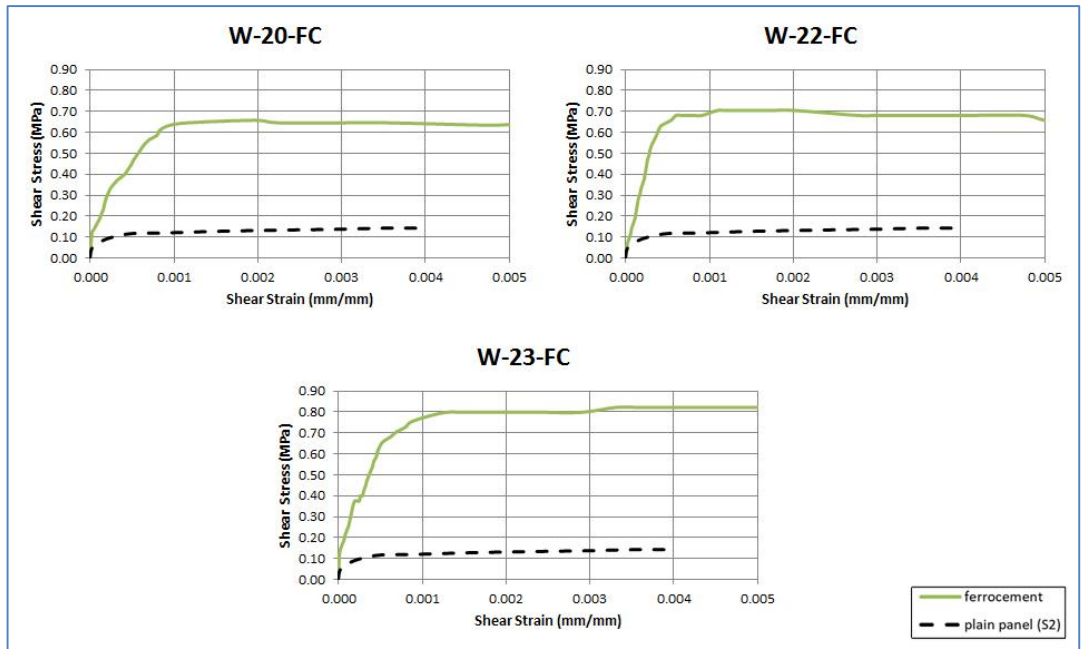


Figure 54. Stress-strain response of ferrocement jacketing reinforced wall panels of Series 2.

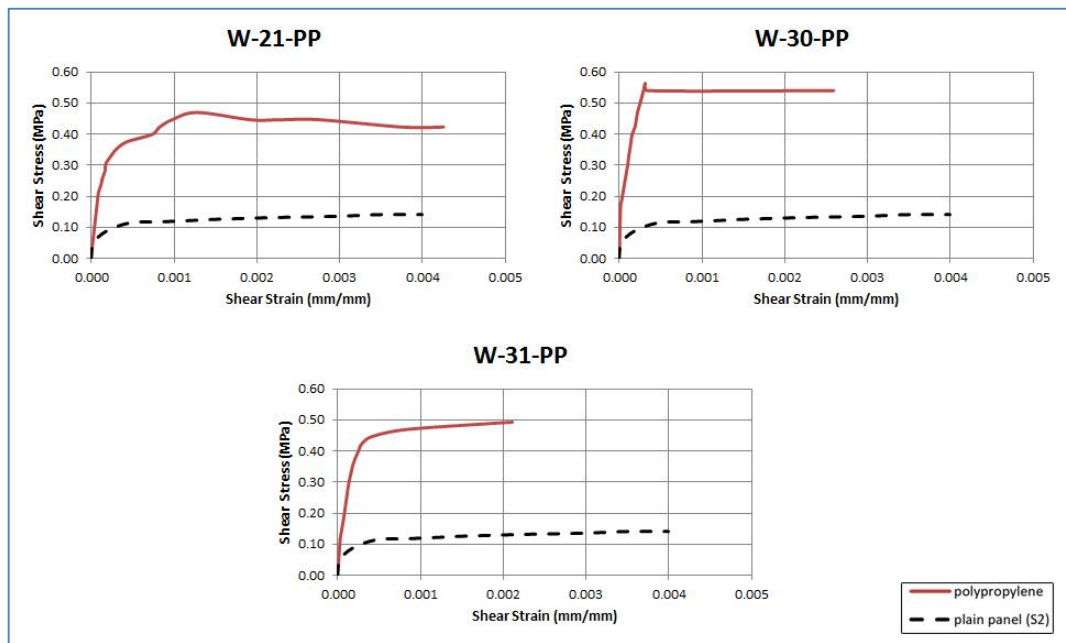


Figure 55. Stress-strain response of polypropylene reinforced wall panels of Series 2.

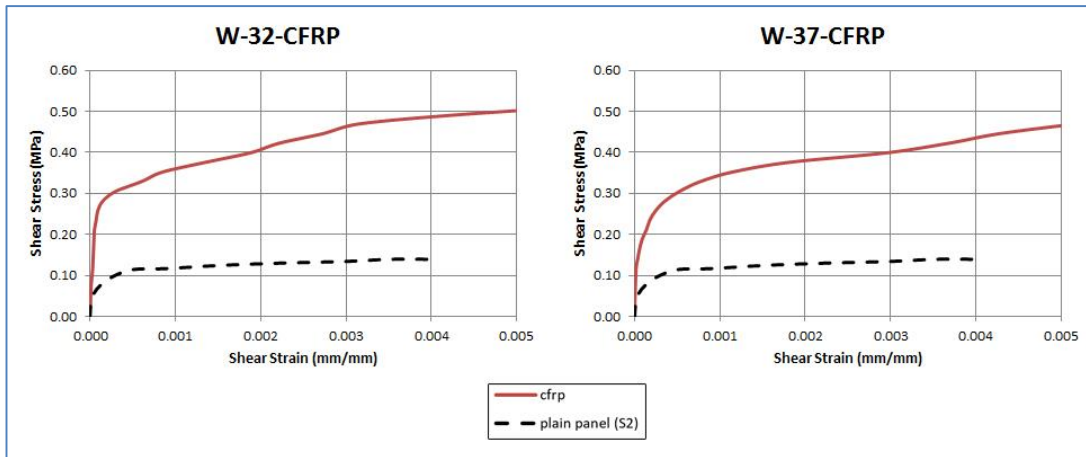


Figure 56. Stress-strain response of C-FRP reinforced wall panels of Series 2.

Figure 57 presents a summary of the shear stress-strain diagrams of the three strengthening techniques of Series 2 having as a reference the average of the plain panels of this series. The maximum strain value was increase from 0.005 to 0.012 in order to have a better perspective related to the deformation capacity of each case.

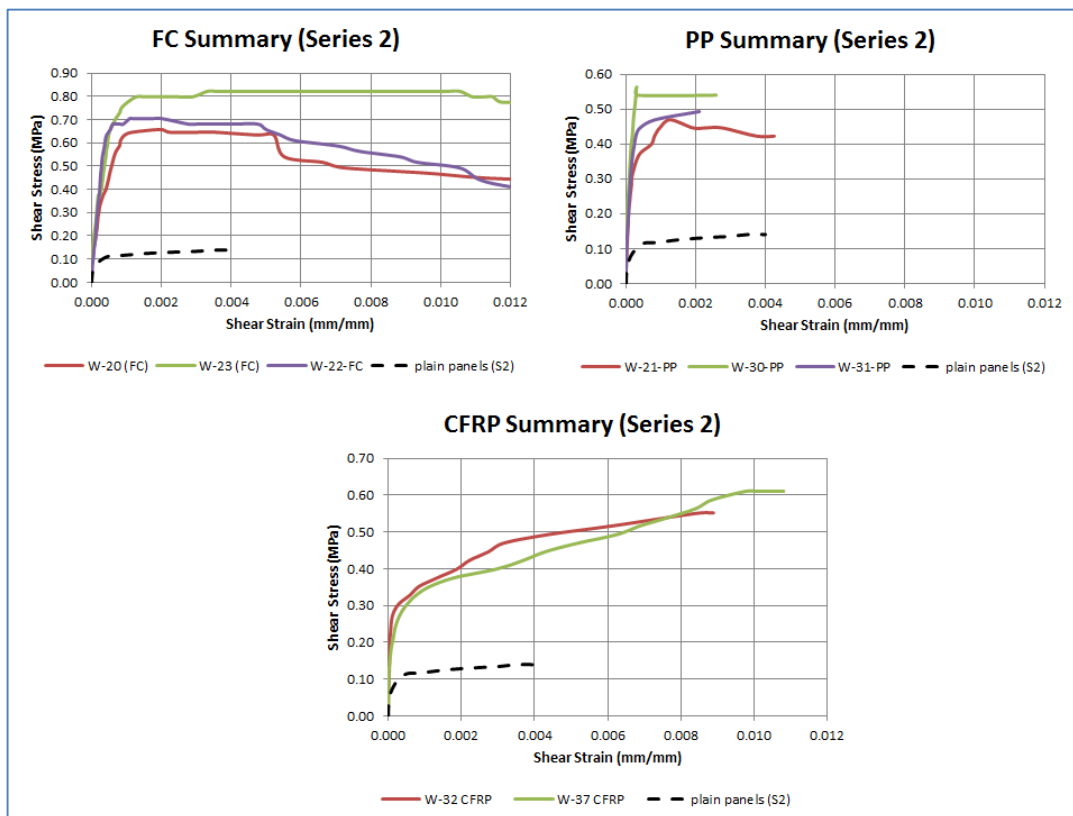


Figure 57. Summary of reinforced wall panels of Series 2.

It is obvious that the panels reinforced using ferrocement jacketing achieved higher strength and a more ductile behavior.

In Figure 58, it is presented the comparison of the average stress-strain diagrams of the strengthening techniques together with the plain panel of Series 2. Ferrocement jacketing exhibits the highest ductility, followed by C-FRP and polypropylene. In the case of the latter one, despite the high shear strength, deformation capacity was limited.

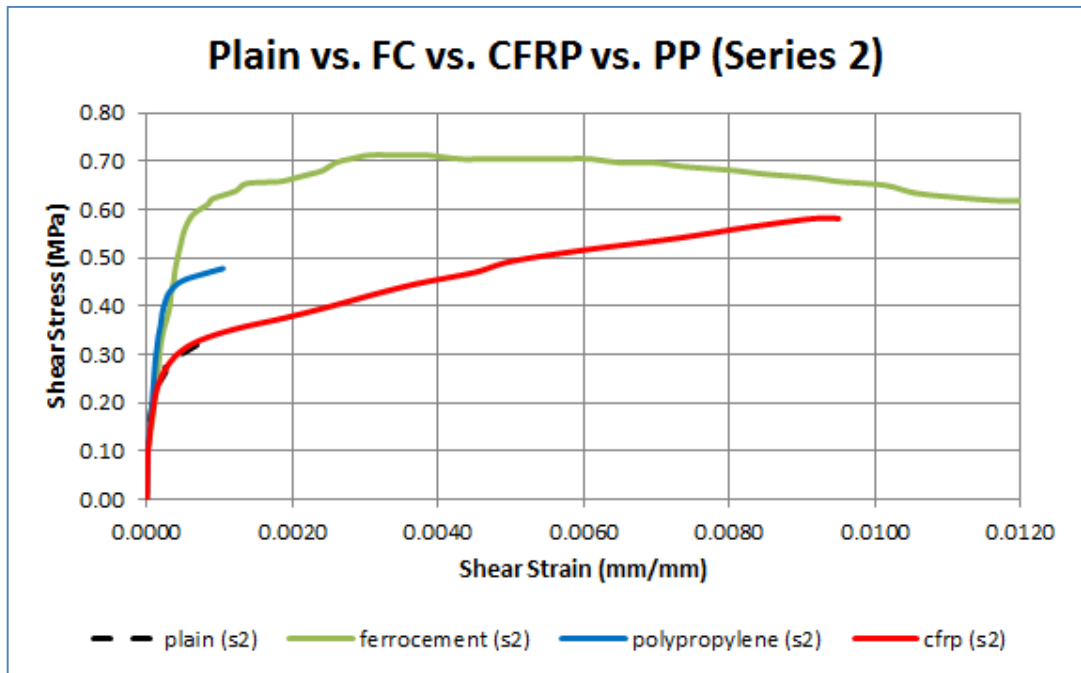


Figure 58. Comparison of strengthening techniques for panels of Series 2.

4.8 Shear Strength, Stiffness, Ultimate drift and Ductility

Another parameter to be taken into consideration while analyzing the behavior of URM is the ultimate drift and ductility. As mentioned in previous chapters, in case of an earthquake, due to seismic shaking, URM buildings are subjected to lateral loads which impose the structure lateral deformation. Ductility is defined as the ability of a material to deform without rupture, or in case of URM buildings, the ability of the structure to deform without collapsing.

The change in stiffness was observed usually for load values close to the ultimate load, as the first crack develops but it cannot expand due to the presence of the external reinforcement.

Stress-strain curve starts with a steep slope indicating the linear stage of masonry, whereas the second stage indicates the plastic phase and it is almost horizontal that usually started after the cracks became visible to naked eye. In this stage, the degraded stiffness can be observed.

4.8.1 Plain Wall Panels

For the panels of Series 1, the average shear strength was 0.364 MPa, with a maximum value of 0.470 MPa occurring at W-03 and a minimum value of 0.282 MPa occurring at W-08. A summary of mechanical parameters of plain wall panels of Series 1 is presented in Table 26.

The average drift was calculated to be 0.115%, with a maximum value of 0.150% occurring at W-07 and a minimum of 0.024% occurring at W-03.

As it is inferred from Table 27, the panels of Series 2, exhibited lower shear strengths compared to their homologous panels of Series 1. The average value was 0.142 MPa, where W-36 reached a maximum of 0.189 MPa and W-24 reached the minimum strength of 0.082 MPa. The average ultimate drift was computed as 0.344% with a maximum of 0.901% occurring at W-28 and a minimum of 0.131% at W-35.

Table 26. Summary of mechanical parameters for plain wall panels of Series 1.

<i>Wall panel</i>	<i>P_{max} (kN)</i>	<i>v_{max} (MPa)</i>	<i>δ (%)</i>	<i>G (MPa)</i>	<i>E (MPa)</i>
W-01	189.316	0.446	0.068	656.176	1640.441
W-02	169.388	0.399	0.062	643.919	1609.798
W-03	199.280	0.470	0.024	1958.833	4897.083
W-04	149.460	0.352	0.036	978.333	2445.833
W-05	139.496	0.329	0.093	353.495	883.737
W-06	179.352	0.423	0.082	515.488	1288.720
W-07	119.568	0.282	0.150	187.880	469.700
W-08	129.532	0.305	0.078	391.359	978.397
W-09	149.460	0.352	0.083	424.373	1060.934
Average (W-S1)	154.442	0.364	0.115	616.999	1542.496

Table 27. Summary of mechanical parameters for plain wall panels of Series 2.

<i>Wall panel</i>	<i>P_{max} (kN)</i>	<i>v_{max} (MPa)</i>	<i>δ (%)</i>	<i>G (MPa)</i>	<i>E (MPa)</i>
W-19	49.820	0.117	0.338	34.615	86.538
W-24	34.874	0.082	0.876	9.361	23.402
W-25	49.820	0.177	0.384	46.094	115.234
W-26	54.802	0.129	0.784	16.454	41.135
W-27	54.802	0.129	0.343	37.700	94.249
W-28	49.820	0.177	0.910	19.451	48.626
W-29	64.766	0.153	0.281	54.448	136.121
W-33	59.784	0.141	0.109	129.358	323.394
W-34	49.820	0.177	0.193	91.710	229.275
W-35	59.784	0.141	0.131	107.902	269.756
W-36	79.712	0.189	0.145	130.099	325.247
Average (W-S2)	54.802	0.142	0.344	70.384	173.960

4.8.2 Ferrocement jacketing reinforced panels (W-FC)

The panels reinforced with ferrocement jacketing of Series 1 resulted in an average shear strength of 0.822 MPa with a maximum value of 0.892 MPa and minimum of 0.775 MPa. The average ultimate drift was calculated to be 0.692% with a maximum value of 0.890% and a minimum of 0.512% (Table 28). The average ultimate diagonal

load was 348.740 kN; with a maximum of 378.632 kN occurring at W-10-FC and minimum of 328.812 kN at W-11-FC.

Table 28. Summary of mechanical parameters for ferrocement jacketing reinforced panels of Series 1.

<i>Wall panel</i>	<i>P_{max} (kN)</i>	<i>v_{max} (MPa)</i>	<i>δ_u (%)</i>	<i>G (MPa)</i>	<i>E (MPa)</i>
W-10-FC	378.632	0.892	0.512	174.238	435.596
W-11-FC	328.812	0.775	0.675	114.800	287.000
W-12-FC	338.776	0.798	0.890	89.708	224.270
Average (W-S1-FC)	348.740	0.822	0.692	126.249	315.622

The panels of Series 2 exhibited lower shear strength; an average of 0.728 MPa with a maximum value of 0.822 MPa and a minimum 0.657 MPa occurring at W-20-FC. On the other hand, the ultimate drift levels were considerably higher, with an average of 2.286%; maximum value of 2.676% at W-22-FC and minimum 1.872% at W-20-FC (Table 29). The average ultimate diagonal load was lower when compared to Series 1; 308.844 kN, with a maximum of 348.70 kN at W-23-FC and a minimum of 278.992 kN at W-20-FC.

Table 29. Summary of mechanical parameters for ferrocement jacketing reinforced panels of Series 2.

<i>Wall panel</i>	<i>P_{max} (kN)</i>	<i>v_{max} (MPa)</i>	<i>δ_u (%)</i>	<i>G (MPa)</i>	<i>E (MPa)</i>
W-20-FC	278.992	0.657	1.872	35.122	87.806
W-22-FC	298.920	0.704	2.676	26.325	65.813
W-23-FC	348.740	0.822	2.311	35.563	88.907
Average (W-S2-FC)	308.884	0.728	2.286	32.337	80.842

4.8.3 Polypropylene Reinforced wall panels

As described in Table 30 and Table 31, polypropylene reinforced panels exhibited higher ultimate loads and shear strength; 358.704 kN and 0.845 MPa, respectively. The highest shear strength was achieved by W-13-PP with a value of 0.986 MPa and the lowest value was recorded from W-21-PP, 0.470 MPa. On the other hand, W-21-PP achieved the highest ultimate drift, 0.426% and W-13-PP, the lowest one with only 0.073%. It was observed that the panels of Series 1 had higher shear and elastic moduli, indicating that were stiffer than panels of Series 2.

Table 30. Summary of mechanical parameters for polypropylene reinforced panels of Series 1.

<i>Wall panel</i>	<i>P_{max} (kN)</i>	<i>v_{max} (MPa)</i>	<i>δ_u (%)</i>	<i>G (MPa)</i>	<i>E (MPa)</i>
W-13-PP	418.488	0.986	0.096	1027.396	2568.490
W-14-PP	298.920	0.704	0.073	2428.966	5870.000
W-15-PP	358.704	0.845	0.084	1006.310	2515.774
Average (W-S1-PP)	358.704	0.845	0.084	1487.557	3651.421

The polypropylene reinforced panels of Series 2 exhibited lower ultimate loads and shear strengths when compared to Series 1; 215.887 kN and 0.509 MPa, respectively. The highest shear strength was achieved by W-30-PP with a value of 0.564 MPa and the lowest value was recorded from W-21-PP, 0.470 MPa. The highest ultimate drift was achieved by W-21-PP of 0.426% and the lowest one with only 0.211% by W-31-PP.

Table 31. Summary of mechanical parameters for polypropylene reinforced panels of Series 2.

<i>Wall panel</i>	<i>P_{max} (kN)</i>	<i>v_{max} (MPa)</i>	<i>δ_u (%)</i>	<i>G (MPa)</i>	<i>E (MPa)</i>
W-21-PP	199.280	0.470	0.426	110.373	275.932
W-30-PP	239.136	0.564	0.259	217.592	543.981
W-31-PP	209.244	0.493	0.211	233.706	584.265
Average (W-S2-PP)	215.887	0.509	0.299	187.224	468.060

4.8.4 G-FRP reinforced wall panels (W-X-GFRP)

G-FRP reinforced wall panels achieved average values of shear strengths and ultimate drifts as 0.538 MPa and 0.637%, respectively. These panels exhibited a more ductile behavior but lower shear strengths when compared to polypropylene reinforced panels.

Table 32. Summary of mechanical parameters for G-FRP reinforced panels of Series 1.

<i>Wall panel</i>	<i>P_{max} (kN)</i>	<i>v_{max} (MPa)</i>	<i>δ_u (%)</i>	<i>G (MPa)</i>	<i>E (MPa)</i>
W-16-GFRP	278.992	0.675	0.684	98.716	246.791
W-17-GFRP	209.244	0.493	0.975	50.589	126.472
W-18-GFRP	189.316	0.446	0.253	176.413	441.032
Average (W-S1-GFRP)	225.851	0.538	0.637	108.573	271.431

The maximum values were recorded on W-16-GFRP, 0.675 MPa and on W-17-GFRP as 0.975% and the minimum values of 0.446 MPa and 0.253% both on W-18-GFRP. The summary of the mechanical parameters is presented in Table 32.

4.8.5 C-FRP reinforced wall panels (W-X-CFRP)

As presented in Table 33, C-FRP reinforced panels exhibited average shear strength and ultimate drifts as 0.582 MPa and 1.351%, respectively. The highest value was reached at W-37-CFRP on ultimate load, shear strength and ultimate drift as 259.064 kN, 0.611 MPa and 1.813%, respectively.

Table 33. Summary of mechanical parameters for C-FRP reinforced panels of Series 2.

<i>Wall panel</i>	<i>P_{max} (kN)</i>	<i>v_{max} (MPa)</i>	<i>δ_u (%)</i>	<i>G (MPa)</i>	<i>E (MPa)</i>
W-32-CFRP	234.154	0.552	0.889	62.136	155.340
W-37-CFRP	259.064	0.611	1.813	33.725	84.312
Average (W-S2-CFRP)	246.609	0.582	1.351	47.930	119.826

4.8.6 Ferrocement jacketing repaired panels (W-X-R-FC)

The repaired panels with ferrocement jacketing for Series 1 and Series 2 exhibited considerable improvement of shear strength and ultimate drifts when compared to their plain counterparts. As it may be seen from Table 34, the average values of ultimate diagonal load, shear strength and ultimate drift are 255.743 kN, 0.603 MPa and 1.366%, respectively. The maximum ultimate load and shear strengths were achieved from W-06-R-FC (288.956 kN and 0.681 MPa), whereas the minimum values were recorded from W-07-R-FC (209.244 kN and 0.493 MPa). Nevertheless, W-07-R-FC achieved the highest ultimate drift of 2.229%.

Table 34. Summary of mechanical parameters for ferrocement jacketing repaired panels of Series 1.

<i>Wall panel</i>	<i>P_{max} (kN)</i>	<i>v_{max} (MPa)</i>	<i>δ_u (%)</i>	<i>G (MPa)</i>	<i>E (MPa)</i>
W-06-R-FC	288.956	0.681	1.075	63.346	158.365
W-07-R-FC	209.244	0.493	2.229	22.123	55.307
W-08-R-FC	269.028	0.634	0.794	79.864	199.660
Average (W-S1-R-FC)	255.743	0.603	1.366	55.111	137.777

Table 35. Summary of mechanical parameters for ferrocement jacketing repaired panels of Series 2.

<i>Wall panel</i>	<i>P_{max} (kN)</i>	<i>v_{max} (MPa)</i>	<i>δ_u (%)</i>	<i>G (MPa)</i>	<i>E (MPa)</i>
W-27-R-FC	249.100	0.587	3.510	16.725	41.813
W-28-R-FC	199.280	0.470	0.785	59.827	149.567
W-29-R-FC	269.028	0.634	2.514	25.219	63.047
Average (W-S2-R-FC)	239.136	0.564	2.270	33.924	84.809

For the Series 2, as it is presented in Table 35, the average values of ultimate diagonal load, shear strength and ultimate drift are 239.136 kN, 0.564 MPa and 2.270%, respectively. The maximum ultimate load and shear strengths were achieved from W-

29-R-FC (269.028 kN and 0.634 MPa), whereas the minimum values were recorded from W-28-R-FC (199.280 kN and 0.470 MPa).

4.8.7 Polypropylene repaired wall panels (W-X-R-PP)

The results of polypropylene repaired panels are presented in Table 36 and Table 37. The average shear strength for Series 1 was 0.525 MPa and 0.376 MPa for Series 2, whereas the ultimate drift levels were considerably low 0.261% (Series 1) and 1.400% (Series 2). W-05-R-PP achieved the highest ultimate load of 269.028 kN, consequently the highest shear strength of 0.634 MPa. The lowest ultimate load and shear strength were recorded in W-26-R-PP of 139.496 kN and 0.329 MPa, respectively. W-03-R-PP achieved the lowest ultimate drift of 0.076%.

Table 36. Summary of mechanical parameters for polypropylene repaired panels of Series 1.

<i>Wall panel</i>	<i>P_{max} (kN)</i>	<i>v_{max} (MPa)</i>	<i>δ_u (%)</i>	<i>G (MPa)</i>	<i>E (MPa)</i>
W-03-R-PP	219.208	0.517	0.076	680.566	1701.414
W-05-R-PP	269.028	0.634	0.305	207.902	519.754
W-09-R-PP	179.352	0.423	0.401	105.411	263.529
Average (W-S1-R-PP)	222.529	0.525	0.261	331.293	828.232

Table 37. Summary of mechanical parameters for polypropylene repaired panels of Series 2.

<i>Wall panel</i>	<i>P_{max} (kN)</i>	<i>v_{max} (MPa)</i>	<i>δ_u (%)</i>	<i>G (MPa)</i>	<i>E (MPa)</i>
W-24-R-PP	149.460	0.352	1.820	19.357	48.393
W-25-R-PP	189.316	0.446	0.750	59.493	148.733
W-26-R-PP	139.496	0.329	1.630	20.168	50.421
Average (W-S2-R-PP)	159.424	0.376	1.400	33.006	82.516

4.8.8 C-FRP repaired panels (W-X-R-CFRP)

C-FRP repaired panels achieved an average ultimate load and shear strength of 215.887 kN and 0.509 MPa and an ultimate drift level of 1.295 %. The results of all panels are summarized in Table 38. W-36-R-CFRP achieved the highest ultimate load and shear strengths of 259.064 kN and 0.611 MPa, whereas the lowest values were recorded in W-34-R-CFRP.

Table 38. Summary of mechanical parameters for C-FRP repaired panels of Series 2.

<i>Wall panel</i>	<i>P_{max} (kN)</i>	<i>v_{max} (MPa)</i>	<i>δ_u (%)</i>	<i>G (MPa)</i>	<i>E (MPa)</i>
W-34-R-CFRP	189.316	0.447	1.673	26.690	66.726
W-35-R-CFRP	199.280	0.470	1.177	39.957	99.892
W-36-R-CFRP	259.064	0.611	1.034	59.121	147.802
Average (W-S2-R-CFRP)	215.887	0.509	1.295	41.923	104.807

4.8.9 Summary of Shear Strength, Stiffness, Ultimate drift and Ductility

The experimental results showed that the shear strength of the panel is strongly dependent upon the mortar type (mortar strength) since in almost all the cases, the cracks propagated through the joints, without damaging the bricks. The ultimate diagonal load and shear resistance of the panels of Series 2 (made of type “O” mortar) is very low when compared with Series 1.

The highest average shear strength was achieved by W-s1-PP, 0.845 MPa which was 2.322 times higher than the average shear strength of the plain panels of Series 1. Additionally, W-s1-PP achieved higher ultimate diagonal load of 358.704 kN. Nevertheless, polypropylene strengthened panels exhibited limited deformation capacity and had a more brittle behavior than the plain panels with an ultimate drift ratio of 0.735.

Table 39. Comparison of the average reinforced techniques vs. plain wall panels of Series 1.

<i>Wall panel</i>	<i>P_{max} (kN)</i>	<i>v_{max} (MPa)</i>	<i>v_{max}/v₀</i>	<i>δ_u (%)</i>	<i>δ_u/δ₀</i>	<i>G (MPa)</i>	<i>E (MPa)</i>
W-X-s1	154.442	0.364	-	0.115	-	616.999	1542.496
W-s1-FC	348.740	0.822	2.257	0.692	6.047	126.249	315.622
W-s1-PP	358.704	0.845	2.322	0.084	0.735	1487.557	3651.421
W-s1-GFRP	225.851	0.538	1.479	0.637	5.566	108.573	271.431
W-s1-R-PP	222.529	0.525	1.441	0.261	2.277	331.293	828.232
W-s1-R-FC	255.743	0.603	1.656	1.366	11.930	55.111	137.777

Ferrocement strengthened panels on the other hand, achieved the second highest value of shear strength, 0.822 MPa and considerably higher ultimate drift ratio of 6.047 times (Table 39). The highest improvement was observed in ferrocement repaired panels (W-s1-R-FC) where the ultimate drift to plain panels' ratio was 11.930.

In Series 2, ferrocement strengthening method was deemed the best one in terms of shear strength and deformation capacity. The average shear strength of 0.728 MPa and the increase in ultimate drift was 5.746 times higher in comparison to the plain panels of Series 2 (Table 40).

Table 40. Comparison of the average reinforced techniques vs. plain wall panels of Series 2.

<i>Wall panel</i>	<i>P_{max} (kN)</i>	<i>v_{max} (MPa)</i>	<i>v_{max}/v₀</i>	<i>δ_u (%)</i>	<i>δ_u/δ₀</i>	<i>G (MPa)</i>	<i>E (MPa)</i>
W-X-s2	54.802	0.142	-	0.334	-	70.384	175.960
W-s2-FC	308.884	0.728	5.111	1.920	5.746	49.018	122.546
W-s2-PP	215.887	0.509	3.573	0.299	0.893	187.224	468.060
W-s2-CFRP	246.609	0.582	4.086	1.351	4.044	47.930	119.826
W-s2-R-PP	159.424	0.376	2.638	1.400	4.190	33.006	82.516
W-s2-R-FC	239.136	0.564	3.957	2.270	6.794	33.924	84.809
W-s2-R-CFRP	215.887	0.509	3.576	1.295	3.875	41.923	104.807

Additionally, as expected, the influence of type of mortar is very high: the panels with type "N" mortar exhibited shear strength 256 % higher than the panels made of type

“O” mortar. In Figure 59 it is presented the comparison of both series for plain, polypropylene and ferrocement reinforced panels.

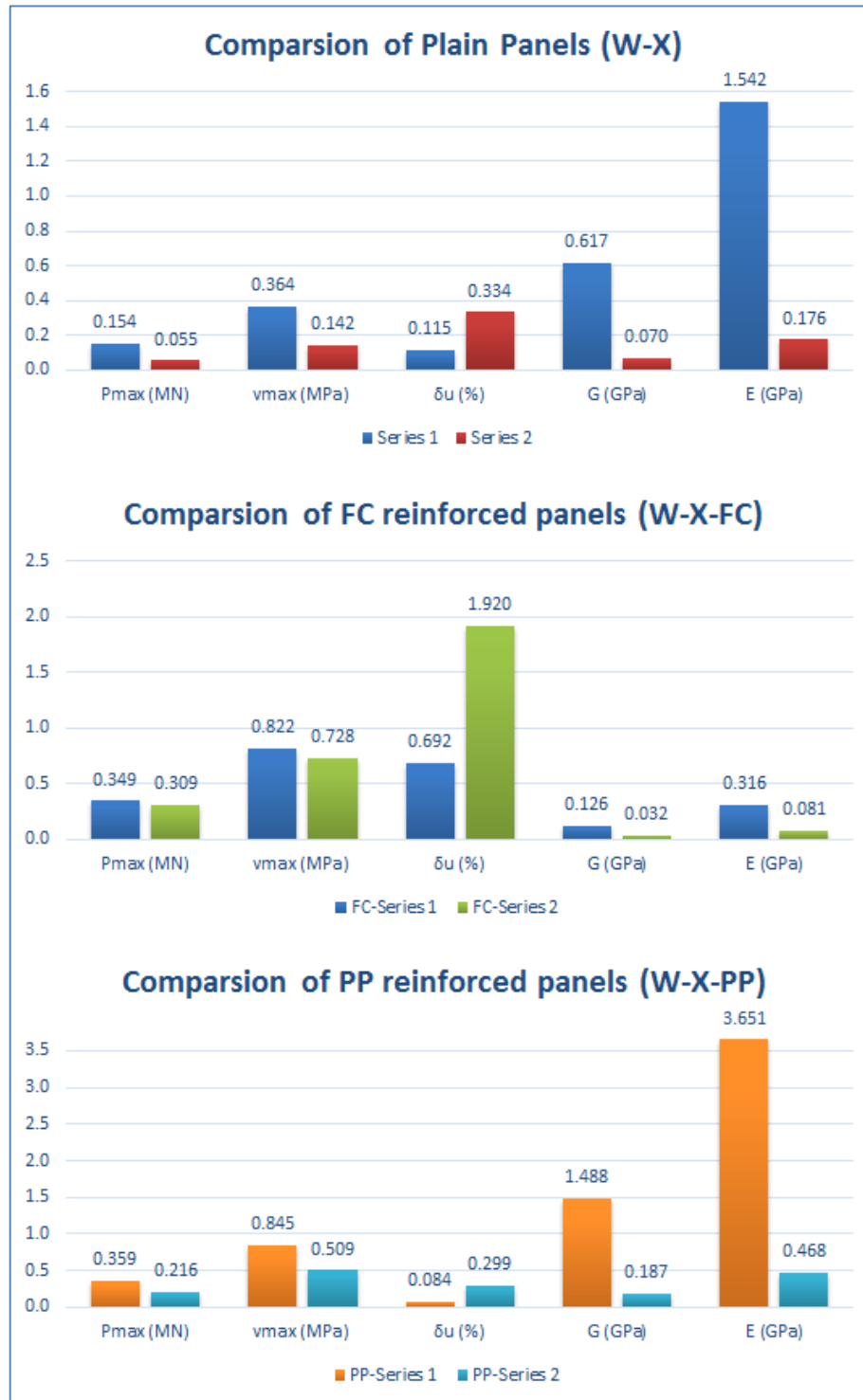


Figure 59. Comparison between panels of Series 1 and Series 2.

4.9 Summary of diagonal compression test

The diagonal compression test results showed that, as expected, the unreinforced panels of both series exhibited a very brittle behavior. The main failure mode occurred predominately through mortar joints and can be categorized as a diagonal tension failure followed by a shear sliding along the cracked diagonal stepped joints. The similar failure modes can be observed in polypropylene, G-FRP and C-FRP reinforced panels with a sharp crack along the loaded diagonal.

Ferrocement jacketing repaired and reinforced panels exhibited a different behavior, where development of hair like cracks was seen prior to main cracks. The overall failure was attributed to the loss of adhesion of the jacketing layer with the panel which resulted in thick radial cracks around the unloaded corners of the panels.

The experimental test results showed that the effect of ferrocement jacketing technique were quite satisfactory in terms of both shear strength and deformation capacity. The reinforced wall panels were much more ductile and stronger than the plain ones. Moreover, when comparing all the techniques, the deformation capacity of ferrocement is the highest.

It was also observed that, as expected, the performance of the wall panels of type “N” mortar (Series 1) was better than the ones made of type “O” mortar (Series 2).

All the repair methods were found to be more influential when applied to low strength mortar. This fact could be explained with the high resistive capacity of the plaster layer.

The main problem that resulted when applying ferrocement jacketing was the anchorage of the mesh to the wall panels. When loading, the pullout of the mesh was observed. Nevertheless, it may be concluded that the strengthening methods performed satisfactory. After removing the plaster layer, it was seen that, after yielding, the bricks were crushed not only along the loaded diagonal.

CHAPTER 5

FINITE ELEMENT MODELLING

5.1. Introduction

In this chapter the finite element model used to simulate the behavior of the specimens is described. Three main panel types were taken into consideration: plain, ferrocement and polypropylene strengthened specimen for Series 1 and Series 2. The FE model was used to help understand and compare the results of the diagonal compression tests described in Section 3.

The nonlinear analysis was conducted using Diana 9.6 commercial software with the cutback based automated incremental procedure. During this analysis, after defining the final loading, the algorithm was taking as few load steps as possible in order to limit the number of steps in iterative procedure. The non-convergence recovery was achieved by decreasing the load step and restarting the calculation in case of a divergence. This procedure consists of Newton Raphson method.

5.2. Modelling procedure

The FE analysis was performed using the software package DIANA 9.6 adopting the simplified micro-modelling approach for modelling of masonry. The software is based on the displacement finite element method.

In order to make a comprehensive comparison of the suggested strengthening methods, the numerical model was the one suggested by Zijl et al. [165]. The modelling of the panels was done using a “*Simplified Modelling Method with Brick Crack Interface*”.

This approach consists of having the bricks and mortar are modelled separately as two different materials using the following elements: for bricks Q8MEM element (isoperimetric, 4-node plane stress, based on linear interpolation and Gauss

integration) with CL12I, an interface element between two lines in a two-dimensional configuration for the brick-joint and brick-crack interfaces (Figure 60) [166]. The mortar joint and the mortar/brick unit interface lumped into a zero thickness a discontinuous interface element that relates the (normal stress σ_n and shear stress τ) to the interface normal displacement u and shear displacement v . The nominal width of the interface is 0.5 mm. In this model there were eight plane stress elements and two interface elements. The mortar joints are the ones where the crack can be developed.

On the other hand, the brick units were modelled with continuum elements with elastic properties that were expanded to maintain the overall geometry of the masonry. At the middle of the brick potential cracking interface elements were used. Additionally, all of the non-linear behavior (cracking, shear sliding and crushing) was modelled in the interface elements.

One of the main reasons of using micro-modelling approach is its ability to reproduce crack patterns and the complete load displacement path of a masonry structure, and its suitability to have better insights for understanding the experimental results.

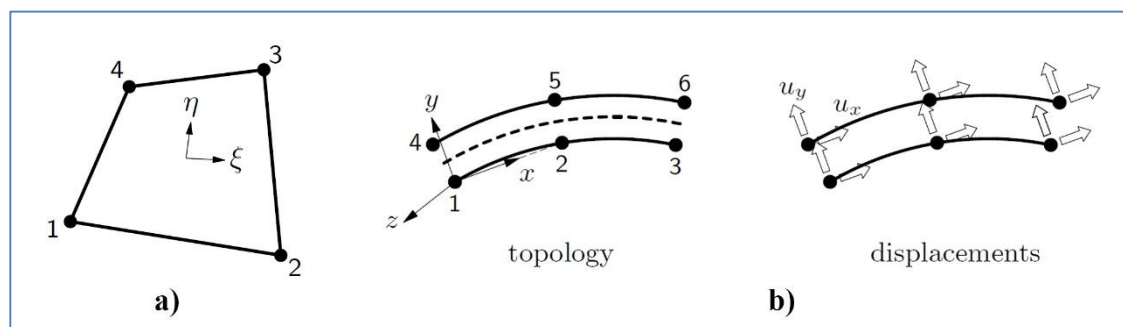


Figure 60. DIANA 9.6 elements used for modelling: a) Q8MEM, plane stress element and b) CL12I, interface element.

5.2.1. Adopted Crack-Shear-Crush (CSC) Interface Material Model

The different modes of failure of masonry such as joint tensile and sliding cracking, diagonal tensile cracking of the brick and masonry crushing, are governed by three main criteria:

- i) Tension cut-off criterion;
- ii) Coulomb friction criterion;
- iii) Elliptical compressive cap criterion represented in (Figure 61).

The interface elements friction and relative displacement vectors are represented by $\sigma = [\sigma \ \tau]^T$ and $\varepsilon = [u \ v]^T$, where σ and u are friction and relative displacement in the normal direction of the interface, whereas τ and v are the friction and relative displacement in the perpendicular direction. The elastic stiffness matrix D , used in the elastic constitutive relationship $\sigma = D\varepsilon$ is defined as:

$$D = \begin{bmatrix} k_n & 0 \\ 0 & k_s \end{bmatrix}$$

where k_n is stiffness in the normal direction, and k_s is stiffness in shear.

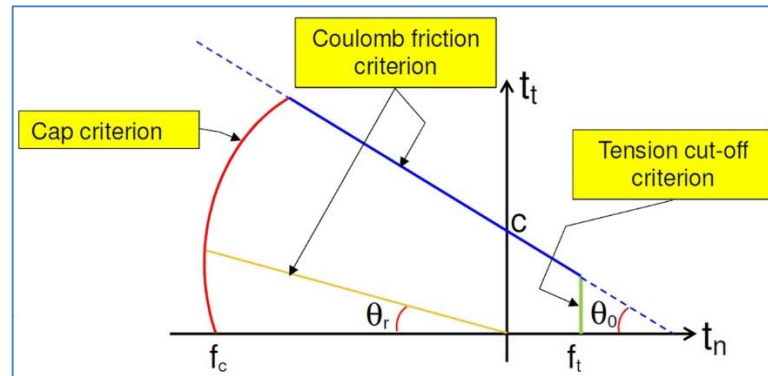


Figure 61. Interface model used in this study [2].

(1) Tension cut-off criterion

$$f_1 = \sigma - \sigma_t, \quad \sigma_t = f_t e^{-\frac{f_t}{\sigma_f} k_1}$$

where σ_t is the tensile strength between brick and mortar, f_t the bond strength, G_f^I mode I fracture energy and k_1 the equivalent plastic strain.

(2) Coulomb-friction criterion for Shear slipping

The Coulomb friction yield/crack initiation criterion is used to define shear-slipping.

At this stage both adhesion softening and friction softening are captured. The shear strength is proportional to the confining pressure with an initial offset (adhesion, c) and the angle of $\tau - \sigma$ with horizontal defines the friction angle, Φ . Cohesion will be zero, when the shear resistance will decrease sufficiently, and the yield surface will be defined as:

$$f_2 = |\tau| + \sigma\Phi - c, \quad c = c_0 e^{-\frac{c_0}{G_f^{II}} k_2}, \quad \Phi = \Phi_0 + (\Phi_r - \Phi_0) \frac{c_0 - c}{c_0}$$

where Φ is the friction coefficient defined as the tangent of the friction angle $\Phi = \tan(\Phi)$, c is the adhesion, Φ_0 and Φ_r are the initial and residual friction coefficients, respectively, G_f^{II} is the mode II fracture energy and k_2 is the equivalent plastic strain [166] [167].

(3) Compressive cap criterion

The yield function for the compression cap, is

$$f_3 = \sigma^2 + C_s \tau^2 - \sigma_C^2$$

where C_s is a parameter that controls shear stress contribution to failure and σ_C^2 the yield value.

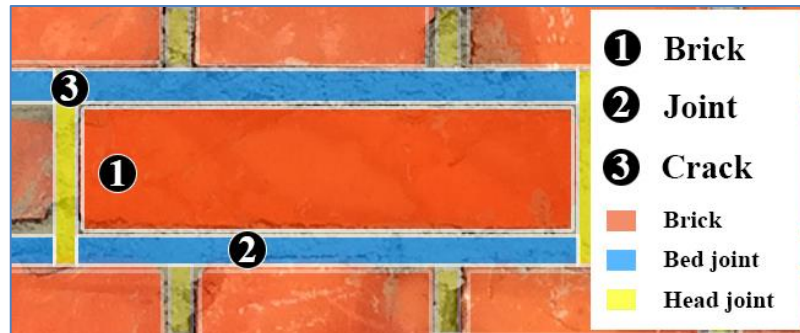


Figure 62. Division of the masonry elements into elements ready for modelling.

5.2.2. FE Model

The model, based on the micro-scale approach, was created in midas FX+ for DIANA 9.6. The mesh of the model was done following three main stages: firstly, the half-brick was created with interface elements to represent the brick crack and the brick joint, then the basic brick was duplicated in order to create the two-brick model with all the interface elements required for simulation. Lastly, the two-brick model was replicated in horizontal and vertical direction in order to achieve the required dimensions of 1.2 x 1.2 m.

5.2.3. Assigning of material properties

As the main aim of the modelling strategy was to investigate and compare the overall performance of the panels, some of the material parameters such as normal stiffness, k_n , shear stiffness, k_s , (obtained by Lourenco [2]) bond strength, f_t , etc. were assumed based on previous literature; Van der Pluijm [168] who conducted an extensive research on determination of mechanical behavior of brick-mortar interfaces where bond strength, f_t , mode I and mode II fracture energies were determined together with some other parameters such as internal friction angle, dilatancy coefficient, etc.

The material in the bricks and brick crack interface were kept as linear indicating that the cracks would be developed only in the mortar joints (as it was clearly seen during the experimental stage of the campaign). The material properties are presented in Table 41.

Table 41. Material properties used for the model [165]

Masonry	Elastic Modulus	E	*	N/mm ²
	Poisson's ratio	ν	0.15	
Cracks	Linear normal stiffness	D ₁₁	1.0 x 10 ⁴	N/mm ³
	Linear tangential stiffness	D ₁₂	1.0 x 10 ³	N/mm ³
Joints	Linear normal stiffness	D ₁₁	83.0	N/mm ³
	Linear tangential stiffness	D ₁₂	36.0	N/mm ³
	Tensile strength	f _t	*	N/mm ²
	Fracture energy	G _f	0.018	N/mm
	Cohesion	c	0.35	N/mm ²
	Friction angle	tan ϕ	0.75	
	Dilatancy angle	tan ψ	0.60	
	Residual friction coefficient	Φ	0.75	
	Confining normal stress for ψ_0	σ_u	-1.3	N/mm ²
	Exponential degradation coefficient	δ	5.0	
	Cap critical compressive strength	f _c	*	N/mm ²
	Shear traction control factor	C _s	9.0	
	Compressive fracture energy	G _{fc}	5.0	N/mm
	Equivalent plastic relative displacement	K _p	0.093	
Fracture energy factor	b	0.05		
* dependent upon the type of the panel.				

Table 42. Variable parameters for each model type.

Panel type	f _c (N/mm ²)	f _t (N/mm ²)	E (N/mm ²)	G (N/mm ²)
Plain (s1)	5.675	0.551	1542	617
Ferrocement (s1)	5.675	0.551	316	126
Polypropylene (s1)	5.675	0.551	3651	1488
Plain (s2)	2.816	0.268	174	70.3
Ferrocement (s2)	2.816	0.268	81	32
Polypropylene (s2)	2.816	0.268	468	109

f_c – compressive strength, f_t – tensile strength, E – modulus of elasticity, G – shear modulus

5.2.4. Boundary constrains and loading

In order to effectively apply the load and to simulate the shear behavior of masonry, the bottom edges of the model were constrained in horizontal and vertical direction, whereas for the top edges, only for vertical direction. Additionally, in order to prevent horizontal deformation of the upper edge, a multi-point constraint was applied.

The loading consists of application of a unit horizontal displacement along the top of the panel which would be transferred uniformly along the entire upper edge due to the multi-point constraint applied earlier (Figure 63).

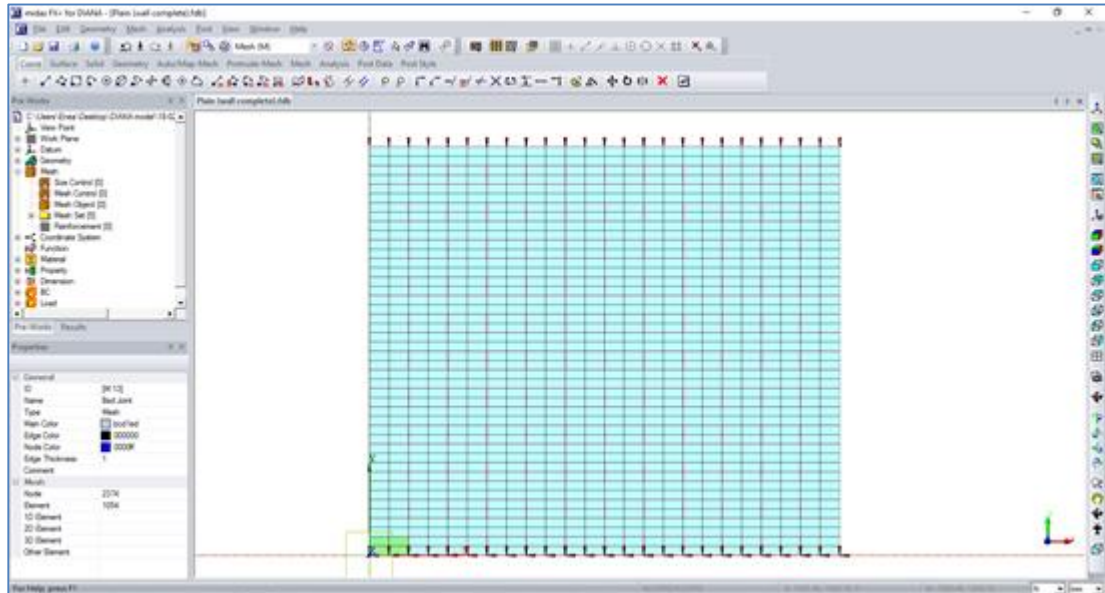


Figure 63. The finished model in midas FX+ for DIANA.

5.2.5. Modelling of strengthened walls

The strengthened panels were modeled using an additional reinforcement layer made of a reinforcement grid (in the case of ferrocement) and a plastering layer in case of polypropylene fibers. The additional reinforcing material properties are summarized in Table 42.

5.3. Analysis results

The analysis results are presented in Table 43 and Table 44. As it can be seen, Series 1 panels exhibited a higher resistance in comparison to the ones of Series 2.

Table 43. Summary of Linear Analysis Results.

	<i>plain - S1</i>	<i>plain - S2</i>	<i>FC-S1</i>	<i>FC-S2</i>	<i>PP-S1</i>	<i>PP-S2</i>
FBXYZ (V)	89.428	22.357	1156.777	131.884	11.921	16.558
	95376.496	23844.124	1444377.843	40005.422	108528.127	43725.000
NXX	-29.609	-13.324	783.485	-	874.477	-
NXY	-29.240	-9.248	-4.594	4.853	-25.934	-16.976
	695.429	227.215	215.986	48.131	742.698	167.060
Principal Stress S3	-2.015	-0.806	-6.400	-1.132	-7.707	-4.370
	-7.054	-2.822	0.000	0.000	0.000	0.000
SXY	-4.511	-	-	-	-	0.136
	0.226	-	-	-	-	-2.073
SXX	-	-	-3.308	-0.138	-9.569	-
	-	-	2.630	0.111	-	-
Mean Stress Nodes	-4.315	-	-2.403	-	-	-
	-2.540	-	2.403	-	-	-
Von Misses Stress	-	-	0.179	-	-	-
	-	-	6.037	-	-	-

“-” the results were too small

Table 44. Summary of nonlinear analysis results.

	<i>plain - S1</i>	<i>plain - S2</i>	<i>FC-S1</i>	<i>FC-S2</i>	<i>PP-S1</i>	<i>PP-S2</i>
FBXYZ (V)	0	0.292	0	0.047	15.613	27.535
	34.000	17.895	27023.743	23334.742	35849.000	22.420
TDtX(V)	-0.151	0.401			-0.092	
	0.181	-1.703			0.162	
Principal Stress S1			5.462	1.152		
Principal Stress S2			-2.204			
			0.689			
Principal Stress S3	-0.275	-0.300	0.000	0.000	0.000	0.000
	-2.748	-2.397	5.044	-4.159	-2.794	-1.886
SXX	0	0	-3.493	-1.000	0	-2.017
	-2.902	-1.443	3.886	0.181	3.147	1.293
SXY		0.103		0.015	1.529	0.104
		-1.196		-0.863	-2.545	-1.517
SYX	0.112		0.004	-2.841		-1.544
	-2.181		-2.223	0.260		-1.178
Von Misses Stress			1.160	0.000		0.011
			3.866	2.234		2.712

PTx	-0.094	-0.249	-1.380	-0.876	-0.163
	0.181	0.301	1.424	0.876	0.236
Mean Stress				0.208	0.476
Nodes				-1.521	-2.154

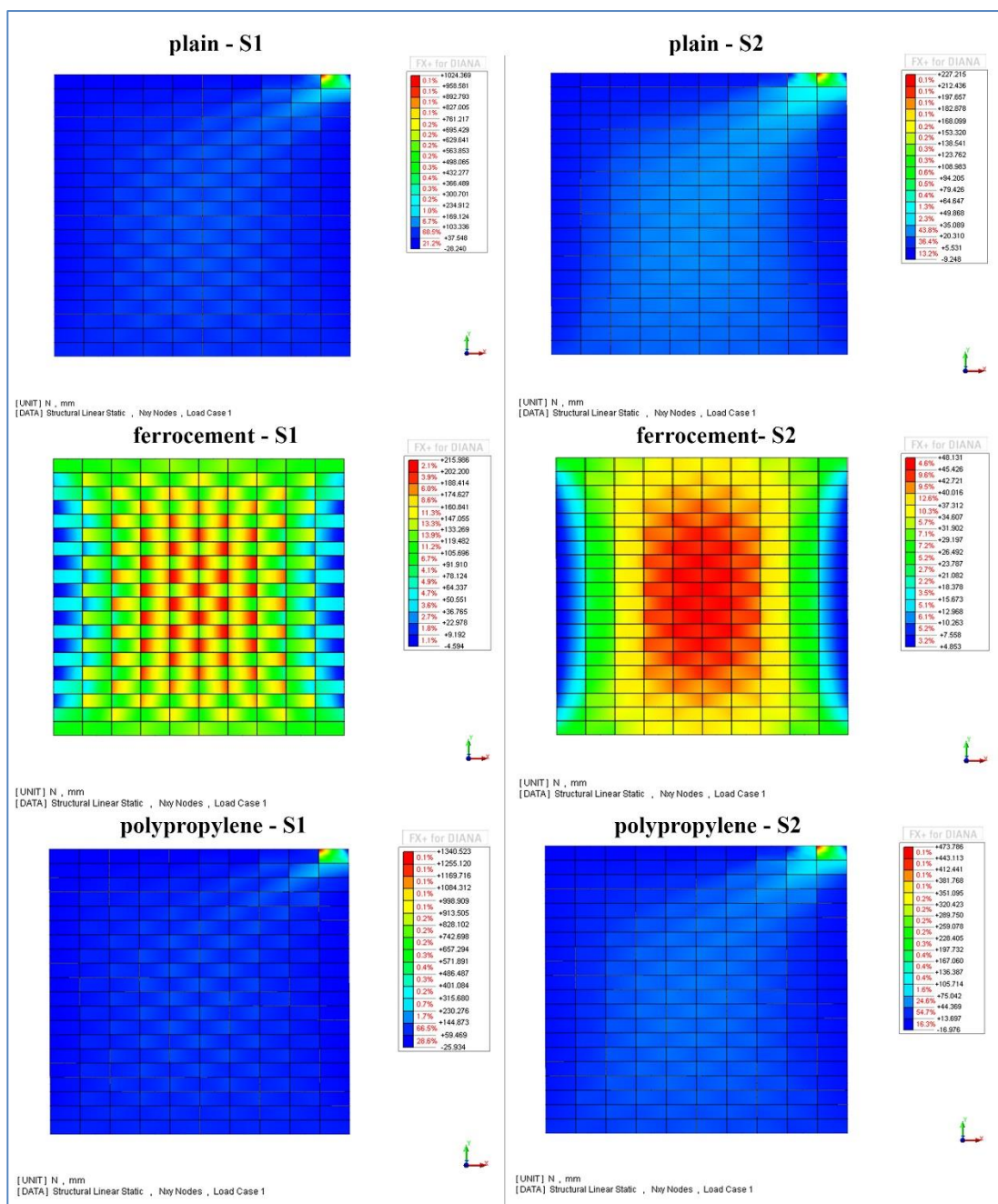


Figure 64. Comparison of Nxy stresses after linear analysis.

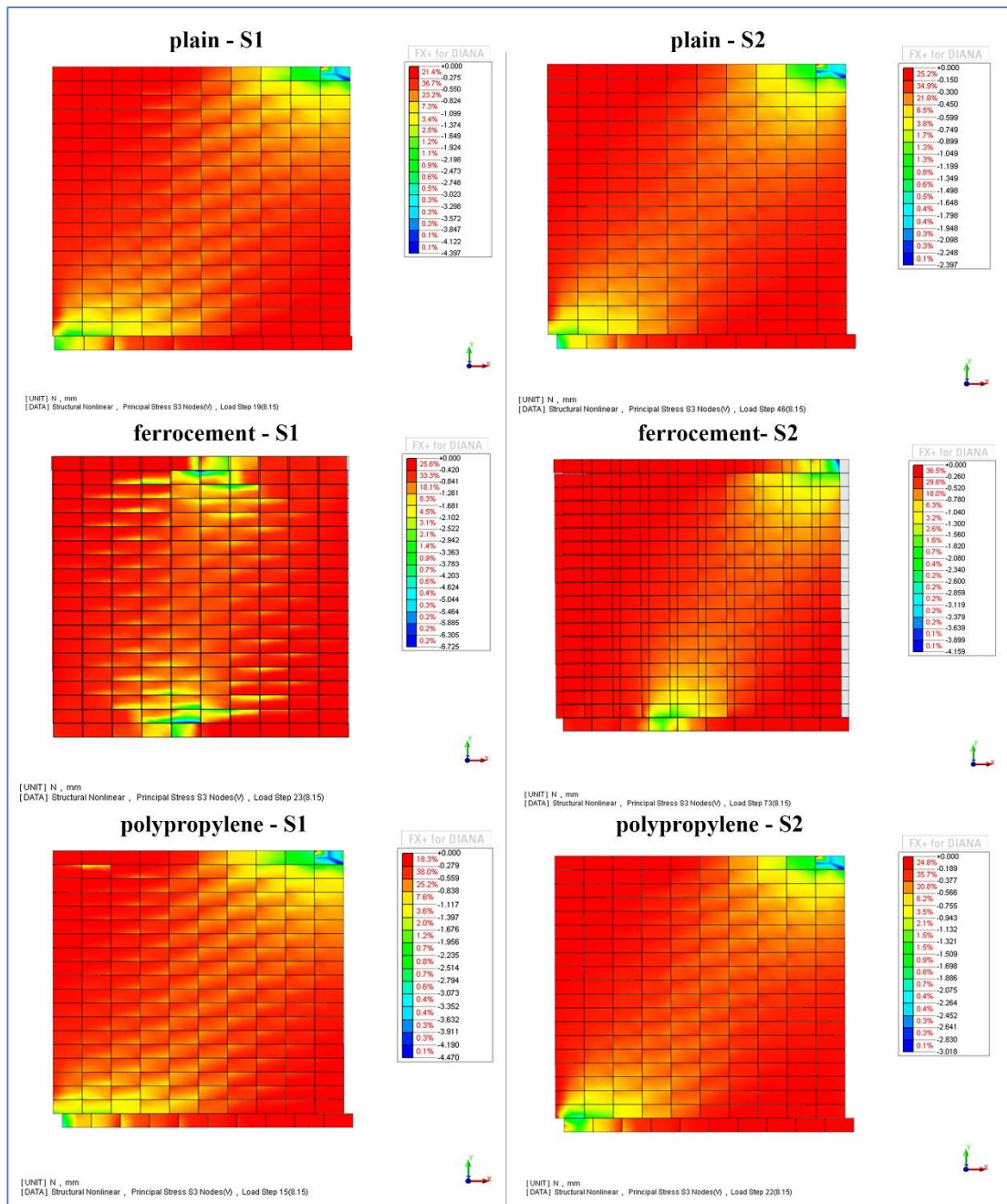


Figure 65. Comparison of Principal stresses S3 after nonlinear analysis.

An important parameter to determine the overall behavior of the panel under the induced unit deformation is the Load-displacement diagram. In Figure 66 and Figure 67 it is shown the comparison between plain, ferrocement and polypropylene strengthened panels for Series 1 and Series 2 panels. In both cases, the highest

deformation and force is achieved from ferrocement strengthened panel which highlights the effectiveness of this technique.

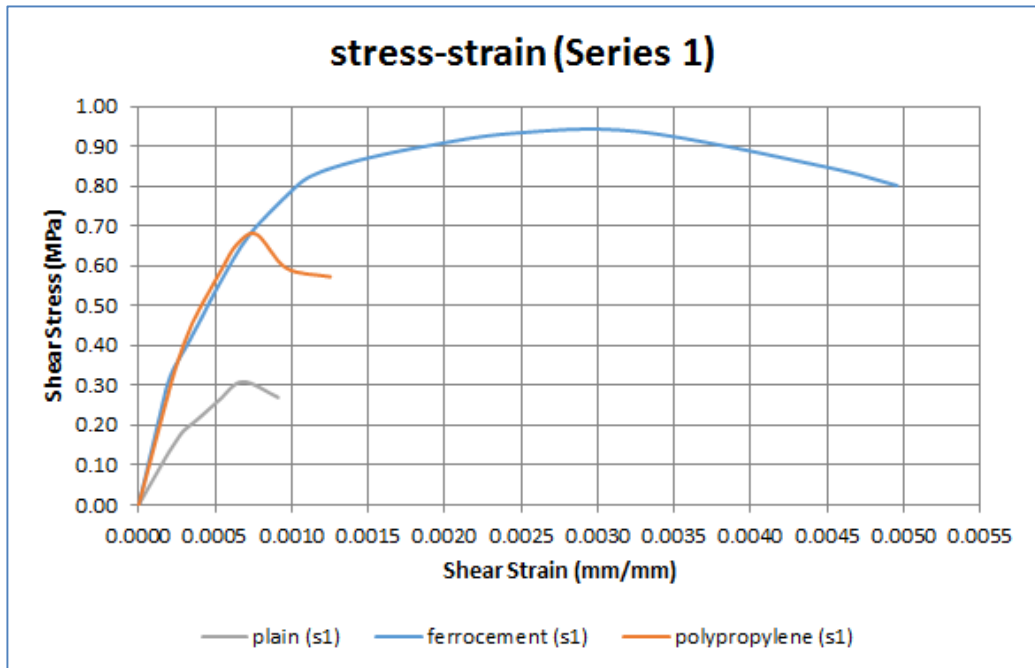


Figure 66. Comparison of stress-strain response for Series 1.

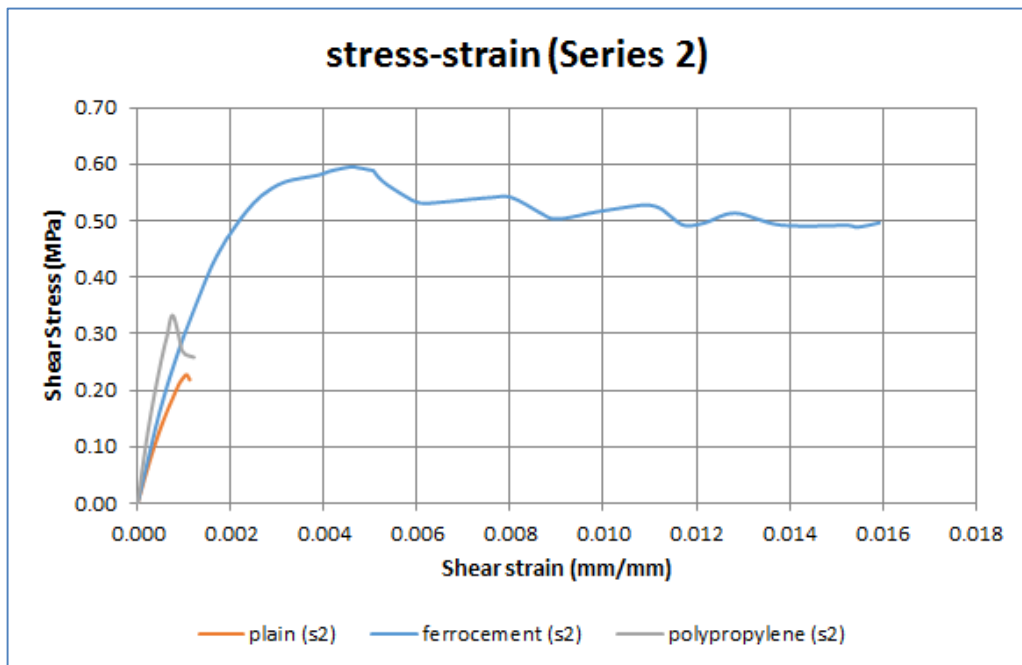


Figure 67. Comparison of load displacement diagrams for Series 2.

5.4. Experimental vs Numerical comparisons

In this section a comparison between experimental and numerical results is discussed. The main parameter that was used to understand the trend of the behavior of the panels is the comparison between stress-strain diagrams described in Figure 68.

In the panels of Series 1, ferrocement strengthened specimens exhibited a higher shear stress of 0.80 MPa and a total shear strain of about 0.0053. The stress-strain diagram obtained after nonlinear analysis showed that ferrocement strengthened specimens achieved the highest shear stress of 0.937 MPa and a maximum strain of 0.0050, considerably higher than other two panels.

Polypropylene strengthened panels exhibited similar behavior in both cases; high shear stress (0.750 MPa) but very low shear strain value (0.0005), and in the numerical analysis a shear strength of 0.679 MPa and a maximum strain of 0.0013.

Plain panels, as expected showed a very brittle behavior and much lower values in both analyses; 0.228 MPa shear strength and a maximum strain of 0.0012.

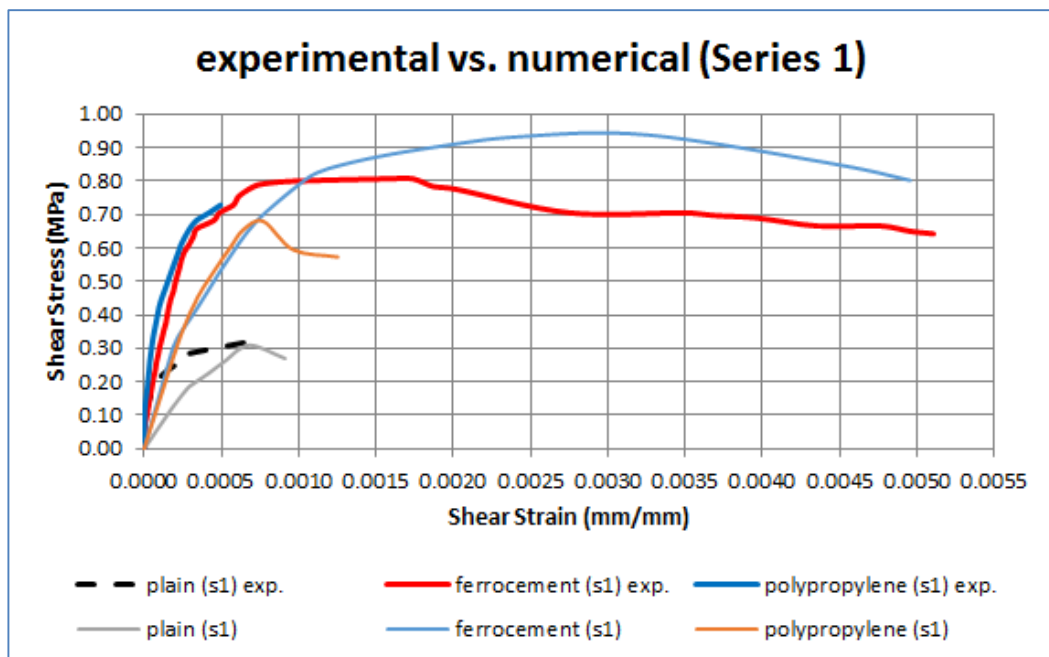


Figure 68. Summary of stress-strain response of experimental and numerical results for Series 1.

In Figure 69 it is presented the individual comparison between each of the investigated panel types. For Series 1, apart from the ferrocement strengthened specimen, plain and polypropylene strengthened panels exhibited similar values of maximum shear stress. Nevertheless, it was observed that all the modelled panels were more ductile. It may be explained by the linearity assumptions of assumed the material properties used for modelling.

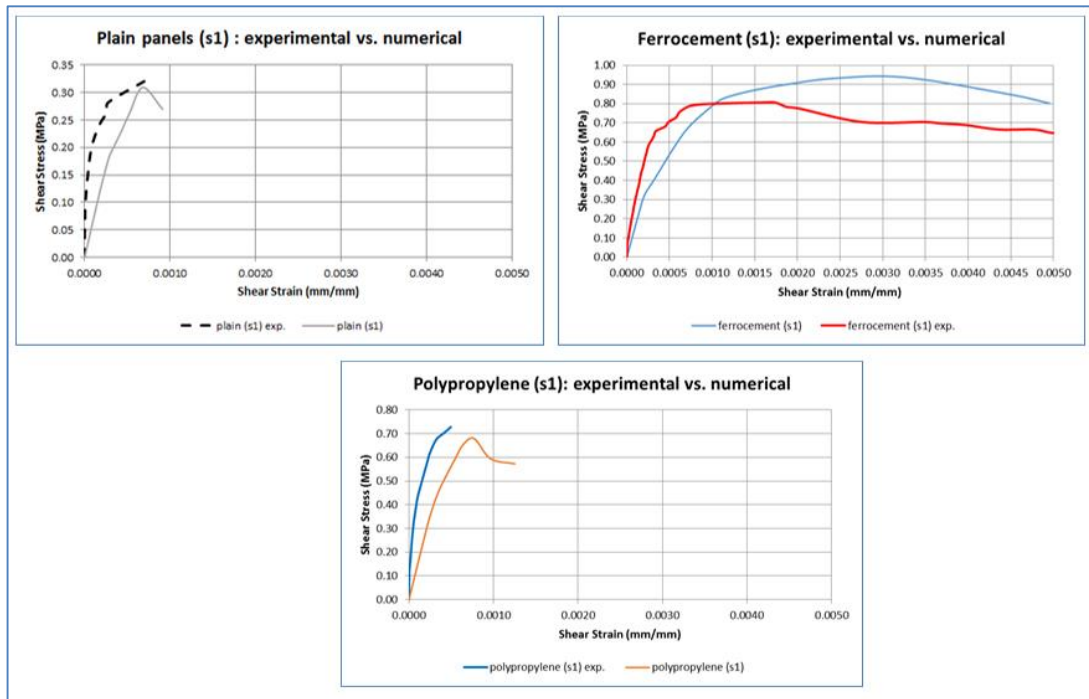


Figure 69. Comparison between experimental and numerical results of plain, ferrocement and polypropylene strengthened panels for Series 1.

In the panels of Series 2, ferrocement strengthened specimens exhibited a higher shear stress of 0.70 MPa and a total shear strain of about 0.025. The stress-strain diagram obtained after nonlinear analysis showed that ferrocement strengthened specimens achieved the highest shear stress of load of 0.595 MPa and a maximum strain of 0.0159 considerably higher than other two panels (Figure 70).

Polypropylene strengthened panels exhibited similar behavior in both cases; high shear stress (0.480 MPa) but very low shear strain value (0.0015), and in the numerical analysis a maximum shear stress of 0.332 MPa and a maximum strain 0.00121.

Plain panels exhibited a lower shear stress of 0.233 MPa and a maximum strain of 0.0011.

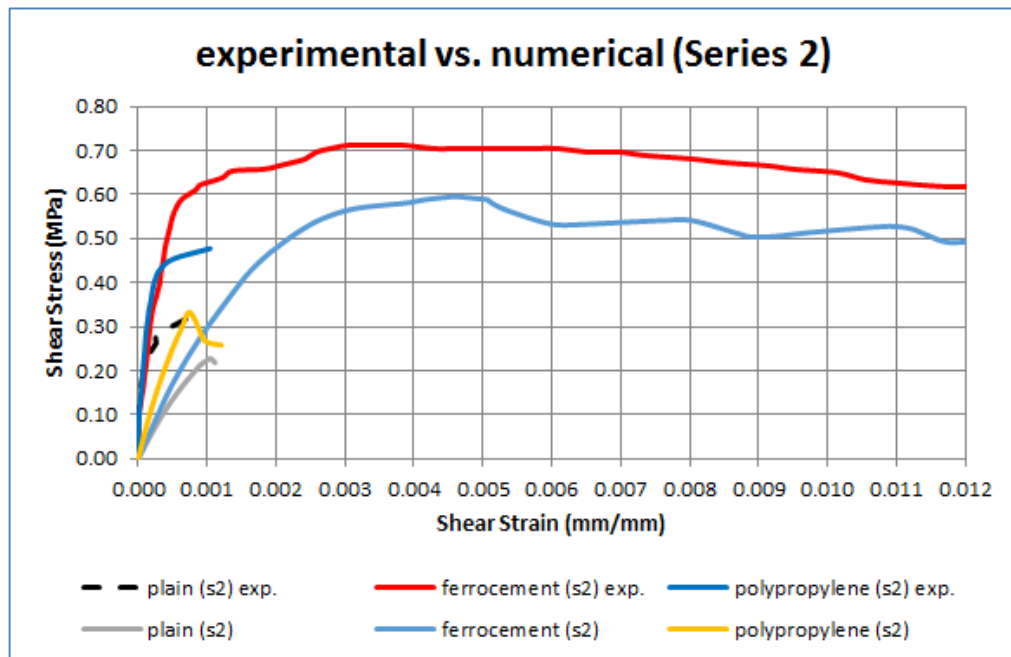


Figure 70. Summary of stress-strain response of experimental and numerical results for Series 2.

In Figure 71 it is presented the comparison between the studied specimens. It was observed that for all Series 2 specimens, the numerical analysis provided lower shear stresses and strains compared to the experimental results emphasizing the fact that some of the assumed parameters were more conservative.

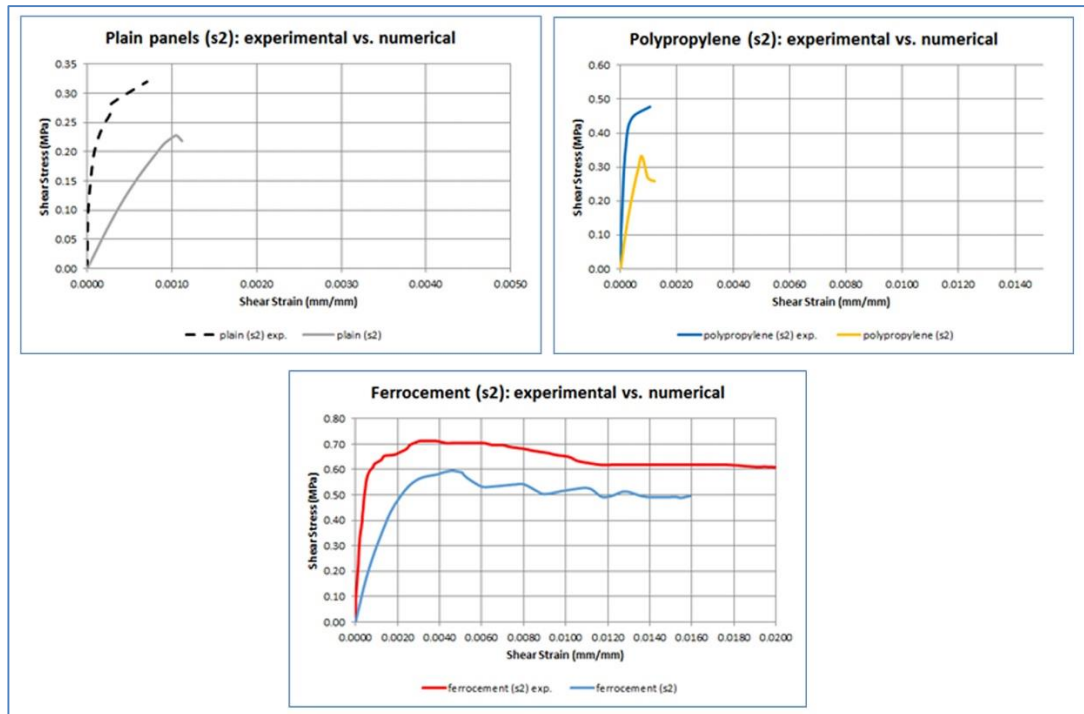


Figure 71. Comparison between experimental and numerical results of plain, ferrocement and polypropylene strengthened panels for Series 2.

5.5. Concluding remarks

Numerical analysis, even though based on several assumptions, provided good insights of the behavior of the panels during linear and nonlinear analysis. The aim of the analysis was to compare the experimental results with a previously done and well-established numerical procedures.

At the end of the results, it may be concluded that the ferrocement jacketing strengthening technique provided the best results in terms of both load and deformation, making the panel more resistant against horizontal loads.

CHAPTER 6

CONCLUSIONS

6.1 Conclusions

In this study, structural performance of unreinforced and reinforced masonry panels was investigated. The panels were built using local materials made of same characteristics: all the clay bricks were obtained from a factory using a 50-year-old technology and were fired at the same time, in order to have a much as possible a representation of current masonry buildings' condition. Additionally, two different types of mortars were used (type "N" and type "O") which would represent the very old and modern unreinforced masonry buildings, respectively. The panels, having nominal dimensions of 1.2 x 1.2 x 0.25 m, were built in a controlled environment by professional masons, inside the civil engineering laboratory of Epoka University.

In the first group of panels, Series 1; four were plain (unstrengthened) walls, six were pre-cracked and later repaired with either ferrocement (3) or polypropylene and nine strengthened with ferrocement (3), polypropylene (3) or G-FRP (3) prior to testing.

In the second group of panels, Series 2; two were plain walls, nine were pre-cracked and later repaired with either ferrocement (3), polypropylene (3) or C-FRP (3) and eight were strengthened either with ferrocement (3), polypropylene (3) or C-FRP (2) prior to testing.

A total of 52 diagonal compression tests were conducted strictly following the technical specifications of American Society for Testing and Materials (ASTM International). Prior to testing, material characteristics of masonry constituent materials were determined for each panel.

Additionally, numerical simulation using DIANA 9.6 software was performed in order to make a comprehensive evaluation of the structural behavior of the studied specimens.

Based on the test results and the outcome of the numerical analysis, the following conclusions may be drawn:

1. The experimental results showed that all the tested specimens presented a similar failure mode, mainly characterized by a step-like crack along the compressed diagonal, predominantly through the mortar joints in a diagonal step pattern. However, crack propagation, maximum deformation as well as ultimate load carrying capacity of the panels was dependent upon the mortar type as well as the strengthening method.
2. As expected, the plain wall panels of both series exhibited a very brittle behavior and low shear resistance; average shear strength for Series 1 was 0.364 MPa and 0.142 MPa for Series 2. The highest shear resistance was achieved from the group of the panels reinforced with polypropylene fibers, 0.845 MPa which was slightly higher than ferrocement strengthened panels of 0.822 MPa. Nevertheless, ferrocement strengthened panels exhibited much higher deformations prior to failure.
3. In all the reinforced panels, it was observed a noticeable increase in the ultimate shear strength; an improvement from 140-160% (Series 1) to 260-396% (Series 2). Deformation capacity on the other hand, was improved from 228%-1193% (Series 1) to 419-679% (Series 2).
4. The suggested strengthening techniques were proven to be more effective on low grade mortar.
5. Numerical analysis showed that ferrocement jacketing technique provided more satisfactory results in terms of higher resistance and more ductility levels.
6. The URM brittle failure was corrected by the considered strengthening techniques, especially by ferrocement jacketing. In this case together with C-FRP and G-FRP, the crack spreading and the debonding sound reduced sufficient warnings of a developing failure.

Repair and reinforcement of URM buildings with externally bonded strengthening materials appears to be an attractive alternative for improvement of structural performance against lateral loadings.

6.2 Recommendations for future research

These experiments have only been carried out considering static loading. All the tests were done static loading. There is a need for a further research for assessment of structural performance of the panels under dynamic loading conditions as well as considering out-of-plane performance.

Damaged masonry panels could be studied in more detail and a numerical model could be suggested.

REFERENCES

- [1] C. Faella, E. Martinelli, E. Nigro and S. Paciello, "Shear capacity of masonry walls externally strengthened by a cement-based composite material: An experimental campaign," *Construction and Building Materials*, vol. 24, p. 84–93, 2010.
- [2] P. B. Lourenço, "Computational strategies for masonry structures," Delft University of Technology, Delft, Netherlands, 1996.
- [3] W. A. Wood, "Load distribution of masonry walls subject to concentrated loads over openings," University of Pittsburgh, Pittsburgh, USA, 1998.
- [4] R. Drysdale, A. Hamid and L. Baker, "Masonry Structures: Behaviour and Design,," *The Masonry Society*, 1999.
- [5] G. Croci, The conservation and structural restoration of the architectural heritage, Southampton, UK: Computational Mechanics Publications, 1998.
- [6] E. Mustafaraj, Assessment of historical structures: A case study of five Ottoman mosques in Albania., Germany: LAP Lambert Academic Publishing., 2014.
- [7] H. B. Kaushik, D. C. Rai and S. K. Jain, "Uniaxial compressive stress-strain model for clay brick masonry," *Current Science*, vol. 92, no. 4, pp. 497-501., 2007.
- [8] R. Lumantarna, "Material characterization of New Zealand clay brick unreinforced masonry buildings," University of Auckland, Auckland, New Zealand, 2012.
- [9] S. Karaman, H. Gunal and S. Ersahin, "Assesment of clay bricks compressive strength using quantitative values of colour components," *Construction and Building Materials*, vol. 20, no. 5, pp. 348-354, 2006.
- [10] K. Elert, G. Cultrone, C. R. Navarro and E. S. Pardo, "Durability of bricks used in the conservation of historic buildings - influence of composition and microstructure," *Journal of Cultural Heritage*, vol. 4, no. 2, pp. 91-99, 2003.

- [11] ASTM, "ASTM C 62-04 Standard Specification for Building Brick (solid masonry units made from clay or shale)," ASTM International, West Conshohocken, PA, 2004.
- [12] T. Sneek, "Dependence of masonry properties on the interaction between masonry units and mortar," in *Proceedings of the North American masonry Conference.* , Colorado, USA, 1978.
- [13] ASTM International, "ASTM C67-14, Standard Test Methods for Sampling and Testing Brick and Structural Clay Tile,," West Conshohocken, PA, 2014.
- [14] ASTM International, "ASTM C1006-07 - Standard Test Method for Splitting Tensile Strength of Masonry Units," West Conshohocken, PA, 2013.
- [15] H. Hilsdorf, "Investigation Into the Failure Mechanism of Brick Masonry Loaded in Axial Compression," in *International Conference on Masonry Structural Systems,* , University of Texas, Austin., 1967.
- [16] S. Sahlin, *Structural Masonry*, Englewood Cliffs, New Jersey: Prentice-Hall Inc., 1971.
- [17] W. B. McKay, *Brickwork*, Longmans, London, United Kingdom.: Green and Co., 1947.
- [18] J. A. Mulligan, *Handbook of brick masonry construction*, New York, United States.: McGraw-Hill, 1942.
- [19] A. Palomo, M. T. Blanco-Varela, S. Martinez-Ramirez, F. Puertas and C. Fortes, "Historic Mortars: Characterisation and Durability. New Tendencies for Research," in *European Research on Cultural Heritage: State-of-the-Art Studies,* , Prague, Czech Republic, 2004.
- [20] ASTM, "ASTM C 270-03, Standard Specification for Mortar for Unit Masonry," ASTM International, West Conshohocken, PA, 2003.
- [21] T. Bakeer, *Collapse analysis of masonry structures under earthquake actions*, 8th Edition ed., Dresden, Germany: TU Dresden, 2009.
- [22] S. V. Deodhar, "Strength of Brick Masonry Prisms in Compression," *Journal of the Institution of Engineers (India)*, vol. 81, no. 3, pp. 133-137, 2000.

- [23] K. S. Gumaste, K. S. Nanjunda Rao, B. V. Venkatarama Reddy and K. S. Jagadish, "Strength and elasticity of brick masonry prisms and wallettes under compression," *Materials and Structures*, vol. 40, no. 2, pp. 241-253, 2006.
- [24] H. B. Kaushik, D. C. Rai and S. K. Jain, "Stress-Strain Characteristics of Clay Brick Masonry under Uniaxial Compression," *Journal of Materials in Civil Engineering*, vol. 19, no. 9, pp. 728-738, 2007.
- [25] A. W. Hendry and F. M. and Khalaf, *Masonry wall construction*, London, United Kingdom and New York, United States: Spon Press, 2001.
- [26] P. B. Lourenço, "Experimental and numerical issues in the modelling of the mechanical behavior of masonry," in *Structural Analysis of Historical Constructions II. CIMNE*, Barcelona, Spain, 1998.
- [27] T. Paulay and M. J. N. Priestley, "Seismic design of reinforced concrete and masonry buildings," John Wiley & Sons, , New York, USA, 1992.
- [28] R. G. Drysdale, A. A. Hamid and L. R. Baker, *Masonry Structures, Behavior and Design*, Englewood Cliff: Prentice Hall Inc, 1994, p. 784.
- [29] L. Berto, A. Saetta, R. Scotta and R. Vitaliani, "Failure mechanism of masonry prism loaded in axial compression: computational aspects," *Materials and structures*, vol. 38, no. 2, pp. 249-256, 2005.
- [30] R. H. Atkinson and J. L. Noland, "A proposed failure theory for brick masonry in compression," in *3rd Canadian Masonry Symposium*, , Edmonton, Alberta, Canada, , 1983.
- [31] W. S. McNary and D. P. Abrams, ""Mechanics of masonry in compression," *Journal of Structural Engineering*, vol. 111, no. 4, pp. 857-870, 1985.
- [32] H. K. Hilsdorf, "An investigation into the failure of brick masonry loaded in axial compression," in *Designing, engineering, and constructing with Masonry Products*, Houston, 1969.
- [33] CEN, "EN 1996-1-1: Design of masonry structures - Part 1-1: General rules for reinforced and unreinforced masonry structures.," " European Committee for Standardization, Brussels, Belgium, 2005.

- [34] MSJC, "Building code requirements for masonry structures, ACI 530-02/ASCE 5- 02/TMS 402-02.," America Concrete Institute, Structural Engineering Institute of the American Society of Civil Engineers, The Masonry Society, Detroit, Michigan, USA, 2002.
- [35] A. Hendry, B. Sinha and S. Davies, *Design of Masonry Structures, Load Bearing Brickwork Design*, Third Edition ed., UK: E&FN Spon, UK, 1997.
- [36] M. Tomazevic, "Earthquake-Resistant Design of Masonry Buildings," in *Series on Innovation in Structures and Construction, Masonry Materials and Construction Systems*, vol. 1, Imperial College Press, 1999.
- [37] P. Schubert, "The influence of mortar on the strength of masonry," in *8th International Brick and Block Masonry Conference*, London, UK, 1988.
- [38] H. P. Backes, "On the Behavior of Masonry Under Tension in the Direction of the Bed Joints," Aachen University of Technology, Aachen, Germany, 1985.
- [39] F. J. Crisafulli, A. J. Carr and R. Park, "Shear Strength of Unreinforced Masonry Panels," in *Pacific Conference on Earthquake Engineering*, Melbourne, Australia, 1995.
- [40] P. Hofmann and S. Stockl, "Tests on the shear-bond behavior in the bed-joints of masonry," *Masonry International* , vol. 9, p. 1–15, 1986.
- [41] R. H. Atkinson, B. P. Amadei, S. Saeb and S. Sture, "Response of masonry bed joints in direct shear.," *ASCE Journal of Structural Engineering ASCE*, vol. 115, no. 9, p. 2276–2296, 1989.
- [42] R. Van der Pluijm, "Shear behaviour of bed joints," in *Proc. 6th North American masonry conf.*, Philadelphia, USA, 1993.
- [43] EN 1052-3:2002, "Methods of test for masonry – part 3: determination of initial shear strength," European Committee for Standardization, Brussels, Belgium, 2003.
- [44] P. B. Lourenço and L. F. Ramos, "Characterization of cyclic behaviour of dry masonry joints," *Journal of Structural Engineering 2004*, vol. 130, no. 5, p. 779–786, 2004.

- [45] V. Turnšek and P. Sheppard, "The shear and flexure resistance of masonry walls.," in *International Research Conference on Earthquake Engineering*, Skopje, Macedonia, 1980.
- [46] EN 1998-1:2004, "Eurocode 8: Design of structures for earthquake resistance – Part 1: General rules, seismic actions and rules for buildings," 2004.
- [47] ASTM International, ASTM E519-02, Standard Test Method for Diagonal Tension (Shear) in Masonry Assemblages, West Conshohocken, PA, 2002.
- [48] RILEM TC, "LUM B6 Diagonal tensile strength tests of small wall specimens," E & FN SPON, 1994.
- [49] V. Turnšek and F. Cacovic, "Some experimental results on the strength of brick masonry walls," in *2nd international brick masonry conference*, Stoke-on-Trent, UK, 1971.
- [50] C. Faella, E. Martinelli, E. Nigro and S. Paciello, "Shear capacity of masonry walls externally strengthened by a cement-based composite material: An experimental campaign," *Construction and Building Materials*, vol. 24, p. 84–93, 2010.
- [51] M. Corradi, A. Borri and A. Vignoli, "Strengthening techniques tested on masonry structures struck by the Umbria–Marche earthquake of 1997–1998," *Constr Build Mater*, vol. 16, no. 4, p. 229–239, 2002.
- [52] M. Corradi, A. Borri, G. Castori and R. Sisti, "Shear strengthening of wall panels through jacketing with cement mortar reinforced by GFRP grids," *Composites: Part B*, vol. 64, p. 33–42, 2014.
- [53] J. Milosevic, A. S. Gago, M. Lopes and R. Bento, "Experimental assessment of shear strength parameters on rubble stone masonry specimens," *Construction and Building Materials*, vol. 47, pp. 1372-1380, 2013.
- [54] A. Borri, G. Castori, M. Corradi and E. Speranzini, "Shear behavior of unreinforced and reinforced masonry panels subjected to in situ diagonal compression tests," *Construction and Building Materials*, vol. 25, p. 4403–4414, 2011.

- [55] V. Alecci, M. Fagone, T. Rotunno and M. De Stefano, "Shear strength of brick masonry walls assembled with different types of mortar," *Construction and Building Materials*, vol. 40, pp. 1038-1045, 2013.
- [56] D. Dizhur and J. M. Ingham, "Diagonal tension strength of vintage unreinforced clay brick masonry wall panels," *Construction and Building Materials*, vol. 43, p. 418–427, 2013.
- [57] N. Ismail, R. B. Petersen, M. J. Masia and J. M. Ingham, "Diagonal shear behavior of unreinforced masonry wallettes strengthened using twisted steel bars.," *Construction and Building Materials*, vol. 25, pp. 4386-4393, 2011.
- [58] A. Kalali and M. Z. Kabir, "Experimental response of double-wythe masonry panels strengthened with glass fiber reinforced polymers subjected to diagonal compression tests," *Engineering Structures*, vol. 39, pp. 24-37, 2012.
- [59] Y. W. Lin, L. Wotherspoon, A. Scott and J. M. Ingham, "In-plane strengthening of clay brick unreinforced masonry wallettes," *Engineering Structures*, vol. 66, pp. 57-65, 2014.
- [60] N. Gattesco and A. Dudine, "Effectiveness of a masonry strengthening technique made with a GFRP-mesh-reinforced mortar coating," in *8th International Masonry Conference*, Dresden, Germany, 2010.
- [61] M. A. Najafgholipour, M. R. Maheri and P. B. Lourenço, "Capacity interaction in brick masonry under simultaneous in-plane and out-of-plane loads," *Construction and Building Materials*, vol. 38, p. 619–626., 2013.
- [62] Y. Yardim and O. Lalaj, "Shear strengthening of unreinforced masonry wall with different fiber reinforced mortar jacketing," *Construction and Building Materials*, vol. 102, pp. 149-154, 2016.
- [63] N. Gattesco and I. Boem, "Experimental and analytical study to evaluate the effectiveness of an in-plane reinforcement for masonry walls using GFRP meshes," *Construction and Building Materials*, vol. 88, pp. 94-104, 2015.
- [64] H. Mahmood and J. M. Ingham, "Diagonal compression testing of FRP-retrofitted unreinforced clay brick masonry wallettes," *ASCE Journal of Composite Construction*, vol. 15, no. 5, p. 810–20., 2011.

- [65] M. Corradi, C. Tedeschi, L. Binda and A. Borri, "Experimental evaluation of shear and compression strength of masonry wall before and after reinforcement: Deep repointing," *Construction and Building Materials*, vol. 22, no. 4, pp. 463-472, 2008.
- [66] A. Prota, G. Marcari, G. Fabbrocino, G. Manfredi and C. Aldea, "Experimental In-Plane Behavior of Tuff Masonry Strengthened with Cementitious Matrix–Grid Composites," *Journal of Composites in Construction*, vol. 3, no. 223, pp. 223-233, 2006.
- [67] M. R. Valluzzi, D. Tinazzi and C. Modena, "Shear behavior of masonry panels strengthened by FRP laminates," *Construction and Building Materials*, vol. 16, p. 409–416, 2002.
- [68] A. Borri, G. Castori and M. Corradi, "Determination of shear strength of masonry panels through different tests," *International Journal of Architectural Heritage*, vol. 9, p. 913–927, 2015.
- [69] FEMA 273, "NEHRP Guidelines for The Seismic Rehabilitation of Buildings," Washington D.C, 1997.
- [70] NEHRP, "Recommended Provisions for Seismic Regulations for New Buildings and Other Structures," 2000.
- [71] Canadian Masonry Code, "CSA S304.1 - Design of masonry structures," CSA, 2004.
- [72] ASCE, *Seismic Rehabilitation of Existing Buildings – SEI/ASCE 41-06*, Reston. VA: American Society of Civil Engineers; 2007, 2007.
- [73] A. H. Harris, "Masonry: Materials, Design, Construction and Maintenance," in *American Society for Testing and Materials*, Baltimore, USA, 1988.
- [74] G. Pande, J. Middleton and B. Krajl, *Computer Methods in structural masonry*, London, UK: E & FN Spon, 1998.
- [75] S. M. Alcocer and R. E. Klinger, "Masonry Research in the Americas," *Masonry in the Americas*, vol. 147, pp. 127-169, 1994.

- [76] S. G. Fattal and L. E. Cattaneo, "Evaluation of Structural Properties of Masonry in Existing Buildings," National Bureau of Standards, Department of Commerce, Washington, USA, 1977.
- [77] D. M. McCann and M. C. Forde, "Review of NDT methods in the assessment of concrete and masonry structures," *NDT&E International*, vol. 34, pp. 71-84, 2001.
- [78] M. Schuller, M. Berra, R. Atkinson and L. Binda, "Acoustic tomography for evaluation of unreinforced masonry," *Construction and Building Materials*, vol. 11, no. 3, pp. 199-204, 1997.
- [79] B. P. Sinha and A. W. Hendry, "Racking tests on storey-height shear-wall structures with openings subjected to precompression," in *Designing, engineering and constructing with masonry products*, Houston, Texas, 1969.
- [80] A. W. Hendry and B. P. Sinha, "Shear tests on the full-scale single-storey brickwork structures subjected to pre-compression," *Journal of Civil Engineering Public Works Review*, pp. 1339-1344, 1971.
- [81] R. Engermann, D. Cook and A. Anzani, "An investigation into the behavior of scale model brick walls," in *9th International Brick/Block Masonry Conference*, Berlin, Germany, 1991.
- [82] D. A. Abrams, "Effects of scale and loading rate with tests of concrete and masonry structures," *Earthquake Spectra*, vol. 12, no. 1, pp. 13-28, 1996.
- [83] H. Krawlinker, "Possibilities and limitations of scale-model testing in earthquake engineering.," in *Proceedings of the second US national conference on earthquake engineering*, Stanford, California, 1979.
- [84] A. Mohammed, "Experimental comparison of brickwork behavior at prototype and model scales," Cardiff University, Cardiff, UK, 2006.
- [85] A. Mohammed and T. Huges, "Prototype and model masonry behavior under different loading conditions," *Materials & Structures*, vol. 44, no. 1, pp. 53-65, 2011.
- [86] M. Tomasevic and I. Klemenc, "Seismic behaviour of confined masonry walls," *Earthquake Engineering Structural Dynamics*, vol. 26, p. 1059-1071, 1997.

- [87] N. R. El-Sakhawy, H. A. Raof and A. Gouhar, "Shearing behaviour of joints in load bearing masonry wall," *Journal of Materials in Civil Engineering*, vol. 14, no. 2, p. 145–150, 2002.
- [88] A. L, S. R A, M. F and M. A, "Experimental investigation of the brick–mortar interface behavior. Experimental investigation of the mortar joint in masonry structures.," *Mechanics Research Communications, MRC*, 2005.
- [89] M. R. Maheri and M. A. Sherafati, "The effects of humidity and other environmental parameters on the shear strength of brick walls; evaluation of field test data," *Matererial Structures*, vol. 45, no. 6, pp. 941-956, 2012.
- [90] R. M. Maheri, M. A. Najafgholipour and A. R. Rajabi, "The influence of mortar head joints on the in-plane and out of plane seismic strength of brick masonry walls.," *Iranian J Sci Technol 2011;35:*, vol. 35, p. 63–79, 2011.
- [91] C. T. Grimm and R. L. Tucker, "Flexural strength of masonry prisms versus wall panels," *ASCE Journal of Structural Engineering*, vol. 111, no. 9, pp. 2021-2032, 1985.
- [92] K. V. M. Rao, B. V. V. Reddy and K. S. Jagadish, "Flexural bond strength of masonry using various blocks and mortars," *Materials and Structure*, vol. 29, p. 119–124, 1996.
- [93] S. Pavia and R. Hanley, "Flexural bond strength of natural hydraulic lime mortar and clay brick," *Materials and Structures*, vol. 40, p. 230–245, 2009.
- [94] M. A. Najafgholipour, M. R. Maheri and P. B. Lourenço, "Capacity interaction in brick masonry under simultaneous in-plane and out-of-plane loads," *Construction and Building Materials*, vol. 38, p. 619–626, 2013.
- [95] A. Brignola, S. Frumento, S. Lagomarsino and S. Podesta, " Identification of shear parameters of masonry panels through the in situ diagonal compression test.," *International Journal of Architectural Heritage*, vol. 3, p. 52–73, 2008.
- [96] N. Sathiparan, P. Mayorco, K. N. R. Guragain and K. Meguro, "Experimental study on In-plane and Out-of-plane behaviour of masonry walletes retrofitted by PP Band meshes," *Seisan Kenkyu*, vol. 57, no. 6, pp. 530- 533, 2005.

- [97] M. Badoux, M. A. Elgwady and P. Lestuzzi, "Earthquake Simulator Tests on Unreinforced Masonry Walls before and after Upgrading with Composites," in *12th European Conference on Earthquake Engineering*, 2002.
- [98] V. Turco, S. Secondin, A. Morbin, M. R. Valluzzi and C. Modena, "Flexural and shear strengthening of un-reinforced masonry with FRP bars," *Composites Science and Technology*, vol. 66, p. 289–296, 2006.
- [99] A. Fam, D. Musiker, M. Kowalsky and S. Rizkalla, "In-plane testing of damaged masonry wall repaired with FRP," *Adv Compos Lett*, vol. 11, no. 6, p. 275–281, 2008.
- [100] Q. Wang, Z. Chai, Y. Huang and Y. Zhang, "Seismic shear capacity of brick masonry wall reinforced by GFRP," *Asian Journal of Civil Engineering (Building and Housing)*, vol. 7, no. 6, p. 563–580, 2006.
- [101] Y. A. Al-Salloum and T. H. Almusallam, "Walls strengthened with epoxy-bonded GFRP sheets," *Journal of Composite Materials*, vol. 39, p. 1719–1745, 2005.
- [102] H. Mahmood, A. P. Russel and J. M. Ingham, "Monotonic testing of unreinforced and FRP-retrofitted masonry walls with external CFRP reinforcement," in *Proceedings of the 14th world conference on earthquake engineering*, Beijing, China, 2008.
- [103] L. Pela, "Continuum damage model for non-linear analysis of masonry structures," Polytechnic University of Cataluña, Barcelona, Spain, 2008.
- [104] G. Uva and G. Salerno, "Towards a multiscale analysis of periodic masonry brickwork: A FEM algorithm with damage and friction," *International Journal of Solids and Structures*, vol. 43, p. 3739–3769, 2006.
- [105] A. W. Page, "The biaxial compressive strength of brick masonry," *Proceedings of the Institution of Civil Engineers*, vol. 71, no. 2, p. 893–906, 1981.
- [106] A. W. Page, "The strength of brick masonry under biaxial tension–compression," *International Journal of Masonry Constructions*, vol. 3, no. 1, p. 26–31, 1983.

- [107] M. Bruneau, "State-of-the-art report on seismic performance of unreinforced masonry buildings," *Journal of Structural Engineering*, vol. 120, no. 1, pp. 230–251, 1994.
- [108] G. Magenes and M. G. Calvi, "In-plane seismic response of brick masonry walls," *Earthquake Engineering Structure Dynamics*, vol. 26, no. 11, p. 1091–1112, 1997.
- [109] C. Calderini, S. Cattari and S. Lagomarsino, "In-plane strength of unreinforced masonry piers," *Earthquake Engineering Structure Dynamics*, vol. 38, no. 2, p. 243–267, 2009.
- [110] W. Mann and H. Müller, "Failure criteria for laterally loaded masonry and their application to shear walls (in German)," *Die Bautechnik*, vol. 50, no. 12, p. 421–425, 1973.
- [111] R. Mayes and R. W. Clough, "State-of-the-art in seismic shear strength of masonry-an evaluation and review," in *EERC 75-21*, College of Engineering, University of California. , 1975.
- [112] F. Y. Yokel and S. G. Fattal, "Failure hypothesis for masonry shear walls," *Journal of Structural Division*, vol. 102, no. 3, p. 515–532, 1976.
- [113] A. W. Page, "An experimental investigation of the biaxial strength of brick masonry," in *6th International Brick/Block Masonry Conference*, Rome, Italy, 1982.
- [114] B. Ghiassi, M. Soltani and A. Tasnimi, "A simplified model for analysis of unreinforced masonry shear walls under combined axial, shear and flexural loading," *Engineering Structures*, vol. 42, p. 396–409, 2012.
- [115] S. Casolo and G. Milani, "Simplified out-of-plane modelling of three-leaf masonry walls accounting for the material texture," *Construction and Building Materials*, vol. 40, p. 330–351, 2013.
- [116] C. Sandoval and P. Roca, "Study of the influence of different parameters on the buckling behaviour of masonry walls," *Construction and Building Materials*, p. 888–899, 2012.

- [117] M. Javed, A. N. Khan, A. Penna and G. Magenes, "Behaviour of masonry structures during the Kashmir 2005 Earthquake," in *First European Conference on Earthquake Engineering and Seismology (1st ECEES)*, Geneva, Switzerland, 2006.
- [118] H. Mahmood and J. M. Ingham, "Diagonal compression testing of FRP-retrofitted unreinforced clay brick masonry wallettes," *ASCE Journal of Composites in Construction*, vol. 15, no. 5, p. 810–820, 2011.
- [119] H. Houben and H. Guillard, *Earth construction – a comprehensive guide*, ITDG Publishing, 1994.
- [120] S. Bhattacharya, S. Nayak and S. C. Dutta, "A critical review of retrofitting methods for unreinforced masonry structures," *International Journal of Disaster Risk Reduction*, vol. 7, pp. 51-67, 2014.
- [121] CENAPRED, "Metodos de Refuerzo para la Vivienda Rural de Autoconstruccion (Spanish)," Centro Nacional de Prevencion de Desastres, Primera Jornada Nacional De Simulacros Para La revencion de Riesgos, Mexico, 2002.
- [122] F. Kadiu, *Shkenca dhe Teknologjia e Materialeve (Albanian)*, Tirane, Albania: Erik Botime, 2007.
- [123] Albanian Institute of Statistics, INSTAT, "Population and housing, Census 2011," Tirana, Albania, 2012.
- [124] B. C. Papazachos, "Active tectonics in Aegean and surrounding area," in *Proceedings Summer School on Seismic Hazard in Mediterranean Regions*, , Strasbourg, France, 1988.
- [125] T. C. Triantafillou, "Strengthening of masonry structures using epoxy-bonded FRP laminates," *ASCE Journal of Composites for Construction*, vol. 2, pp. 96-104, 1998.
- [126] P. F. A. Montes, "Behaviour of a hemispherical dome subjected to wind loading," *Journal of Wind Engineering and Industrial Aerodynamics*, vol. 89, pp. 911-924, 2001.

- [127] I. Rosenthal, "Precast ferrocement columns," *Journal of Ferrocement*, vol. 16, pp. 273-284, 1986.
- [128] A. Winokur and I. Rosenthal, "Ferrocement in centrally loaded compression elements," *Journal of Ferrocement*, vol. 12, pp. 357-364, 1982.
- [129] S. Razvi and M. Saatcioglu, "Confinement of reinforced concrete columns with welded wire fabric," *ACI Structural Journal*, vol. 86, pp. 615-623, 1989.
- [130] S. M. Mourad and M. J. Shannag, "Repair and strengthening of reinforced concrete square columns using ferrocement jackets," *Cement & Concrete Composites*, vol. 34, pp. 288-294, 2012.
- [131] S. Kaushik, A. Prakash and A. Singh, "Inelastic buckling of ferrocement encastred columns," in *5th International Symposium on Ferrocement*, 1990.
- [132] T. Ahmed, S. Ali and J. Choudhury, "Experimental study of ferrocement as a retrofit material for masonry columns," in *5th International Symposium on Ferrocement*, 1990.
- [133] P. Nedwell, M. Ramesht and R. S. Tabhanaki, "Investigation into the repair of short square columns using ferrocement," in *5th International Symposium on Ferrocement*, 1990.
- [134] D. Abrams, T. Smith, J. Lynch and S. Franklin, "Effectiveness of rehabilitation on seismic behavior of masonry piers," *ASCE Journal of Structural Engineering*, vol. 133, no. 1, pp. 32-43, 2007.
- [135] Forta Ferro Corporation, "Forta for Concrete," September 2015. [Online]. Available: www.forta-ferro.com.
- [136] American Concrete Institute, "State-of-the-art Report on Fiber Reinforced Concrete," ACI, 2002.
- [137] M. Jabarov, S. Kozharinov and A. Lunyov, "Strengthening of damaged masonry by reinforced mortar layers," in *7th WCEE*, Istanbul, Turkey, 1980.
- [138] C. Papanicolaou, T. Triantafillou and M. Lekka, "Externally bonded grids as strengthening and seismic retrofitting materials for masonry panels," *Construction Building Materials*, vol. 25, no. 2, pp. 504-514, 2001.

- [139] P. Roca and G. Araiza, "Shear response of brick masonry small assemblages strengthened with bonded FRP laminates for in-plane reinforcement," *Construction and Building Materials*, vol. 24, p. 1372–1384, 2010.
- [140] A. Nanni and J. Tumialan, "Fiber reinforced composites for strengthening of masonry structures," *Structural Engineering International*, vol. 4, pp. 271-278, 2003.
- [141] T. Zhao, J. Xie and H. Li, "Strengthening of cracked concrete block masonry walls using continuous carbon fiber sheet," in *9th NAMC*, Clemson, South Carolina, USA, 2003.
- [142] S. Hamoush, W. McGinley, P. Mlakar, D. Scott and K. Murray, "Out-of-plane strengthening of masonry walls with reinforced composites," *ASCE Journal of Composites for Construction*, vol. 5, pp. 139-145, 2001.
- [143] J. Gilstrap and C. Dolan, "Out of plane bending of FRP-reinforced masonry walls", *Composites Science and Technology*, vol. 58, pp. 1277-1284, 1998.
- [144] S. Hamoush, W. McGinley, S. Woodson and P. Mlakar, "Influence of the FRP reinforcement ratio on the out-of-plane shear strength of externally reinforced masonry wall systems," in *9th NAMC*, Clemson, South Carolina, USA, 2003.
- [145] A. Gabor, A. Bennani, E. Jacquelin and F. Lebon, "Modelling approaches of the in-plane shear behaviour of unreinforced and FRP strengthened masonry panels," *Composite Structures*, vol. 74, p. 277–288, 2006.
- [146] J. G. Rots, "Numerical simulation of cracking in structural masonry," *Heron*, vol. 36, no. 2, p. 49–63, 1991.
- [147] V. I. Lishak, V. I. Yagust and D. Z. Yankelevsky, "2-D orthotropic failure criteria for masonry," *Engineering Structures*, vol. 36, p. 360–371, 2012.
- [148] G. Magenes and A. Della Fontana, "Simplified non-linear seismic analysis of masonry buildings," in *Proc. of the British Masonry Society*, 1998.
- [149] A. W. Page, "Finite element model for masonry," *ASCE Journal of Structural Division*, vol. 104, no. 8, p. 1267–1285, 1978.

- [150] P. B. Lourenço and J. G. Rots, "A multi-surface interface model for the analysis of masonry structures," *ASCE Journal of Engineering Mechanics*, vol. 123, no. 7, p. 660–668, 1997.
- [151] R. Senthivel and P. B. Lourenço, "Finite element modelling of deformation characteristics of historical stone masonry shear walls," *Engineering Structures*, vol. 31, no. 9, p. 1930–1943, 2009.
- [152] K. M. Dolatshahi and A. K. Aref, "Two-dimensional computational framework of mesoscale rigid and line interface elements for masonry structures," *Engineering Structures*, vol. 33, no. 12, p. 3657–3667, 2011.
- [153] I. Calio, M. Marletta and B. Panto, "A new discrete element model for the evaluation of the seismic behaviour of unreinforced masonry buildings," *Engineering Structures*, vol. 40, p. 327–338, 2012.
- [154] H. R. Lotfi and P. B. Shing, "Interface model applied to fracture of masonry structures," *ASCE Journal of Structural Engineering*, vol. 120, no. 1, p. 63–80, 1994.
- [155] A. D. Tzamtzis, "Dynamic finite element analysis of complex discontinuous and jointed structural systems using interface elements," QMWC, University of London, London, UK, 1994.
- [156] L. Gambarotta and S. Lagomarsino, "Damage models for the seismic response of brick masonry shear walls. Part II: the continuum model and its applications," *Earthquake Engineering & Structural Dynamics*, vol. 26, no. 4, p. 441–462, 1997.
- [157] R. Luciano and E. Sacco, "Homogenisation technique and damage model for old masonry material," *International Journal of Solids and Structures*, vol. 34, no. 24, pp. 3191-3208, 1997.
- [158] A. Zucchini and P. B. Lourenço, "Mechanics of masonry in compression: Results from a homogenization approach," *Computers and Structures*, vol. 85, p. 193–204, 2007.

- [159] G. Milani, P. B. Lourenço and A. Tralli, "A homogenization approach for the limit analysis of out-of-plane loaded masonry walls," *ASCE Journal of Structural Engineering*, vol. 132, no. 10, p. 1650–1663, 2006.
- [160] G. Milani, P. B. Lourenço and A. Tralli, "Homogenised limit analysis of masonry walls. Part I: Failure surfaces," *Computers and Structures*, vol. 84, pp. 166-180, 2006.
- [161] G. Milani, P. B. Lourenço and A. Tralli, "Homogenised limit analysis of masonry walls. Part II: Structural examples," *Computers and Structures*, vol. 84, p. 181–195, 2006.
- [162] R. Phillips, "Multiscale modeling in the mechanics of materials," *Current Opinion in Solid State & Materials Science*, vol. 3, p. 526–532, 1998.
- [163] F. Parisi, "Non-linear analysis of masonry buildings," Naples, Italy, 2010.
- [164] ASTM International, "ASTM C1314-04-Standard Test Method for Compressive Strength of Masonry Prisms," West Conshohocken, PA, 2004.
- [165] G. Van Zijl, P. De Vries and A. Vermeltoort, "Masonry wall damage by restraint to shrinkage," *ASCE Journal of Structural Engineering*, vol. 130, no. 7, pp. 1075-1086, 2004.
- [166] TNO DIANA, "DIANA – Finite Element Analysis-User’s Manual release 9.6-Element Library," TNO DIANA, Delft, Netherlands, 2014.
- [167] v. Z. G.P.A.G, "Modeling Masonry Shear-Compression: Role of Dilatancy Highlighted," *ASCE Journal of Engineering Mechanics*, vol. 130, no. 11, pp. 1289-1296, 2004.
- [168] R. V. d. Pluijm, "Material properties of masonry and its components under tension and shear," in *6th Canadian masonry symposium*, Saskatchewan, Canada, 1992.

CURRICULUM VITAE

PERSONAL INFORMATION

Surname, Name: Mustafaraj, Enea
Nationality: Albanian
Date and Place of Birth: 25.03.1989, Laç
Marital Status: Single
Phone: +355 69 5143816
Fax: -
E-mail: eneamustafaraj@gmail.com
emustafaraj@epoka.edu.al

EDUCATION

Date: 2012-2016
Degree: PhD in Civil Engineering
University: Epoka University

Date: 2011-2012
Degree: MSc in Civil Engineering, Profile: Structural Engineering
University: Epoka University

Date: 2007-2011
Degree: Bachelor in Civil Engineering
University: Epoka University

ACADEMIC EXPERIENCE

Date: September 2012 - present
Position: Lecturer
Employer: Epoka University

Date: September 2011 – August 2012

Position: Research Assistant

Employer: Epoka University

FOREIGN LANGUAGES

	Understanding				Speaking				Writing	
	Listening		Reading		Spoken interaction		Spoken production			
English	C2	Proficient User	C2	Proficient User	C2	Proficient User	C2	Proficient User	C2	Proficient User
Turkish	B2	Independent User	B2	Independent User	B2	Independent User	B2	Independent User	B2	Independent User
Italian	B1	Independent User	A2	Basic User	B1	Independent User	B1	Independent User	A2	Basic User

LIST OF PUBLICATIONS

- JOURNAL ARTICLES

Mustafaraj, E. and Yardim, Y. (2016) Determination of structural behavior of an unreinforced masonry Clock Tower using FEM analysis. American Journal of Engineering Research (AJER), 5(1), 100-104, ISSN (e): 2320-0847.

Mustafaraj, E. and Saliko, D. (2016) Structural optimization of a reinforced concrete building. American Journal of Engineering Research (AJER), 5(1), 73-79 ISSN (e): 2320-0847.

Mustafaraj, E., and Yardim, Y. (2013). “**Strengthening and Restoration of Historical Structures—Mirahor Ilyas Beg Mosque in Korça**” Journal of Literature and Art Studies, ISSN 2159-5836, Vol. 3, No. 12, 809-818.

Yardim, Y., and **Mustafaraj, E.,** (2013). “**Effects of soil settlement and deformed geometry on a historical structure**” -, Natural Hazards and Earth System Sciences, 15, 1051-1059, 2015. doi:10.5194/nhess-15-1051-2015.

Yardim, Y., and **Mustafaraj, E.,** (2012). "**Structural Assessment and Restoration of the Leaden Mosque in Berat, Albania**", KSU. Journal of Engineering Sciences, 15(2)

- **CONFERENCE PROCEEDINGS**

Mustafaraj, E., and Yardim, Y. (2016). “External shear strengthening of unreinforced masonry panels using ferrocement jacketing”, XVI International Scientific Conference VSU'2016, 9-10 June, 2016 Sofia, Bulgaria

Mustafaraj, E., and Yardim, Y. (2016). “Usage of ferrocement jacketing for strengthening of damaged unreinforced masonry (URM) walls”, 3rd International Balkans Conference on Challenges of Civil Engineering, 3-BCCCE 2016, 19-21 May 2016, Tirana, Albania

Mustafaraj, E., and Yardim, Y. (2014). “Structural Assessment of Preza Clock Tower, Albania” - ICESA 2014-International Civil Engineering & Architecture Symposium for Academicians 2014, 17-20 May 2014, Side, Turkey.

Barushi, K., and Mustafaraj, E., (2013). “A case study on structural assessment and restoration of King Zog's villa in Durres, Albania”. 2-BCCCE 2013, 23-25 May, Tirana, Albania.

Rexhaj, G., and Mustafaraj, E., (2013). “Conditional assessment of Kiri Bridge in Shkoder, Albania”. 2-BCCCE 2013, 23-25 May, Tirana, Albania.

Mustafaraj, E. (2013). “Structural assessment of historical buildings: a case study of five Ottoman Mosques in Albania”, 2-BCCCE 2013, 23-25 May, Tirana, Albania.

Mustafaraj, E., and Yardim, Y. (2013). “Repair and Strengthening of Historical Structures: Naziresha’s Mosque in Elbasan”. 3rd Annual International Conference on Civil Engineering, 10-13 June 2013, Athens, Greece.

Keci, J., and Mustafaraj, E. (2013). “Practices, Barriers and Challenges of Risk Management Implementation in Albanian Construction Industry”. 3rd Annual International Conference on Civil Engineering, 10-13 June 2013, Athens, Greece.

Yardim, Y., and **Mustafaraj, E.**, (2013). “**Geometric imperfection effect on historical building under earthquake load**”. Vienna Congress on Recent Advances in Earthquake Engineering and Structural Dynamics 2013 (VEESD 2013), C. Adam, R. Heuer, W. Lenhardt & C. Schranz (eds), 28-30 August 2013, Vienna, Austria.

Mustafaraj, E., and Yardim, Y. (2012) “**Strengthening and restoration of historical structures -Mirahor Ilyas Beg Mosque in Korça**”, 1st International Conference on Architecture and Urban Design, 19-21 April 2012, Tirana, Albania.

Mustafaraj, E., and Yardim, Y. (2012) “**Conditional Assessment of Historical Structures: Earthquake Performance of Naziresha Mosque**”, International Students’ Conference of Civil Engineering, 10-11 May 2012, Tirana, Albania.

- **BOOK CHAPTERS**

Yardim, Y. and **Mustafaraj, E.** (2015). **Chapter 17 “Selected Assessment and Retrofitting Application Techniques for Historical Unreinforced Masonry Buildings”** In book: Seismic Assessment and Rehabilitation of Historic Structures, Publisher: IGI Global, Editors: Panagiotis G. Asteris, Vagelis Plevris.

Keci, J. and **Mustafaraj, E.** (2015). **Chapter 13 “Practices, Barriers and Challenges of Risk Management Implementation in Albanian Construction Industry”** In book: Urban Planning and Civil Engineering, Edited by Virginia P. Sisiopiku Ossama E. Ramadan, Athens Institute for Education & Research (ATINER).

- **BOOKS**

Mustafaraj E, Gjonaj, I., and Ponari, K. (2015): "**SIGURIA NE PUNE**" **Manual per punen ne kantier.** 02/2015; Dita 2000, ISBN: 978-9928-187-17-8.

Mustafaraj, E. (2014). **“Assessment of Historical Structures, A case study of five Ottoman Mosques in Albania”**, LAP Lambert Academic Publishing, ISBN: 978-3-659-21414-1, March 13, 2014.